AD-A136 702 ANALYTICAL AND NUMERICAL MODELLING OF FLOW DRIVEN BY SURFACE DIFFERENTIAL HEATING(U) RISOE NATIONAL LAB ROSKILDE (DENMARK) I TROEN SEP 82 RISOE-R-452 1/2

UNCLASSIFIED F/G 4/1 NL

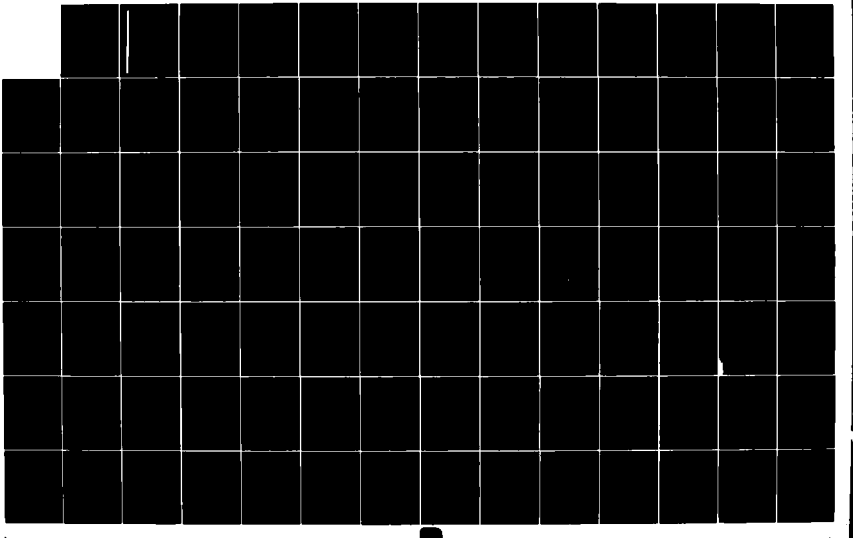

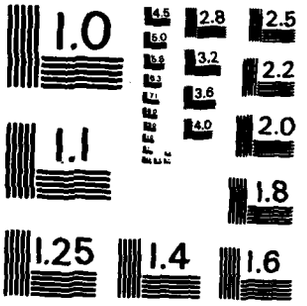

MICROCOPY RESOLUTION TEST CHART
NATIONAL BUREAU OF STANDARDS-1963-A

Risø-R-452

RISØ

Risø-R-452

AD-A136702

Analytical and Numerical Modelling of Flow driven by Surface differential Heating

Ib Troen

Risø National Laboratory, DK-4000 Roskilde, Denmark
September 1982

RISØ-R-452

ANALYTICAL AND NUMERICAL MODELLING OF FLOW DRIVEN BY SURFACE DIFFERENTIAL HEATING.

Ib Troen

Abstract. The atmospheric flow generated in response to horizontal gradients in the surface temperature or heatflux is investigated. A linear model is described that can treat the problem for the case of small surface temperature gradients, including the approximate effect of a large-scale flow and the effect of a vertical structure in the heat and momentum diffusivity, and in the stratification. The second part of this report describes a numerical mesoscale model, and results from the application of this model to the simulation of the sea-breeze.

September 1982
Risø National Laboratory, DK 4000 Roskilde, Denmark.

The present thesis is submitted to the University of Copenhagen in partial fulfilment of the requirements for the degree of lic. scient. (Ph.D.). Professor E. Eliasen acted as supervisor.

ISBN 87-550-0923-9
ISSN 0106-2840

Risø Repro 1983

CONTENTS

The sun also ariseth, and the sun
goeth down, and hasteth to his
place where he arose.
The wind goeth toward the south
and turneth about unto the northy;
it whirleth about continually, and
the wind returneth again according
to his circuits.

Ecclesiastes 1:5,6

1. INTRODUCTION

The present report deals with some aspects of the atmospheric response to time-varying horizontal gradients in the surface temperature and heatflux on the mesoscale. The interest is concentrated on the modelling of the sea-breeze circulation in its "pure" form as the two-dimensional flow across a coastline in response to the periodic heating of the land.

In the first part an analytical technique is employed, which enables the study of different scales of the mean flow. The method is based on the linearization of the dynamical equations, and the neglect of any feedback from the mean flow to the stratification and turbulence structure (constant diffusivity and stratification). The model is generalized to include the effect of vertical variation of diffusivity and stratification.

The second part describes a numerical model in which a more sophisticated treatment of the turbulent transport is employed. A large number of theoretical studies of the sea-breeze phenomenon have appeared in the literature. Most of these are based on numerical modelling (Estoque 1961,Neumann and Mahrer 1971,Pielke

1974, and many others) but most of the results presented in these studies relate to only gross features of the flow which in many cases can be inferred from an analysis of the governing equations using analytical techniques (Walsh,1974). The accurate modelling of the development of small-scale structure in the sea-breeze flow, and the interaction with the turbulence field is however possible only by using a numerical technique. In recent years the interest in the detailed structure of the flow and the turbulence fields has been promoted by concern for the implications to dispersion of pollutants in the coastal zone (Keen and Lyons 1978, Anthes 1978), and the level of sophistication of operational dispersion models, in particular "puff" models (Mikkelsen et. al. 1981), has allowed for a direct use in such models of the detailed windfields and turbulence parameters from the flow models. The model presented here has potential for such practical use, but at present it has been applied only for simulations using synthetic "typical" input data.

The physical situation modelled in both chapters, except for Section 2.9, is a straight coastline dividing a heated semiinfinite land area and a sea where the temperature is assumed constant. The coordinate system is defined as a right-handed one with the x-axis pointing inland, the y-axis along the coastline, and z-axis vertical. The flow is assumed to be describable as two-dimensional with no variation along the y-axis. The components of the wind vector u, v, and w, are, as usual, defined as the components along the x-, y-, and z-axis, respectively.

2. LINEARIZED PERIODICALLY FORCED MODEL

2.1. The scaled basic equations

The equations of motion assuming the Boussinesq approximation can be written as:

$$\frac{\partial \hat{\vec{v}}}{\partial t} + \hat{\vec{v}} \cdot \nabla \hat{\vec{v}} + f\hat{k} \times \hat{\vec{v}} = \frac{1}{\rho_s} \nabla p + \frac{\partial}{\partial z} \hat{\tau}$$

$$\frac{\partial \theta'}{\partial t} + \hat{\vec{v}} \cdot \nabla \theta' + w\Gamma = \frac{\partial \hat{\vec{v}}}{\partial z} + Q \qquad (2.1)$$

$$\nabla_3 \cdot \hat{\vec{v}} = 0$$

$$\frac{\partial p}{\partial z} = g\rho_s \frac{\theta'}{\theta} \quad ,$$

Where the hydrostatic approximation has been also assumed and the horizontal diffusion of momentum and heat have been neglected. The hydrostatic approximation is justified if the aspect ratio of the flow can be assumed to be much less than one: We are here considering flow driven by surface heating and therefore the pressure gradient is the important driving force for the flow. We can therefore assume the scaling:

$$\frac{p}{L} \sim \frac{\rho U}{T} \qquad (2.2)$$

from the equation for the horizontal velocity, where L is a characteristic length, T characteristic time, and U velocity. From the equations of continuity and vertical velocity we can write:

$$\frac{W}{\overline{T}} \sim \frac{H}{\overline{L}} \frac{U}{\overline{T}} \sim \rho^{-1} \frac{H^2}{L^2} \frac{p}{\overline{H}} \qquad (2.3)$$

Thus the magnitude of the time change of w is of the order $(H/L)^2\ \rho^{-1}$ times the magnitude of the vertical pressure gradient. Also the omission of the horizontal diffusion of momentum can be justified assuming H << L. In a viscous fluid we have that the horizontal diffusion of momentum is of the order $\nu U/L^2$, where ν is the kinematic viscosity of the fluid; the vertical diffusion term is similarly of the order $\nu U/H^2$, and thus the ratio of the two terms is $(H/L)^2$. In the case of the diffusion by turbulence in the atmospheric boundary layer, the fluxes of momentum and heat are typically of the same order of magnitude in both the horizontal and vertical, and therefore the ratio of the two terms in the flux-divergence terms in the equation of motion and in the thermodynamic equation is of the order (H/L).

For small values of the amplitude of the thermal forcing the amplitude of the flow perturbation will be small and the nonlinear advection terms can be neglected. The equations of motion in the case of vanishing basic state flow becomes in this case

$$\frac{\partial \tilde{u}}{\partial t} - f\tilde{v} = -\frac{1}{\rho_s} \frac{\partial \tilde{p}}{\partial x} + K \frac{\partial^2 \tilde{u}}{\partial z^2}$$

$$\frac{\partial \tilde{v}}{\partial t} + f\tilde{u} = K \frac{\partial^2 \tilde{v}}{\partial z^2}$$

$$\frac{\partial \tilde{\theta}}{\partial t} + \tilde{w}\Gamma = K \frac{\partial^2 \tilde{\theta}}{\partial z^2} \qquad (2.4)$$

$$\frac{\partial \tilde{p}}{\partial z} = g\rho_s \frac{\tilde{\theta}}{\theta}$$

$$\frac{\partial \tilde{u}}{\partial x} + \frac{\partial \tilde{w}}{\partial z} = 0$$

where the further simplification has been made that the vertical diffusion terms can be parameterized employing a constant diffusivity.

We assume the surface forcing to be harmonic in time with frequency ω. Equations (2.4) can then be nondimensionalized by the introduction of the following scaling:

$$\tilde{\theta} = \Theta \cdot \theta$$

$$\tilde{p} = Hg\ \rho_s\ p$$

$$\tilde{u} = \frac{g}{N} u$$

$$\tilde{v} = \frac{g}{N} v$$

$$\tilde{w} = \frac{g\omega}{N^2} w \qquad (2.5)$$

$$t = \tau \cdot \omega^{-1}$$

$$x = \xi \cdot L$$

$$z = \eta \cdot H$$

$$L = H \cdot \frac{N}{\omega} \qquad \text{(horizontal scale)}$$

$$H = \sqrt{\frac{K}{\omega}} \qquad \text{(vertical scale)} \ ,$$

where N is the Brunt-Väisälä frequency corresponding to the basic state stratification, and variables with a "~" denote dimensional quantities. With this scaling the equations of motion can be written as

$$\frac{\partial u}{\partial \tau} - f_s v = -\frac{\partial p}{\partial \xi} + \frac{\partial^2 u}{\partial \eta^2}$$

$$\frac{\partial v}{\partial \tau} + f_s u = \frac{\partial^2 v}{\partial \eta^2}$$

$$\frac{\partial \theta}{\partial \tau} + w = \frac{\partial^2 \theta}{\partial \eta^2} \qquad (2.6)$$

$$\frac{\partial p}{\partial \eta} = \theta$$

$$\frac{\partial u}{\partial \xi} + \frac{\partial w}{\partial \eta} = 0$$

where

$$f_s = f/\omega$$

2.2. Method of solution

In the following we specifically consider the case of flow driven by diurnal variation of surface temperature difference across a straight coastline, in which case $\omega = \Omega$ = angular frequency of the earths rotation; thus with $f = 2\ \Omega \sin \phi$ we have $f_s = 2 \sin \phi$. We wish to obtain periodic solutions to this system of equations with the following boundary conditions:

$$\text{at} \quad z = \eta = 0 \quad : \quad u = v = w = 0$$

$$\theta = \begin{cases} 0 & \text{for } \xi < 0 \\ \cos\tau & \text{for } \xi > 0 \end{cases} \qquad (2.7)$$

$$\text{at} \quad z,\ \eta \to \infty \quad : \quad u,\ v,\ w,\ p,\ \theta \to 0$$

It is convenient to write the fields in terms of Fourier series as follows

$$u(\xi,\eta,\tau) = \frac{1}{\pi}\int_0^\infty u(k,\eta)\,\frac{\cos k\,\xi}{k}\,dk \cdot \exp(-i\tau) \qquad (2.8)$$

and similarly for v, also

$$w(\xi,\eta,\tau) = \frac{1}{\pi}\int_0^\infty w(k,\eta)\,\frac{\sin k\xi}{k}\,dk \cdot \exp(-i\tau) \qquad (2.9)$$

and for p as well. The boundary condition at $\eta = 0$ for θ means that θ must be expanded as

$$\theta(\xi,\eta,\tau) = \left(\frac{1}{2}\,\theta_o(\eta) + \frac{1}{\pi}\int_0^\infty \frac{\sin k\xi}{k}\,\theta(k,\eta)dk\right)\exp(-i\tau) \qquad (2.10)$$

with $\theta(k,0) = \theta_o(0) = 1$. Because of the linearity of the system it can be solved for each Fourier mode independently. The first term on the right in Eq. (2.10) corresponds to the heating of the surface harmonically in time and independently of ξ. This forcing is easily seen to induce no flow, but to give contributions to the θ and p fields only. When only this forcing term is considered the θ equation simplifies to

$$\left(i + \frac{\partial^2}{\partial\eta^2}\right)\theta_o = 0 \qquad (2.11)$$

then

$$\theta_o(\eta) = \exp\left(-\frac{\sqrt{2}}{2}\,\eta\right)\cos\left(\frac{\sqrt{2}}{2}\,\eta - \tau\right) \qquad (2.12)$$

This is the classical Stokes solution to the problem of a viscous fluid subject to harmonic forcing at the surface. The equation governing the functions $u(k, \eta)$, $v(k, \eta)$ etc. is obtained from the set of Eqs. (2.6):

$$\left(i + \frac{\partial^2}{\partial \eta^2}\right)u + f_s v = kp$$

$$\left(i + \frac{\partial^2}{\partial \eta^2}\right)v - f_s u = 0$$

$$\left(i + \frac{\partial^2}{\partial \eta^2}\right)\theta - w = 0 \qquad (2.13)$$

$$\frac{\partial p}{\partial \eta} = 0$$

$$- ku + \frac{\partial w}{\partial \eta} = 0$$

combining the above equations we can get an equation for the perturbation pressure:

$$\left(i + \frac{\partial^2}{\partial \eta^2}\right)\left[\frac{\partial^6}{\partial \eta^6} + 2i \frac{\partial^4}{\partial \eta^4} + (f_s^2-1) \frac{\partial^2}{\partial \eta^2} - k^2\right]p = 0; \qquad (2.14)$$

the solution can be written as the sum

$$p = \sum_{j=1}^{4} p_j \exp(\alpha_j \eta) \qquad (2.15)$$

with the α's determined as the solutions with negative real part of the following equations:

$$i + \beta = 0$$

and

$$\beta^3 + 2i\beta^2 + (f_s^2-1)\beta - k^2 = 0 \qquad (2.16)$$

with

$$\alpha = \pm\sqrt{\beta}.$$

The terms with $Re(\alpha) > 0$ corresponds to unphysical solutions which increase exponentially with height.

For small values of f_s, corresponding to $\omega >> f$ rotation can be neglected and Eq. (2.14) reduces to

$$\left[\frac{\partial^6}{\partial\eta^6} + 2i\,\frac{\partial^4}{\partial\eta^4} - \frac{\partial^2}{\partial\eta^2} - k^2\right]p = 0 \qquad (2.17)$$

and Eq. (2.16) becomes in this case

$$(i+\alpha^2)\,\alpha \pm k = 0 \qquad (2.18)$$

Here we are interested only in the case where $\omega \cong 1/(24\ h)$, and therefore rotation can only be neglected if we have $\phi \lesssim 10$ deg. It should be noted, however, that if the surface boundary conditions are changed so that the horizontal length scale no longer is determined by L in Eq. (2.5), but rather induced externally as ℓ with $\ell << L$, then only large values of k in Eq. (2.14) need be considered. In this case Eq. (2.14) can be satisfied only if the higher-order terms and k^2 are of comparable magnitude and thus the rotation term can be neglected. It is obvious that the flow structure is determined in this case solely by the parameter ℓ/L. A discussion of the flow structure in this case is given in Kimura and Eguchi (1978), where the governing parameter is defined as $\Omega = (\ell/L)^{2/3}$. They neglect rotation even in the case $\Omega \simeq 1$, however. In Eq. (2.5) we have introduced the time scale as ω^{-1}; alternatively, we could have used f^{-1}. The equation for the perturbation pressure in this case where we have an externally specified horizontal length scale ℓ can be obtained from Eq. (2.14) by the substitution $\eta' = \sqrt{\omega/f}\ \eta$ yielding:

$$\left(i\hat{\omega} + \frac{\partial^2}{\partial\eta'^2}\right)\left[\frac{\partial^6}{\partial\eta'^6} + 2i\hat{\omega}\,\frac{\partial^4}{\partial\eta'^4} + (1-\hat{\omega}^2)\,\frac{\partial^2}{\partial\eta'^2} - m\right]p = 0 \qquad (2.19)$$

with $\hat{\omega} = \omega/f$ and

$$m = \left(\frac{L}{\ell}\right)^2\left(\frac{\omega}{f}\right)^3 = \frac{KN^2}{f^3\ell^2} \qquad (2.20)$$

In this case the vertical scale is the Ekman depth $H = \sqrt{K/f}$, $\eta' = Z/H$. Eq. (19) makes it possible to identify a number of prototype boundary layers by requiring that different combi-

nations of two terms be dominant. This analysis is performed in Park and Mahrt (1979), where it is argued that the stratification paramater m is much more sensitive to the choice of horizontal length scale ℓ than to the stratification. This latter term is given by N because the diffusivity K should not be chosen independently of N, since turbulence is suppressed when N is large. The choice of $\ell >> L$ or equivalently $m << \omega^3$ should, however, be expected to lead to incorrect scaling of the flow parameters because even though a typical length scale characterizing the heating/cooling area is ℓ, then the "internal" flow scale L is the proper length scale. The conclusion is thus that m in actual flows is limited both downwards and upwards.

In the following we return to our original formulation, and are therefore interested in the solution of the system of equations (2.16).

The solution of the cubic equation is easily found by using Newton-Raphson iteration to obtain one root β_1, and the two remaining roots from the quadratic obtained when $(\beta-\beta_1)$ is factored out. the solution for the α_i's depends on the wavenumber k and the scaled Coriolis parameter f_s. Figure 2.1 shows the real and imaginary part of the three values of α from the solution of the cubic as function of k. The value of f_s is 1.5 corresponding to diurnal forcing at middle latitudes ($\phi \simeq 50^o$). The asymptotic solution corresponding to the limit $k \to \infty$ is given as

$$\alpha_j = k^{1/3} \exp\left(i(j+1)\frac{\pi}{3}\right) \quad , \quad j = 1,2,3 \qquad (2.21)$$

This expression is a fair approximation even at moderate values of k. The fourth root in Eq. (2.16) is independent of k and given as $\alpha_4 = -\sqrt{2}/2(1-i)$. As for the pressure the coefficients in the Fourier integrals Eqs. (2.9) and (2.10) can be written as a sum of four exponentials as Eq. (2.15). The coefficients are related through the following relations obtained from substitution of Eq. (2.15) into Eqs. (2.13):

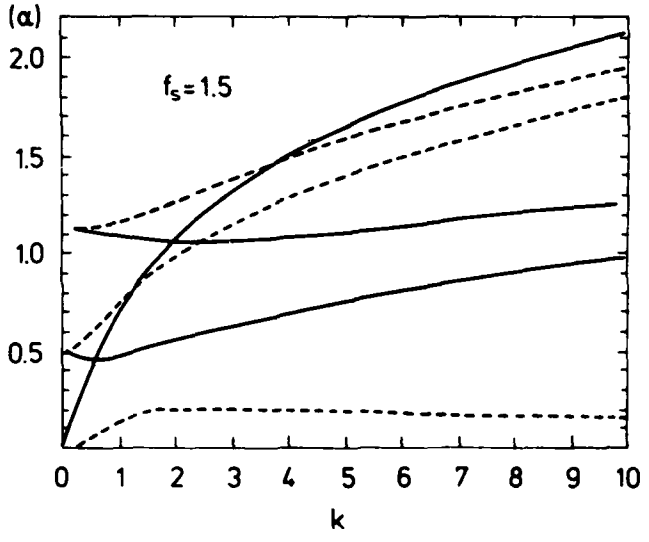

Fig. 2.1. The absolute value of the real part (____), and the imaginary part (---) of the roots α of the characteristic equation (2.16).

$$u_j = k \frac{\gamma_j}{f_s^2 + \gamma_j^2} p_j$$

$$v_j = k \frac{f_s}{f_s^2 + \gamma_j^2} p_j \qquad (2.22)$$

$$w_j = \alpha_j \gamma_j p_j$$

$$\theta_j = \alpha_j p_j$$

with

$$\gamma_j = (\alpha_j^2 + i)$$

The solution for p_j is obtained by application of the boundary conditions Eq. (2.7).

2.3. Limit of large wavenumbers

In the asymptotic limit of $k \to \infty$ we can use α_j from Eq. (2.21) and the system of Eqs. (2.22) can be approximated by the following system:

$$\sum \exp\left(i(j+1)\frac{\pi}{3}\right)p_j = k^{-1/3}$$

$$\sum \exp\left(-i(j+1)\frac{2\pi}{3}\right)p_j = 0 \qquad j = 1,2,3 \qquad (2.23)$$

$$\sum \exp\left(i(j+1)\pi\right)p_j = 0$$

and

$$p_4 = -f_s^2(p_1 + p_2 + p_3).$$

The solution is

$$p_1 = -\left(\frac{1}{4}\,1 + \frac{\sqrt{3}}{3}\,i\right)k^{-1/3}$$

$$p_2 = -\frac{1}{2}\,k^{-1/3}$$

$$p_3 = -\frac{1}{4}\left(1 - \frac{\sqrt{3}}{3}\,i\right)k^{-1/3}$$

$$p_4 = f_s^2\,k^{-1/3}$$

and

$$u_1 = \frac{1}{4}\left(1 - \frac{\sqrt{3}}{3}\, i\right)$$

$$u_2 = -\frac{1}{2}$$

$$u_3 = \frac{1}{4}\left(1 + \frac{\sqrt{3}}{3}\, i\right)$$

$$u_4 = 0$$

The cross isobar flow field $u(k, \eta)$ is therefore given as (Fig. 2.2) for large k:

$$u(k,\eta) = \sum u_j \exp(\alpha_j \eta)$$

$$= -\frac{1}{2}\exp(-\lambda) + \frac{\sqrt{3}}{3}\exp\left(-\frac{1}{2}\lambda\right)\cos\left(\frac{\sqrt{3}}{2}\lambda - \frac{\pi}{6}\right) \qquad (2.24)$$

with

$$\lambda = k^{1/3}\,\eta$$

The appropriate dimensional scale height is thus dependent on the horizontal length scale. Denoting this by ℓ we have $k = L/\ell$ and the scale height therefore becomes

$$h = \left(\frac{\ell}{L}\right)^{1/3} H = \left(\frac{\ell\omega}{\sqrt{K_N \omega}}\right)^{1/3} \sqrt{\frac{K}{\omega}} = \left(\frac{\ell N}{N}\right)^{1/3} \qquad (2.25)$$

In Park and Mahrt (1979) the dynamics in this limit of small ℓ is termed $E^{1/3}$-layer dynamics. In Mahrt (1979) it is noted that this dynamics may describe actual small-scale nocturnal flows even though the initial conditions are complicated since the flow structure is determined only by the balance of the pressure gradient and momentum diffusion. This is brought out in Eq.

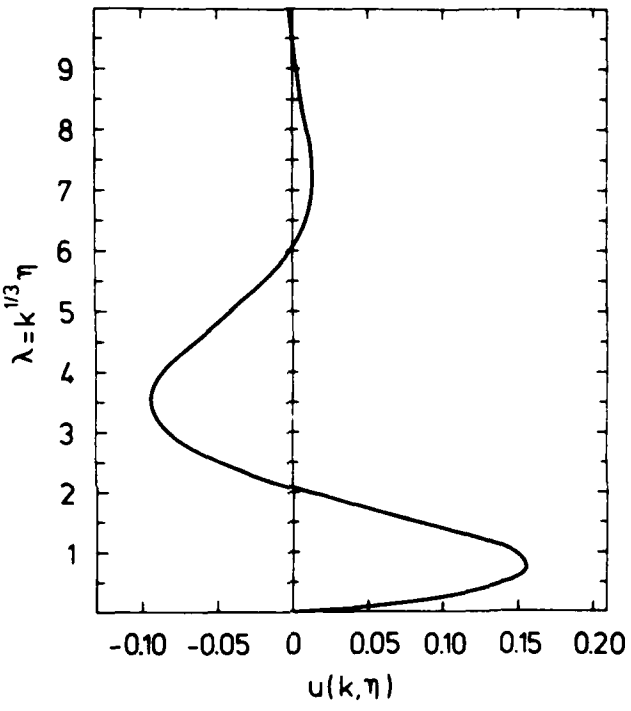

Fig. 2.2. The Cross isobar component $u(k,\eta)$ in the limit of large wavenumbers k as function of $k^{1/3}\eta$, where η is the scaled vertical coordinate.

(2.24), showing $u(k, \eta)$ to be real, and therefore the cross isobar flow to be in phase with the temperature perturbation.

2.4. Solution for small wavenumbers

In the limit of $k^2 \ll 1$ a simple solution can again be obtained: We have for the cubic Eq. (2.16) the approximate roots

$$\beta_1 \cong \frac{k^2}{f_s^2 - 1} + O(k^4)$$

$$\beta_{2,3} = -i(1 \mp f_s) \pm \frac{1}{2f_s} \cdot \frac{k^2}{(1 \mp f_s)} + O(k^4) \qquad (2.26)$$

$$\beta_4 = -i \, .$$

To simplify we will assume $f_s > 1$ in the following: Then

$$\alpha_1 = - a\, b\, k + 0(k^3)$$

$$\alpha_2 = - \frac{1}{b} \cdot \frac{\sqrt{2}}{2} (1 + i) + 0(k^2) \qquad (2.27)$$

$$\alpha_3 = - \frac{1}{a} \cdot \frac{\sqrt{2}}{2} (1 - i) + 0(k^2)$$

$$\alpha^4 = - \frac{\sqrt{2}}{2} (1 - i)$$

with

$$a = (f_s + 1)^{-1/2} \quad \text{and} \quad b = (f_s - 1)^{-1/2} .$$

Eqs. (2.22) and the surface boundary conditions. Eqs. (2.7) lead to the following linear equations for the expansion coefficient for p_j (Eq. 2.15) when the above relations are inserted and terms only up to first order in wavenumber k are retained:

$$\begin{matrix} iabk & -f_s b^{-2} & -f_s a^{-2} & 0 \\ abk & ib^{-2} & -ia^{-2} & \frac{k^2}{f_s^2} \\ -i & r^* f_s b^{-1} & r f_s a^{-1} & 0 \\ -1 & -r b^{-1} & -r^* a^{-1} & -r^* \end{matrix} \begin{matrix} kabp_1 \\ p_2 \\ p_3 \\ p_4 \end{matrix} = \begin{matrix} 0 \\ 0 \\ 0 \\ 1 \end{matrix} \qquad (2.28)$$

where

$$r = \frac{\sqrt{2}}{2} (1 + i)$$

with the solution

$$p_1 = -\frac{k}{2f_s}\left(\sqrt{f_s+1} - i\sqrt{f_s-1}\right)(1 - k\cdot c)$$

$$p_2 = \frac{k^2}{2f_s^2(f_s - 1)} \cdot \frac{\sqrt{2}}{2}(1-i) \cdot \left(1 + k\left(\frac{\sqrt{2}}{2}(1-i)\frac{\sqrt{f_s - 1}}{f_s + 1} - C\right)\right) \tag{2.29}$$

$$p_3 = \frac{-k^2}{2f_s^2(f_s + 1)} \cdot \frac{\sqrt{2}}{2}(1-i) \cdot \left(1 + k\left(\frac{\sqrt{2}}{2}(1-i)\frac{\sqrt{f_s + 1}}{f_s - 1} - C\right)\right)$$

$$p_4 = -\frac{\sqrt{2}}{2}(1+i)$$

..here

$$C = \frac{\sqrt{2}}{4}\frac{1 + i}{f_s^2 - 1}\left((f_s - 1)^{3/2} + i(f_s + 1)^{3/2}\right) .$$

Using Eq. (2.22) the leading terms in the cross isobar flow field for k << 1 becomes

$$u_1 = \frac{-k^2}{2f_s}\left(\frac{i}{(f_s - 1)\sqrt{f_s + 1}} + \frac{1}{(f_s + 1)\sqrt{f_s - 1}}\right)(1 - k\,C)$$

$$u_2 = \frac{-k}{2f_s}\left(\frac{\sqrt{2}}{2}(1-i) - k\left(\frac{1}{(f_s + 1)\sqrt{f_s - 1}} + \frac{\sqrt{2}}{2}(1-i)C\right)\right) \tag{2.30}$$

$$u_3 = \frac{k}{2f_s}\left(\frac{\sqrt{2}}{2}(1-i) + k\left(\frac{i}{(f_s - 1)\sqrt{f_s + 1}} - \frac{\sqrt{2}}{2}(1-i)\,C\right)\right)$$

$$u_4 = 0$$

retaining only the first-order terms we see that the contribution in the Fourier integral Eq. (2.8) is:

$$\mathrm{Re}\left\{u(k,\eta)\,\frac{\cos k\,\xi}{k}\,\exp(-i\tau)\right\} \cong$$

$$\frac{\cos k\,\xi}{2f_s}\left\{\exp\left(-\sqrt{\frac{f_s+1}{2}}\,\eta\right)\cdot\cos\left(\sqrt{\frac{f_s+1}{2}}\,\eta-\frac{\pi}{4}-\tau\right)\right.$$

$$\left.-\exp\left(-\sqrt{\frac{f_s-1}{2}}\,\eta\right)\cdot\cos\left(\sqrt{\frac{f_s-1}{2}}\,\eta+\frac{\pi}{4}+\tau\right)\right\} \qquad (2.31)$$

The u_1-term is of order k^2 and can be neglected for small heights η, however, since the root α_1 is proportional to k (Eq. 2.27) the depth of the disturbance from this component increases as k tends to zero. For decreasing values of k, therefore, part of the return flow will consist of an increasingly deep layer of very weak flow. The contribution to the total profile from the first term takes the form:

$$\mathrm{Re}\left\{u_1\,\frac{\cos k\,\xi}{k}\,\exp(-i\tau)\right\} \cong$$

$$-\frac{k\cos k\,\xi}{(f_s^2-1)\sqrt{2f_s}}\cos(\phi_s-\tau)\,\exp\left(-\frac{k}{\sqrt{f_s^2-1}}\,\eta\right) \qquad (2.32)$$

where

$$\phi_s = \tan^{-1}\sqrt{\frac{f_s+1}{f_s-1}}$$

The expression (2.31) can be rewritten as

$$\mathrm{Re}\left\{u(k,\eta)\,\frac{\cos\kappa\,\xi}{k}\,\exp(-i\tau)\right\} = \cos(k\,\xi)\cdot A(\eta)\cos(\tau+\phi(\eta)) \qquad (2.33)$$

In Fig. 2.3 the amplitude $A(\eta)$ is plotted for different values of the scaled Coriolis parameter f_s. The phase function $\phi(\eta)$ is shown in Fig. 2.4. For large values of f_s the flow structure becomes asymptotically independent of ω, as should be expected, corresponding to a quasi-steady state. The proper depth scale becomes the Ekman depth, as can be seen from Eq. (2.31) with $f_s \gg 1$

$$\mathrm{Re}\left\{u(k,\eta \frac{\cos k\,\xi}{k} \exp(-i\tau)\right\} \cong$$

$$\frac{\cos k\,\xi}{f_s} \exp(-\eta') \sin(\eta') \cos\left(\tau - \frac{\pi}{4}\right) \qquad (2.34)$$

where

$$\eta' = \sqrt{\frac{f_s}{2}}\,\eta = z \left(\frac{2K}{f}\right)^{-1/2}$$

Thus, for $f_s >> 1$ we have $\phi(\eta) = -\pi/4$ up to the height $\eta = \pi \cdot (1/2f_s)^{-1/2}$ where it becomes equal to $3\pi/4$. This stepwise behaviour is seen to be a fair approximation to ϕ even at $f_s = 2$ (Fig. 2.4). The inflow layer becomes deeper as f_s decreases towards 1.

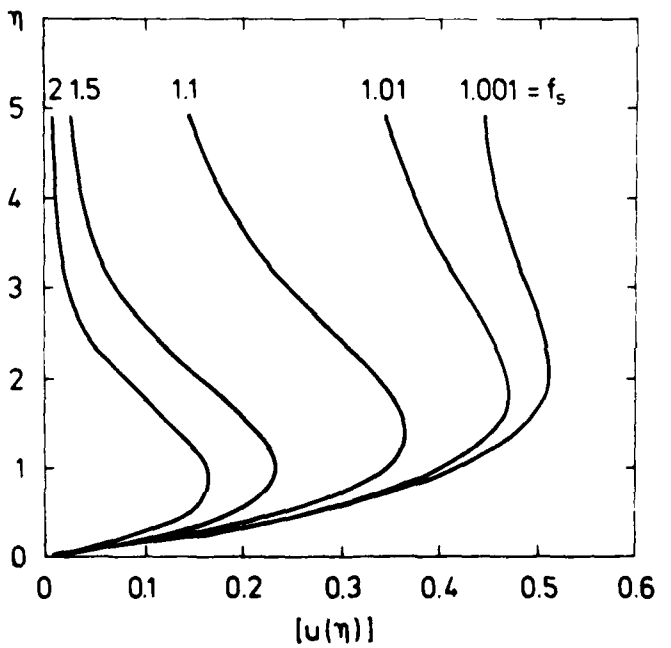

Fig. 2.3. The amplitude A(η) for the u-component at small wavenumbers (Eq. 2.33) for different values of the scaled Coriolis parameter.

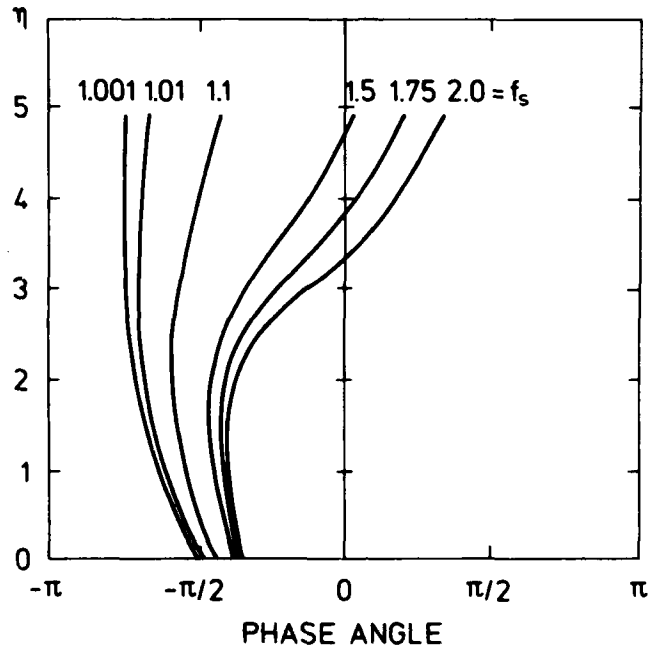

Fig. 2.4. The Phase angle $\phi(n)$ for the u-component at small wavenumbers (Eq. 2.33) for different values of the scaled Coriolis parameter.

2.5. Land-sea breeze circulation

By inspection the dynamics of the small scales are seen to be characterized by a balance between momentum diffusion and pressure gradient force in the u-momentum equation, and between temperature diffusion and adiabatic cooling in the thermodynamic equation. By contrast the large scales are found to be characterized by a balance between the harmonic term, Coriolis force, and the vertical momentum diffusion for the u and v components, whereas in the thermodynamic equation the adiabatic cooling is unimportant and we have the Stokes balance between forcing and vertical diffusion. Well above the surface, however, the diffusion terms are unimportant and the principal momentum balance is between the harmonic terms, Coriolis term, and the pressure gradient, whereas the thermodynamic equation here simplifies to

a balance between the harmonic term and the adiabatic cooling term.

For intermediate wavenumbers all terms are important and even though the cubic characteristic equation can be solved to yield explicit roots for any wavenumber, the final solutions obtained after the solution of the linear equations for the boundary conditions are so complicated that explicit expressions are of little use. The amplitude and phase for different wavenumbers are shown in Fig. 2.5. Also shown is the amplitude and phase functions for the integrated profile at the coast obtained by numerically integrating Eq. (2.8) using Simpsons rule. The upper limit was set to k = 100 and stepsize in the integration was $\Delta k = 0.1$. The profiles corresponding to individual wavenumbers are characterized by a nearly constant "inflow" layer where the phase is essentially constant with height; at the top of this layer the amplitude is close to zero and the phase changes 180 degrees over a rather thin layer. The profiles

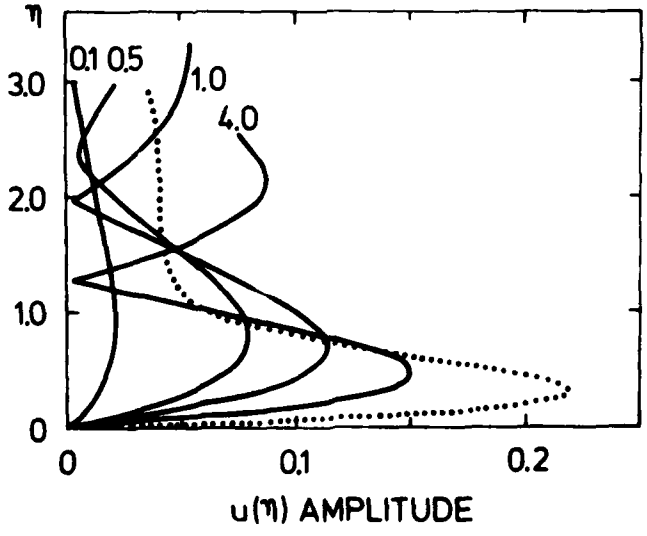

Fig. 2.5a. The amplitude of the modes of the u-component for different wavenumbers. The dotted curve gives the amplitude of the integrated u-profile.

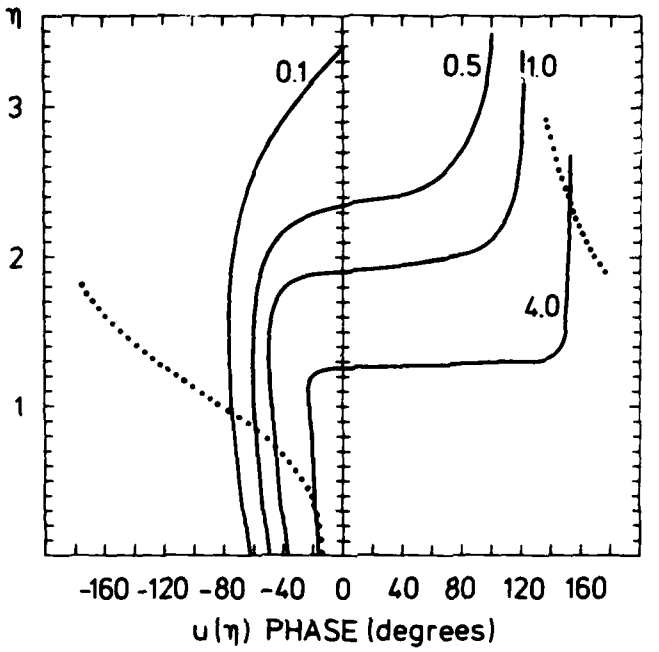

Fig. 2.5b. As fig. 2.5a, but for the phase.

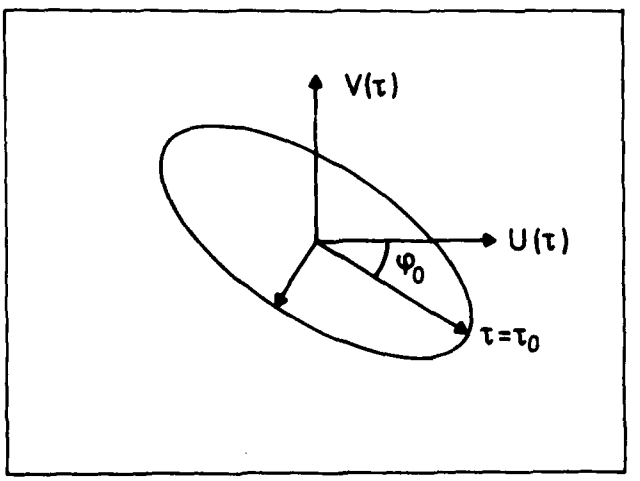

Fig. 2.6. Definition of parameters describing the wind hodograph.

plotted for different values of the time τ differ, therefore, only by a factor nearly independent of height. For the integrated profile the inflow layer is less well defined in depth and changes in the course of one period in the interval from $\eta \cong 1$ to $\eta \cong 2$. For the velocity component along the coast the amplitude and phase functions can likewise be found. The hodograph

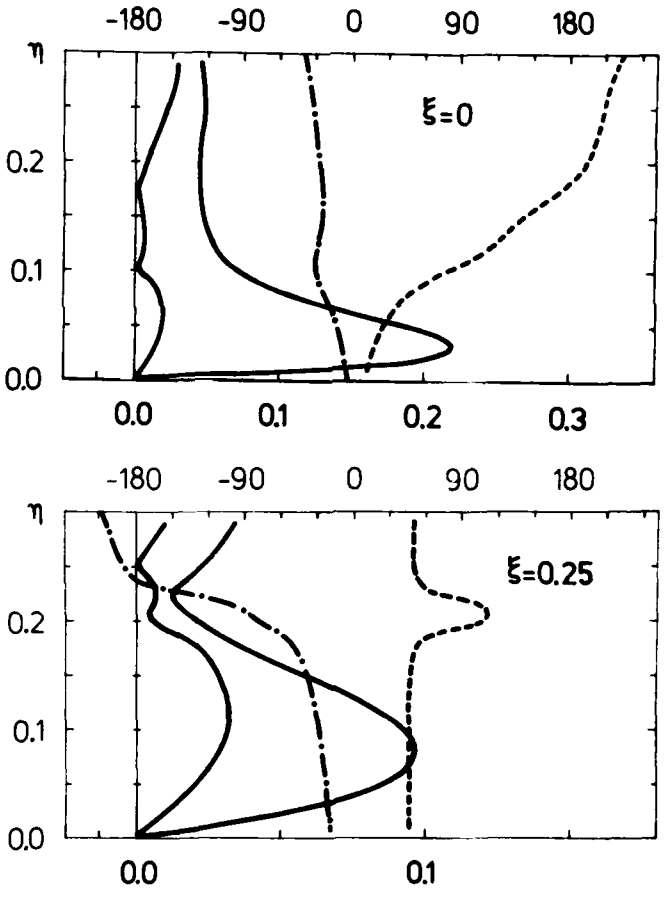

Fig. 2.7. The parameters of the elliptical wind hodograph as function of height for different values of distance from the coastline. The full lines give half the major and minor axes, (-·-·-): ϕ_o, (---): τ_o (fig. 2.6).
The amplitudes refer to the lower scale, and the phase angles ϕ_o, τ_o refer to the upper scale.

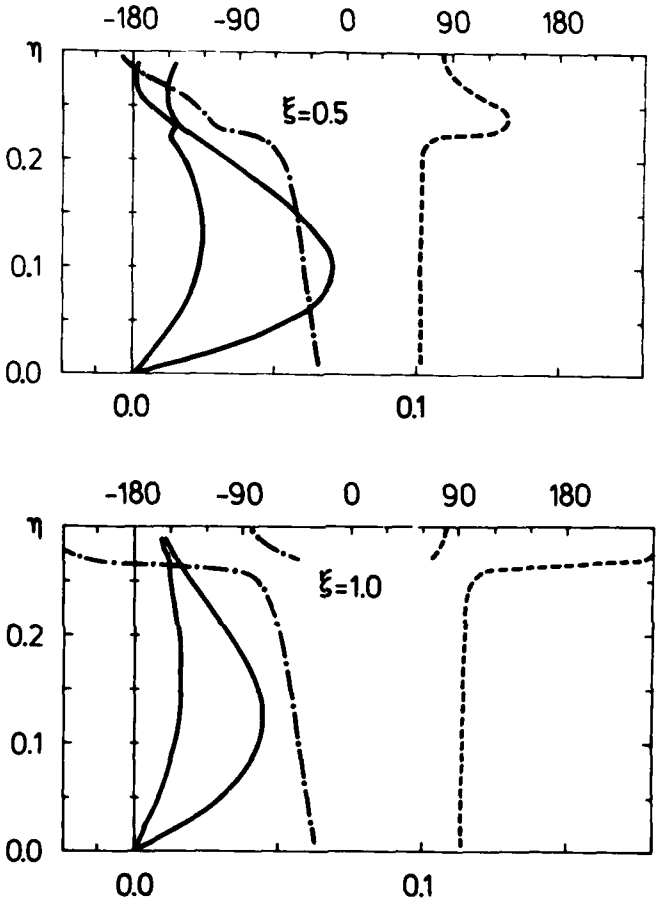

Fig. 2.7. continued

of the horizontal velocity vector at different heights above the coast are given by $|u(\eta)|\cos(\tau+\phi_u(\eta))$, $|v(\eta)|\cos(\tau+\phi_v(\eta))$ where the amplitude and phase functions corresponds to the functions for two components. The hodograph is an ellipse with parameters depending on height and distance from the coast, and the behaviour of the horizontal wind vector can therefore be characterized by the parameters of this ellipse as shown in Fig. 2.6, where vertical profiles of the maximum and minimum magnitude of the wind vector, together with the phase lag of the maximum magnitude relative to the maximum land surface temperature, and the angle between the maximum wind vector and the gradient of sur-

face temperature are plotted for different distances from the coast.

2.6. Effects of horizontal advection

The above results were obtained by assuming the flow to be forced solely by a temperature perturbation at the surface. A crude estimate of the effect of an overlying advective velocity can be obtained assuming the basic state velocity to be constant. This also requires that it is permissible to neglect the wind-shear near the surface in the basic state velocity; furthermore, the neglect of the "self advection" by the perturbation u in comparison with the advection by the background velocity U means $u \ll U$. The solution in this case can be obtained directly as above by noting that the same system of equations and boundary conditions are recovered in the coordinate system moving along with the velocity U in the x-direction. To be more specific, it is easily seen by performing the Galilean transformations, that the solution in the original (non-moving) system can be written for each wavenumber in real notation as:

$$\mathrm{Re}\{u(k,\eta)\ \frac{\cos k\,\xi}{k}\ \exp(-i\tau)\} \equiv u^{(k)} =$$

$$\frac{1}{2}\{A^{(k)}_{\tilde{\omega}+\omega}(z/H_{\tilde{\omega}+\omega})\ \cos(k\xi+\tau+\phi^{(k)}_{\tilde{\omega}+\omega}(z/H_{\tilde{\omega}+\omega}))$$

$$+\ A^{(k)}_{\tilde{\omega}-\omega}(z/H_{\tilde{\omega}-\omega})\ \cos(k\xi-\tau+\phi^{(k)}_{\tilde{\omega}-\omega}(z/H_{\tilde{\omega}-\omega}))\} \qquad (2.35)$$

where $A^{(k)}_m(\eta)$ is the amplitude of the u-component corresponding to the wavenumber k, and the forcing frequency ω in the case of U=0. Similarly, $\phi^{(k)}_\omega(\eta)$ is the corresponding phase function, H_ω is the depth scale corresponding to the frequency ω ($H_\omega = \sqrt{K/\omega}$, and $\tilde{\omega}$ is the "induced" forcing frequency = k U/L. The results from the preceding sections are recovered for $\tilde{\omega} = 0$. Equation (2.35) enables us to identify two limiting cases corresponding to small and large scales considered above. Assuming

$\tilde{\omega} >> \omega$ corresponding to strong advection or $k\,U/L >> \omega$, Eq. (2.35) becomes

$$u^{(k)} \cong A_{\tilde{\omega}}^{(k)}(z/H_{\tilde{\omega}}) \cos(k\xi+\phi_{\tilde{\omega}}^{(k)}(z/H_{\tilde{\omega}})) \cos(\tau) \tag{2.36}$$

The scaling introduced in the preceding sections shows that

$$A_{\tilde{\omega}}^{(k)} = \frac{1}{k} A(\tilde{k},\tilde{\eta}) = \frac{1}{k} A\left(k\left(\frac{\omega}{\tilde{\omega}}\right)^{3/2},\ \eta\left(\frac{\tilde{\omega}}{\omega}\right)^{1/2}\right) \tag{2.37}$$

On introducing $\tilde{\omega}$ into Eq. (2.37) we obtain

$$A_{\omega}^{(k)} = \frac{1}{k} A\left(k_U\sqrt{\frac{k_U}{k}},\ \eta\sqrt{\frac{k}{k_U}}\right) \tag{2.38}$$

where $k_U = N/U\ \sqrt{K/\omega}$. Similarly the phase function can be written as

$$\phi_{\tilde{\omega}} = \phi_{\omega}(\tilde{k},\tilde{\eta}) = \phi_{\omega}\left(k_U\sqrt{\frac{k_U}{k}},\ \eta\sqrt{\frac{k}{k_U}}\right) \tag{2.39}$$

The assumption $\tilde{\omega} >> \omega$ in connection with diurnal forcing, where $f_s \approx 1$ means that $\tilde{\omega} >> f$, and rotation can be neglected. The wavenumber k_U defines a lower limit above which advection by U dominates and $\tilde{\omega} >> \omega$ is equivalent to $k >> k_U$. With this assumption the first argument in the amplitude function in Eq. (2.38) is small compared to one and the value of A can be found by solving for small wavenumbers as in the previous section but for $f_s = 0$.

$$A_{\tilde{\omega}} = \frac{1}{k} \exp\left[-\eta\sqrt{\frac{k}{2k_U}}\right] \sin\left[\frac{1}{2}\, k_U\, \eta\right]. \tag{2.40}$$

For the phase function we obtain

$$\phi_{\tilde{\omega}}^{(k)} = \frac{\pi}{2} - \eta\sqrt{\frac{k}{2k_U}} \tag{2.41}$$

Using these two expressions valid for $k >> k_U$ in Eq. (2.36) the result can be written:

$$u^{(k)} = \frac{1}{k} \exp\left[-\eta\sqrt{\frac{k}{2k_U}}\right] \sin\left[\frac{1}{2} k_U \eta\right] \sin\left[-k\xi+\eta\sqrt{\frac{k}{2k_U}}\right] \cos\tau \qquad (2.42)$$

Comparing with the expression obtained for large wavenumbers in the case of zero advection, Eq. (2.24), the depth scale is decreased in the presence of advection by essentially $k^{1/6}\ k_U^{1/2} \propto \sqrt{U}$. For large scales $\tilde{\omega} << \omega$ and advection have only little effect, and noting that $\phi_\omega = -\phi_{-\omega}$ and $A_\omega = A_{-\omega}$ we can write Eq. (2.35) as:

$$u^{(k)} = A_\omega^{(k)}(\eta) \cos(k\xi) \cos(\tau+\phi_\omega^{(k)}(\eta)) \ . \qquad (2.43)$$

for $k << k_U$. This is identical to the expression valid in the case U = 0 as expected. For intermediate scales $k \approx k_U$ no simple relation exists between the two terms on the right in Eq. (2.35) and each wavenumber must be treated separately. A special case appears as $k = k_U$ equivalent to $\tilde{\omega}=\omega$, where the last term becomes undefined. This "resonance" case corresponds (in the case of zero advection) to steady convection where the diffusive depth scale becomes infinite. The proper depth scale will be the Ekman depth $= \sqrt{K/f}$ in this case. Replacing ω by f in the scaling relations, Eq. (2.5), the set of equations corresponding to Eq.(2.13) becomes

$$\begin{aligned}
&\frac{\partial^2 u}{\partial \eta'^2} + v' = k'p' \\
&\frac{\partial^2 v'}{\partial \eta'^2} - u' = 0 \\
&\frac{\partial^2 \theta}{\partial \eta'^2} - w' = 0 \qquad (2.44) \\
&\frac{\partial \eta'}{\partial \eta'} = \theta' \\
&- k'u' + \frac{\partial w'}{\partial \eta'}
\end{aligned}$$

The equation for the perturbations pressure p becomes:

$$\frac{\partial^2}{\partial \eta'^2}\left[\frac{\partial^6}{\partial \eta'^6} + \frac{\partial^2}{\partial \gamma'^2} - k'^2\right]p' = 0 \qquad (2.45)$$

(The prime on all quantities indicates the deviation in scaling). As above, the solution for the flow can be obtained from Eq. (2.44) and the boundary conditions with the exception that the boundary conditions at infinity for v, θ, and p cannot be satisfied because of the appearance of a linear solution in Eq. (244). Physically this particular solution corresponds to a temperature perturbation independent of height with associated linear pressure variation and linear geostrophic wind, which because of the orientation of the coordinate system appears only in the v-component. The depth of the cross isobar flow u is determined by the Ekman depth.

The effect of a basic state velocity will be pronounced if k_U is not large compared to one ($U \gtrsim N\sqrt{k/\omega}$): Taking reasonable values for the parameters viz. $N = 0.01\ s^{-1}$, $K = 1\ m^2s^{-1}$, $\omega = 0.7 \cdot 10^{-4}\ s^{-1}$ ($= 1\ day^{-1}$) then the requirement is $U \gtrsim 1\ ms^{-1}$. The smaller scales are attenuated at all levels and phase shifted in the direction determined by the sign of U. In the above arguments we have assumed U to be positive; negative U yields by symmetry identical results exept that $-\xi$ should be replaced for ξ in Eq. (2.35).

It is well known that the inland penetration of the sea-breeze is lessened or prevented when a synoptic scale off-shore wind is present. Empirical predictions of the occurrence of sea-breezes have been based on the negative correlation of the synoptically driven wind and sea-breeze occurrence (Biggs and Graves, 1962). Based on a linear model Walsh (1974) finds that this model lends theoretical support to the empirical relations. His analysis is based on the assumption that the requirement for the occurrence of sea-breeze is $u_{max} \geq |U|$ where u_{max} is the maximum velocity predicted by the linear model. Clearly this requirement is inconsistent with the linearization of the advection terms. In addition, large amplitudes of the surface heating

necessary to meet the above requirement for realistic values of the windspeed U and the background stratification N^2 leads to violation of the linearization of the adiabatic heating term in the thermodynamic equation. The necessary assumption here is that the flow-induced perturbation of the stratification can be neglected. This means that the following relation must hold:

$$\Delta N^2 \approx \frac{\Delta\theta_o}{H}\frac{g}{\theta} = \Delta\theta_o \frac{g}{\theta}\sqrt{\frac{\omega}{K}} << N^2 \qquad (2.46)$$

The analysis by Walsh (1974) is based on a particular choice for N since he did not anticipate the possibility of scaling the problem such that only $f_s = f/\omega$ appears as an external parameter as shown in the present analysis. Using his results of the maximum value u_{max} in the linear model as function of a background velocity it is possible to obtain u_{max} as function of the wavenumber k_U as shown in Fig. 2.7. The results are well reproduced by the relation

$$U_{max}^{(U)} = U_{max}^{(0)} \left(1 - \exp(-\alpha k_U)\right) \qquad (2.47)$$

with $\alpha = 0.65$. Eq. (2.47) reproduces the asymptotic behaviour for u_{max} as $U \to 0$ ($k_U \to \infty$) and also as $U \to \infty$ ($k_U \to 0$): $u_{max} \to 0$ as $1/U$. At moderate values of k_U Fig. 2.7 shows Eq. (2.47) to reproduce the model results adequately.

Returning to the requirement Eq. (2.46) in connection with the assumption $\tilde{u}_{max} \gtrsim U$ (where "~" denotes dimensional quantity):

$$U \leq \frac{g}{N}\frac{\Delta\theta_o}{\theta} U_{max}^{(U)} = \frac{g}{N}\frac{\Delta\theta_o}{\theta} U_{max}^{(0)} \left(1-\exp(-\alpha k_U)\right) \qquad (2.48)$$

for $k_U << 1$ we obtain

$$U \leq \frac{\Delta N^2}{N^2} N\sqrt{\frac{K}{\omega}}\, u_{max}^{(0)}\, \alpha k_U \text{ , or}$$

$$1 \leq \left(\frac{\Delta N}{N}\right)^2 k_U^2\, u_{max}^{(0)} \cdot \alpha \qquad (2.49)$$

since our linearization requires $\Delta N/N << 1$ and $u_{max}\ \alpha \approx 0.14$ clearly $\tilde{u}_{max} \approx U$ strongly violates the linearization for U large. Ignoring for a moment this objection Eq. (2.49) can be rewritten as

$$\Delta\theta_o \geq \frac{\Theta}{0.14\ g}\sqrt{\frac{\omega}{K}}\,U^2 \qquad (2.50)$$

This relation is similar to the expression found by Walsh (1974) and has the form of the empirical relation found by Biggs and Graves (1962); furthermore, as shown by Walsh the constant in Eq. (2.50) is very nearly the empirical constant when a realistic value for K is inserted*).

In view of the simplicity of the linear model and the objections raised above it is surprising that the model agrees with observational data with an accuracy as good as that with which the parameters in the model can be determined. The appropriate mean diffusivity K cannot be estimated independently better than as an order of magnitude estimate; also the relation between the gradient wind, which enters in the empirical relation similar to Eq. (2.49) in place of U, and the "bulk" background velocity U used in the model must include a geometrical factor of order one to account for the effect of windshear in the boundary layer.

In the case of zero background velocity the linear model predicts the magnitude of the maximum cross isobar flow $\tilde{u}_{max}$ to be proportional to the amplitude of the land surface temperature. The scaled profile of u obtained from the linear model by solving for all wavenumbers and integrating (Eq. 2.8) is shown in Fig. 2.8 for different values of $\tau = \omega t$. The profile corresponding

---

*) The numerical constant (≈ 0.14) in Eq. (2.49) differs from the constant found by Walsh (0.11) because of the fitting used here by the expression Eq. (2.46). Using (2.49) and the empirical coefficient yields $K = 8\ m^2 s^{-1}$.

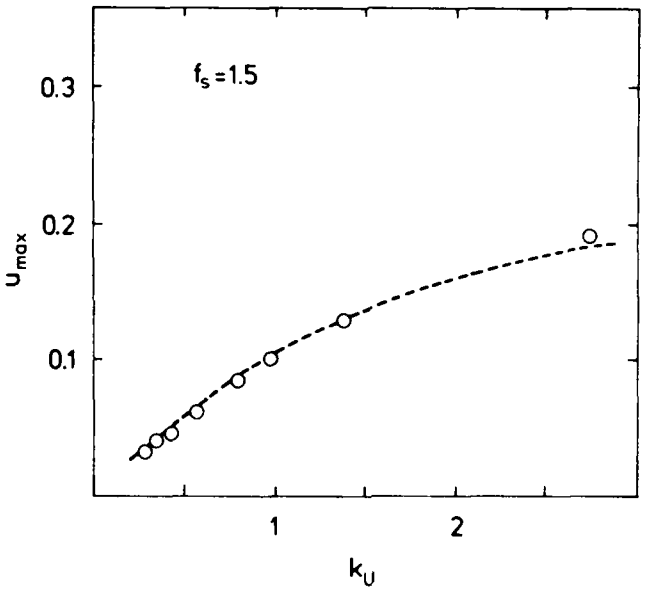

Fig. 2.8. The effect on the maximum value of the u-component of an background velocity U. $k_U=N/U\sqrt{K/\omega}$. (o): Results from rescaling data from Walsh(1974), (---): Eq.(2.47).

to τ = 0.15 corresponds to the profile when the largest value of u is found. The model estimate of $\tilde{u}_{max}$ is therefore

$$\tilde{u}^{(0)}_{max} = 0.22 \cdot \frac{g}{N} \cdot \frac{\Delta\theta_o}{\theta} \qquad (2.51)$$

where the superscript zero indicates zero advection. The numerical constant is valid only for the case of a step change in temperature across a straight coastline which is considered here, and also only valid for the particular choice of the nondimensional Coriolis parameter ($f_s = f/\omega = 1.5$) corresponding to diurnal forcing at mid latitudes. The strong dependence found above on the background velocity and the favorable comparison with empirical data suggest that a reasonable order of magnitude estimate of the maximum velocity taking into account the self-advection at finite values of $\Delta\theta_o$ can be obtained using Eq. (2.47), and assuming the effective advective component to be

proportional to $\tilde{u}_{max}$, viz U = a u_{max}, where a is a geometrical factor of order one. The proposed equation becomes

$$\tilde{u}_{max} = \frac{g}{N}\frac{\Delta\theta_o}{\theta} \cdot u_{max}^{(0)} \cdot (1-\exp(-\alpha k_U)) = \frac{N}{ak_U}\sqrt{\frac{K}{\omega}} \qquad (2.52)$$

where the last equality follows from the definition of k_U. Eq. (2.51) can be solved for k_U by iteration and $\tilde{u}_{max}$ is then determined by the last expression. From Eq. (2.50) it is clear that the linear result becomes questionable as $\Delta\theta_o$ increases and as stratification N^2 decreases. Using Eq. (2.52) in the limit $k_U << 1$ we obtain

$$\tilde{u}_{max} = \sqrt{\frac{\alpha}{a} g u_{max}^{(0)} \frac{\Delta\theta_o}{\theta}\sqrt{\frac{K}{\omega}}} \qquad (2.53)$$

where u_{max} = 0.22, α =0.65. Using a = α =0.65 and K = 5 $m^2\ s^{-1}$ yields

$$\tilde{u}_{max} = 24\ ms^{-1} \left(\frac{\Delta\theta_o}{\theta}\right)^{1/2} \qquad (2.54)$$

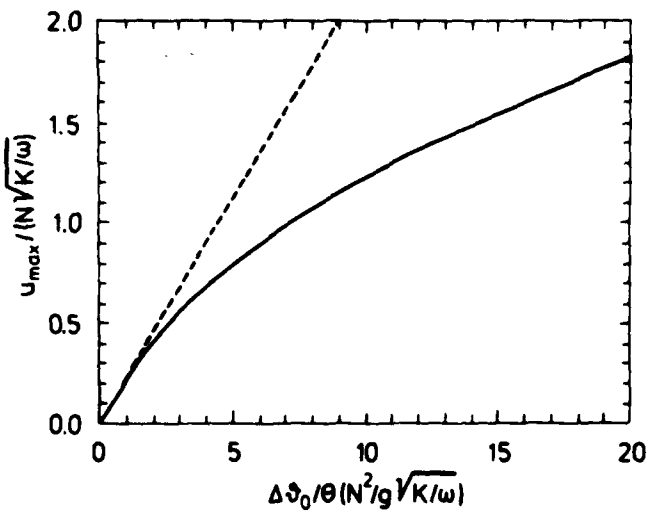

Fig. 2.9. (——): u_{max} from the self advection model from the solution of Eq. (2.52) with a=α=0.65. (---): Linear model.

Comparing Eq. (2.53) with (2.51) we see that the strong dependence on stratification in the linear model disappears and is replaced by a very weak dependence on the diffusivity K in (2.53). Equation (2.53) can be interpreted as a Froude number relationship:

$$Fr = \tilde{u}_{max} \left(gd \frac{\Delta\rho}{\rho_o} \right)^{-1/2} = 1.5 \qquad (2.55)$$

where d is the depthscale $\cong \sqrt{K/\omega}$, $\Delta\rho/\rho_o \cong \Delta\theta_o/\theta$, and we have used $a = \alpha = 0.65$. In studies of the sea-breeze front Simpson et al. (1977) have found that if d is the depth of the intruding (cold) sea air, $\tilde{u}_{max}$ is the rate of advance of the sea-breeze front and $\Delta\rho$ is the density difference between sea- and land air then $Fr \cong 0.7$. In our definition $\tilde{u}_{max}$ represents the maximum air-speed and comparing the two Froude numbers we find that they agree if the rate of advance of the sea-breeze front is 2.1 times slower than the maximum speed. This number agrees surprisingly well with what is found from observations. As an example Kimura and Eguchi (1978) find the average ratio to be 2.2 based on an average over 56 sea-breeze days observed from 13 surface stations in Japan. The maximum speed predicted from Eq. (2.54) can be likewise compared with observations; in the field study of the sea-breeze at the great lakes in the United States Keen and Lyons (1978) found a maximum onshore windspeed of 4.1 ms^{-1} at a height of 150 m above the shoreline, the temperature difference between land and sea was 8 K. Using this value Eq. (2.54) yields $\tilde{u}_{max} = 4.0$ ms^{-1}. Compare this, however, with the variability discussed in connection with the numerical simulations (Chapter 3).

2.7. Comparison with inviscid model

The result from the linear model for the cross isobar flow has already been discussed in the preceding section. The v-component at the coastline at low heights is much smaller than the u-component in magnitude, reflecting the influence of high wavenumbers where rotation is negligible. The hodograph of the hori-

zontal wind is an ellipse in all points because of the assumed periodicity. The assymetry observed for the land and sea breezes can partly be incorporated into the linear model by adding harmonic terms to simulate the typical diurnal land surface temperature. As discussed by Mak and Walsh (1976) this will account for only part of the assymmetry because a large part is caused by the diurnal variation of stratification and diffusivity which cannot be incorporated into the linear model. Because of the strong influence of the small scales on the magnitude of the maximum cross isobar component this quantity is to only a relatively small degree influenced by complicated initial conditions at the beginning of a sea-breeze day. A slowly varying synoptic scale u-component will act to modify the maximum breeze u-component as described above. The v-component, and also the u-component at higher levels, is dominated by larger scales where the Coriolis force is important and the initial conditions will likewise be important. At all points the wind vector exibits the expected clockwise turning (for $f > 0$).

Near the coastline very large gradients exist in the vertical velocity, which is antisymmetric across the coastline. The behaviour of w here is determined by the contribution from large wavenumbers for which advection becomes important even for small values of the forcing. As discussed in the previous section the u-field also is dominated by large wavenumbers near the coastline. Consequently, the detailed results from the linear model cannot be expected to apply to the land- and sea-breeze near the sea-breeze front. If we define the "inner region" in the circulation as the region where the non linear effects are important, then we can expect the linear dynamics to apply in the complementary "outer" region. The reason that such a division is meaningful is that we are dealing with a disturbance generated essentially at one point and propagating in a dispersive medium. The propagation of a disturbance in a stratified inviscid fluid is usually analysed in terms of internal gravity waves, and such an analysis applied to the sea breeze outer region was presented by Geisler and Bretherton (1968) who treated the problem as an initial-value problem by introducing the temperature distribution everywhere instantaneously. They introduced the term the sea-breeze fore-

runner as the disturbance being carried by the gravity waves and reaching points away from the coastline in advance of the sea-breeze proper. In their analysis rotation and diffusion were neglected, and they found in the simplest case where stratification is independent of height that the perturbation in $\tilde{u}$ can be expressed as $g/N(z/h,\tau)$ where h is the depth of the initially imposed temperature perturbation and $\tau = Nh\ t/x$. The connection to the linear harmonic model can be seen if h is interpreted as the diffusive depth scale $\sqrt{K/\omega}$. The dispersion relation for gravity waves in the system is given by (Pearson, 1973):

$$\omega^2 = f^2 + N^2k^2/m^2 \qquad (2.56)$$

when rotation is included. Neglecting rotation the horizontal phase and group speed for waves with vertical wavenumber m is $\omega/k = N/m$, and noting that all modes are excited simultaneously as the temperature contrast is imposed in the Geisler and Bretherton model, at any point away from the coastline a sequence of modes arrive with the largest vertical scales arriving first and eventually modes of smaller and smaller vertical wavelength arrive. In the periodic model three other mechanisms are in effect, firstly rotation is included, affecting the behaviour of the large scales; secondly, the periodic forcing means that the disturbance arriving at a point is a superposition of disturbances generated at different times with a strength given by the harmonic time variation; and thirdly, the effect of surface drag and the internal dissipation is to damp the different modes at different rates. The e-folding time on modes with vertical wavenumber m is of order $m^{-2}\ K^{-1}$ which for modes of vertical extent of $h = \sqrt{K/\omega} = m^{-1}$ becomes equal to $L = N/\omega\sqrt{K/\omega}$, which is the horizontal scale length in the periodic model. The largest perturbation in u occurs at the surface in the inviscid model where a slip-condition is assumed. Employing the scaling introduced for the periodic model, the result found by Geisler and Bretherton for $u(x,z,t)$ can be written as

$$u(\xi,n,\tau) = \frac{1}{\pi} \int_0^{\tau/\xi} \{1 - \cos y\} \cos[yn] \frac{dy}{y} \qquad (2.57)$$

where we have used Eq. (24) in the original paper and $h = \sqrt{K/\omega}$, $L = N/\omega\sqrt{K/\omega}$, etc. from the scaling used in the periodic model described above. It may seem confusing to introduce a forcing frequency ω and a diffusivity K when we are dealing with an inviscid model with steplike forcing, however it makes comparison with the periodic model easier, as will be apparent below. At the surface the result Eq. (2.57) can be written:

$$u(\xi,\tau,0) = \frac{1}{\pi} \sum_{n=1}^{\infty} (-1)^n \frac{(\tau/\xi)^{2n}}{2n \cdot 2n!} \qquad (2.58)$$

This function is shown in Fig. 2.10. It can be seen that the maximum value found in the periodic model ($\cong 0.22$) is exceeded already at values of $\tau/\xi \sim 2$, suggesting the importance of diffusion of momentum. Introducing into the model an internal dissipation of the waves leads to the appearance of the term

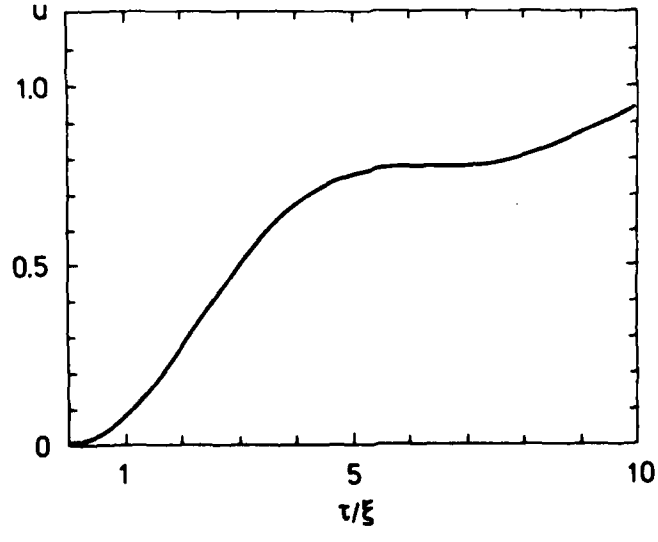

Fig. 2.10. The u-component at the surface from the inviscid model of Geisler and Bretherton (Eq. 2.58).

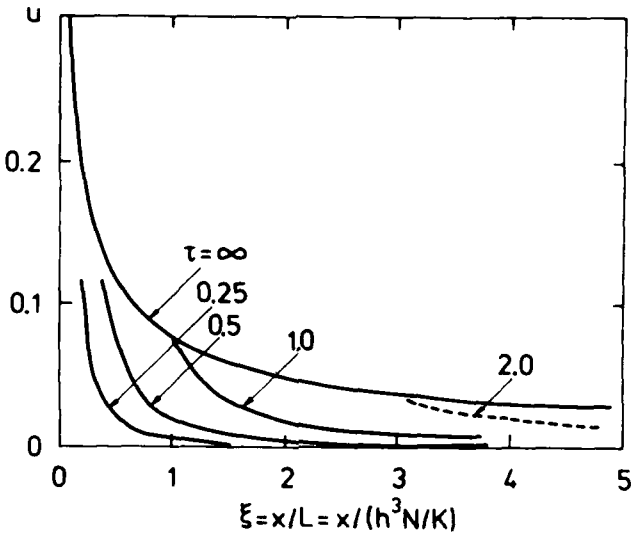

Fig. 2.11. The u-component in the Geisler and Bretherton model, in the case where internal dissipation is included. Numbers on the curves refer to the time τ.

$\exp(-y^3\,\xi)$ inside the integral in Eq. (2.57), as also discussed in the paper by Geisler and Bretherton. The effect of this term is to give a sharp cutoff at $y = \xi^{-1/3}$. The maximum value of u now becomes approximately equal to Eq. (2.58) with $\xi^{-1/3}$ replaced for τ/ξ. The result is shown in Fig. 2.11. The curve labelled $\tau = \infty$ gives the asymptotic value of u_{max}, and the curves labelled with different valves of τ gives $u_{max}\,(\xi,\tau,0)$. These curves follow the asymptotic curve up to the point where the diffusive cutoff occurs at $\xi = \tau^{3/2}$. Note that we can eliminate the dependence on ω by substituting $\omega = K/h^2$ with $\xi = x/(Nh^3/K)$ and $\tau = t/(h^2/K)$. The maximum u-component in the periodic model is shown together with the $\tau = \infty$ curve from Fig. 2.11 in Fig. 2.12. The large difference is a consequence of the mechanisms active in the periodically forced model: the surface drag which becomes infinite at $\xi = 0$ (cf. Eq. 2.24), the finite temperature gradient above the surface at $\xi = 0$ resulting from the action of the vertical velocity in the thermodynamic equation, and the periodic forcing. The horizontal temperature distribution in the periodic model is illustrated in Fig. 2.13 for

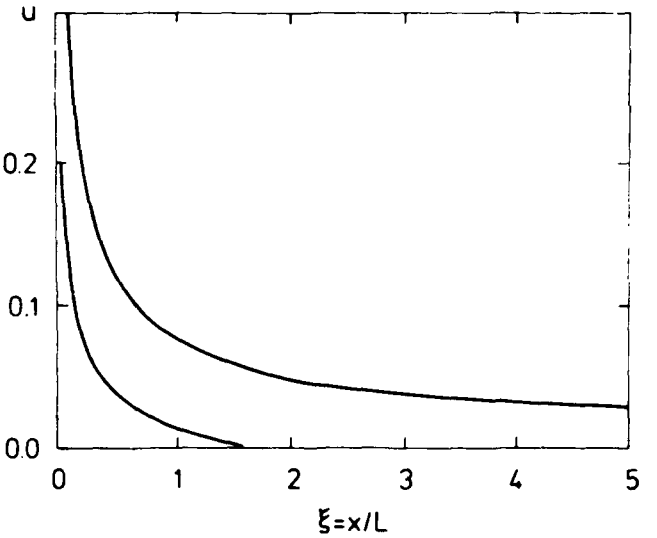

Fig. 2.12. The maximum u-component as function of distance from the coast for the periodic model (lower curve), and the Geisler and Bretherton model with internal dissipation (curve marked $\tau=\infty$ on the previous figure).

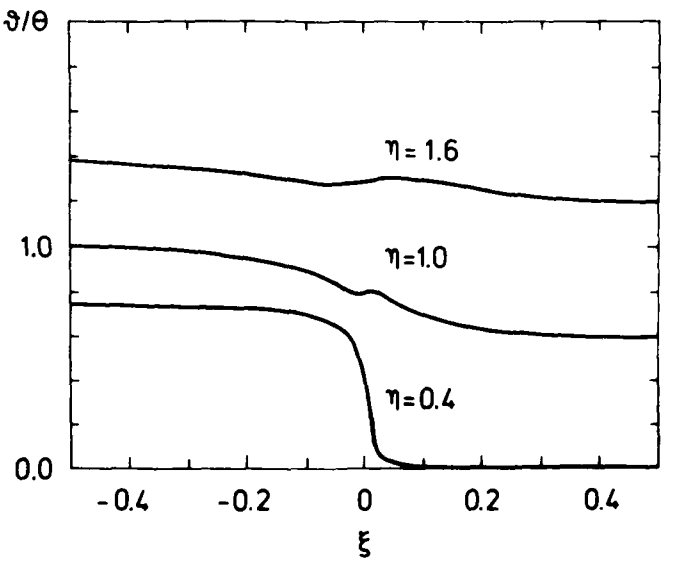

Fig. 2.13. The temperature perturbation at the time of maximum perturbation at the surface in the periodic model for different values of height. (The zero point for θ has been chosen arbitrarily for each curve.)

different values of η at the time of maximum in the surface temperature difference. The curves demonstrate the difference in the forcing function between the viscous periodic model and the model by Geisler and Bretherton where the initial forcing is a stepfunction of amplitude equal to one up to the height $\eta = 1$ and zero above. It should be noted that the vertically integrated temperature perturbation far away from the coast is identical in the two models. The effect of surface drag can be incorporated into the model of Geisler and Bretherton, but only in a crude way, as discussed in their paper. In the periodic model treated sofar the atmosphere is modelled as one layer of constant diffusivity and basic state stratification. This is obviously a gross oversimplification and even in the outer part of the flow large deviations in the structure must be expected, in general, because of temporal and spatial structure in the basic state parameters. The most obvious inhomogeneity is between the boundary layers developed over sea and land because of the difference in surface heating. In the outer part one may expect the conditions over land and sea to be uncoupled and the inviscid model by Geisler and Bretherton (and the periodically forced inviscid model described by Kimura and Eguchi (1978)) could apply in particular over the sea, whereas for conditions over land turbulent diffusion must be incorporated. Over land there may be no outer region in the boundary layer but only above it because as one moves inland from the coast in the convective boundary layer the stratification vanishes except near the surface where it is superadiabatic in the sea-breeze situation. As a consequence, the phase speed of gravity waves tend to zero and the linear dynamics breaks down. In the periodic viscous model the determination of the proper diffusivity presents a problem, since it has a large dependency on height. The values used in the example above are proper only for near surface conditions. The stratification enters only in the thermodynamic equation through the adiabatic cooling term $w \cdot \Gamma$ which is unimportant near the surface but is responsible for the cooling over land/heating over the sea at heights in the upper part of the boundary layer over land and above, generating high pressure over land and the return flow. The stratification parameter N in the linear model should therefore properly be a characteristic

value for the upper boundary layer including the (possible) inversion and the stratification above. With an inversion on top of a mixed layer both the turbulent diffusivity and the stratification depends on height, and the velocity and temperature profiles will deviate from the profiles found in the simple model. The effect of an elevated inversion layer on the profiles in the framework of the linearized periodically forced model is discussed in the next section.

2.8. Vertical variation of diffusivity and stratification

In real boundary layers the diffusivity of heat and momentum are typically functions of height through the dependence of the mean flow structure and the stratification. The inclusion of a height-dependent diffusivity and stratification in the linearized model leads to an eight-order differential equation with non-constant coefficients, and no simple solutions exist in general. Semi analytical solutions can be obtained, however, if the parameters can be assumed to be piecewise constant. For each layer in which K and N are constant the solution is identical to the solutions considered above except for the boundary conditions. The total solution is obtained by applying matching conditions at the interfaces between layers in addition to the boundary conditions at the surface and at infinity. The matching conditions are that all fields ($\tilde{u}$, $\tilde{v}$, $\tilde{w}$, $\tilde{\theta}$ and $\tilde{p}$) and the fluxes of heat and momentum ($K\,\partial\tilde{u}/\partial z$, $K\,\partial\tilde{v}/\partial z$, $K\,\partial\tilde{\theta}\,\partial z$) are continuous across the interfaces. Subdividing into N homogeneous layers gives (N-1) interfaces, and with our previous boundary conditions at the surface ($u=v=w=0$ and θ prescribed) together with the boundary conditions at infinity (four coefficients to exponentially increasing terms vanish) we have 8 N constraints to determine the 8 N coefficients in the pressure profile. The other fields are found from the pressure profile by applying the relations (2.22) for each layer. The large number of equations appearing when we subdivide prohibits any manageable explicit expressions for the vertical profiles, but since the coefficient matrix is sparse the solution is easily obtained numerically even in the case of many sublayers.

With discontinuties in the diffusivity K this means that the fields will not have a continuous first derivative across the interfaces; note, however, that the first derivative of the vertical velocity and the pressure are continuous by virtue of the matching conditions together with the continuity equation and the hydrostatic equation, respectively. The matching conditions ensure non-singular behaviour of all terms in the dynamical equations when applied across interfaces.

With this model we can simulate the effect of an elevated inversion layer by subdividing into 3 layers. If the height of the inversion base is larger than the diffusive scale height in the lower layer ($=\sqrt{K_1/\omega}$) we must expect the scaling Eqs. (2.5) to be applicable but with the flow modified by the inversion. If the inversion is at a height lower than this scale height then no unique scaling exists and the structure and strength of the flow is a function of the basic state parameters in all three layers. If, on the other hand, the inversion base is at a height much larger than the scale height the effect of the inversion is negnegligible.

For scaling the additional non-dimensional parameters the parameters in the lowest layer are used. This the height of the inversion base, inversion thickness, the scale heights and the scale lengths in the two upper layers. The proper diffusivity for each layer is strongly dependent on the stratification and a convective boundary layer is generally capped by an inversion layer effectively reducing diffusive transport above the inversion. With horizontal homogeneous conditions the inversion layer is formed by the entrainment process at the top of the boundary layer. The strength will depend on the stratification above the inversion, the rate of surface heating, and possible subsidence on the synoptic scale. In the sea-breeze situation conditions are complicated by the inhomogeneity across the coastline, the effect on stratification by the vertical motions generated by the sea-breeze itself and horizontal advection. These complications cannot adequately be incorporated into the linear model, and presumably they can be handled only numerically. In spite of this it is of interest to study the effect of an inversion layer

on the flow in the linear model since the linear dynamics still apply in the circulation locally with the possible exception of the region near the sea-breeze front and the coastline. With essentially vanishing diffusivity above the inversion the depth scale of the flow becomes very small and the flow in the boundary layer will be influenced only by the thermal stratification up to a height immidiately above the inversion base. This means that the effect of an inversion in the framework of the linearized model can be modelled using only two layers.

The maximum magnitude of the two-level wind vector is shown as function of the ratio of the Brunt-Väisäla frequencies for different heights of the inversion base on Figs. 2.14a-c. The depth scale in the upper layer is set to 0.1 times the depth scale in

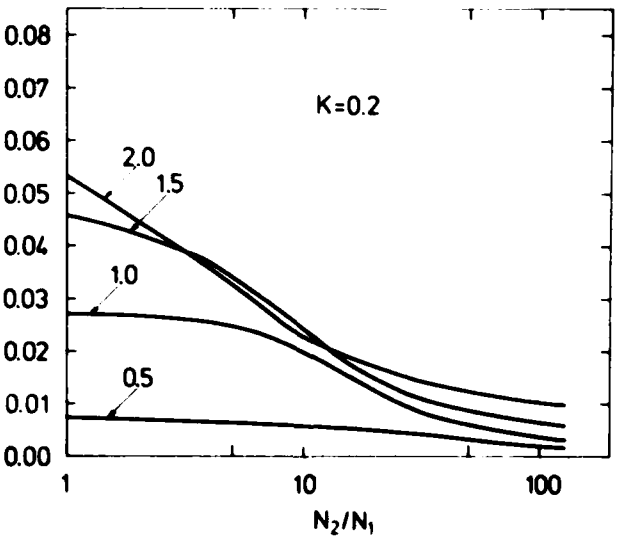

Fig. 2.14. Maximum value of the low level speed as function of the ratio of the values for N in the two layers. Values given on the curves refer to the height of the lower layer (inversion height) scaled with parameters pertaining to the lower layer. K on the figures gives the wavenumber k. (See text).

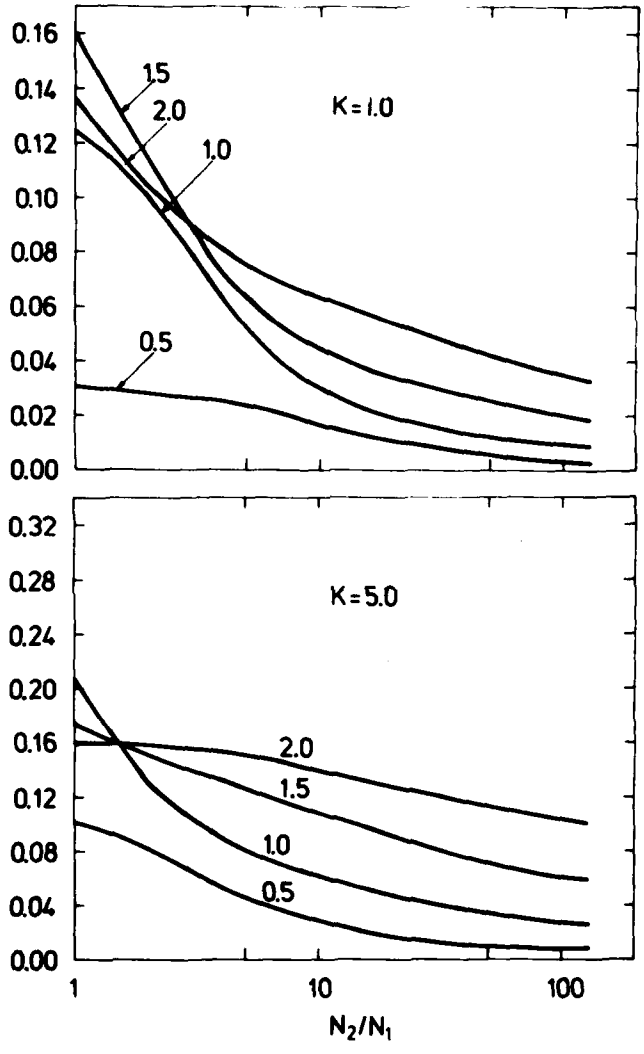

Fig. 2.14. continued

the lower layer corresponding to a decrease of the diffusivity by a factor of 100 across the inversion base. This value is somewhat arbitrary, but using larger values of this ratio results in only very small changes in the maximum low-level wind speed. As expected from the discussion above, however, the depth of the flow above the inversion base is reduced as the depth scale is decreased. For all wavenumbers the wind speed is strongly influ-

enced by the reduced vertical mixing even in the absence of temperature inversion. The values for the homogeneous case ($h = \infty$) are close to the values for $h = 2$ and there occurs obviously an "overshoot" for values of h comparable to one. For larger ratios of the stratification the wind speed decreases toward an asymptotic value determined by the inversion height, the flow becomes confined to the lower layer except for a thin layer with a strong return flow in the inversion layer. The phase angle (τ_0 on Fig. 2.6) decreases as the inversion strength is increased and with a strong low level inversion $\tau_0 \sim 0$ for all wavenumbers, the angle ϕ_0 also tends to zero for strong inversions. This is not surprising in view of the discussion in section 2.7 and the results in section 2.4; the stratification is most important in the dynamics near $n = 1$ (in the homogeneous case), whereas the largest effect of diffusion is near the surface; consequently a two-layer model with an inversion layer at $n \approx 1$ must dynamically become similar to the one-layer model for large wavenumbers. We have used the parameters in the lowest layer for scaling, and if the "effective" stratification increases with the strength of the inversion, then for any wavenumber ($= L_1/\ell$, where ℓ is the physical wavelength and L_1 is the scale length in the lower layer $\propto N_1$) the "effective" wavenumber influenced by the much larger length scale L_2 above the inversion base must be larger than the wavenumber itself. Figure 3.2 shows windprofiles for the more complicated situation where we have employed several layers simulating a parabolic diffusivity profile and a jump in the Brunt-Väisälä frequency at the top of the layer of strong mixing. The increase of the diffusivity with height near the ground tends to concentrate a strong windshear near the ground to lower the level of maximum wind speed compared to the homogeneous case. the return flow is concentrated near the top of the layer with strong mixing, as expected from the discussion above.

In connection with an inversion layer with an effective decoupling of the horizontal wind a synoptic pressure gradient can give rise to a strong wind shear across the inversion, and the role of horizontal advection by such a basic state wind velocity is complicated by the different advection rates acting on the

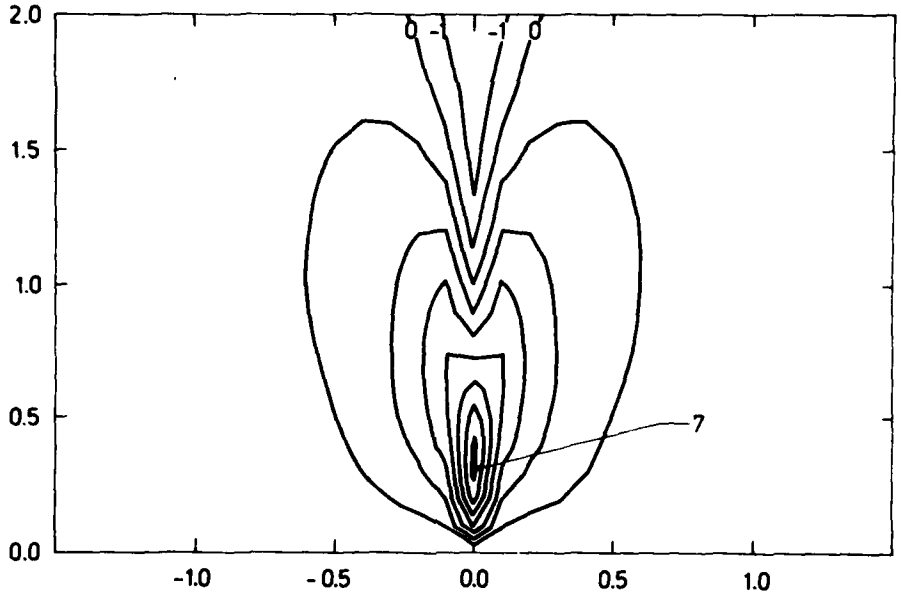

Fig. 2.15a. Contour plot of the u-component at the time of maximum surface temperature perturbation as function of ξ (abcissa) and η (ordinate). Contour interval is 0.025. (Max value is $7 \cdot 0.025 = 0.18$).

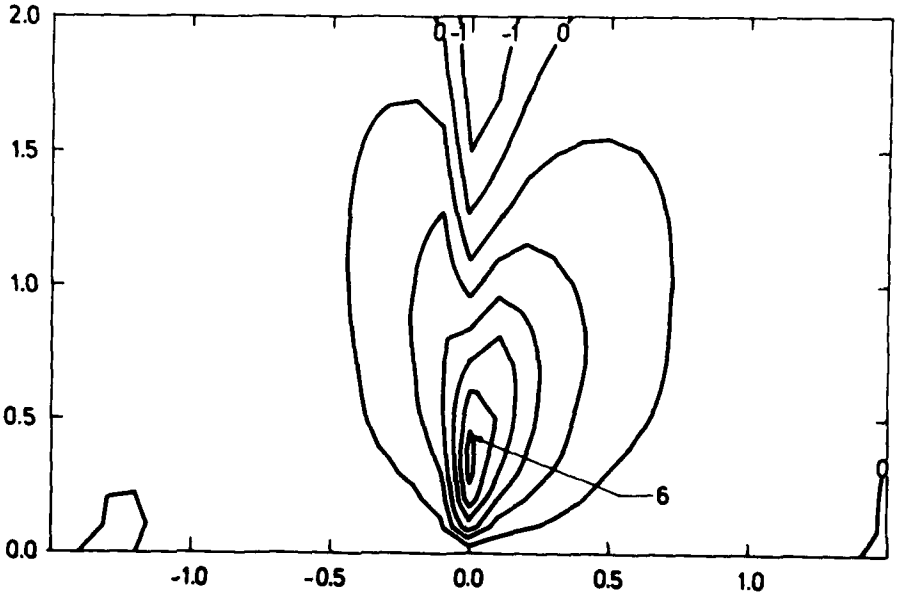

Fig. 2.15b. As fig. 2.15a, but for the case with background velocity U with $k_U=4$.

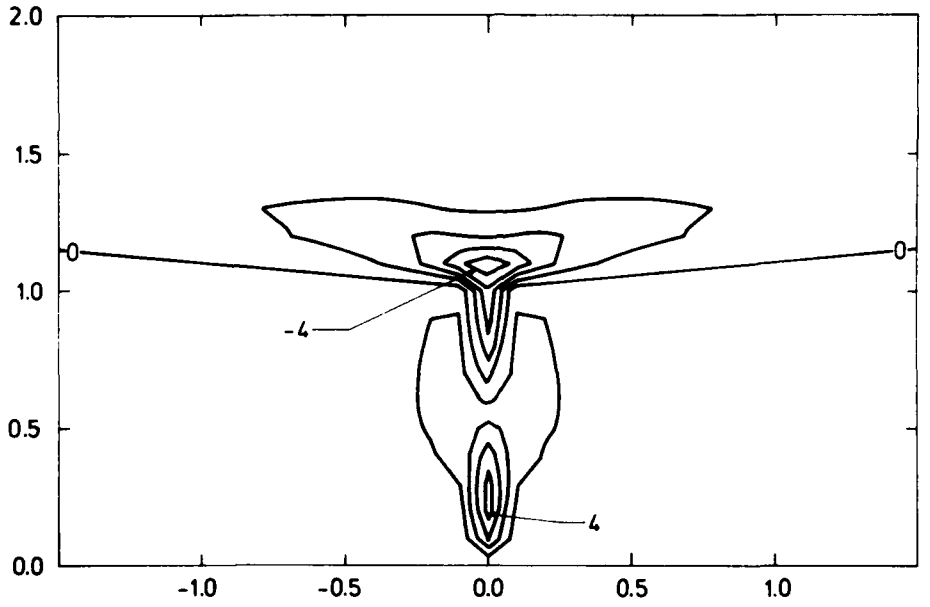

Fig. 2.16a. As fig. 2.15a, but in the case of a two layer structure (inversion) with N_2 in the layer above n=1 given as $N_2=100^{*}N_1$, and $K_2=0.01^{*}K_1$. Scaling with lower layer parameters.

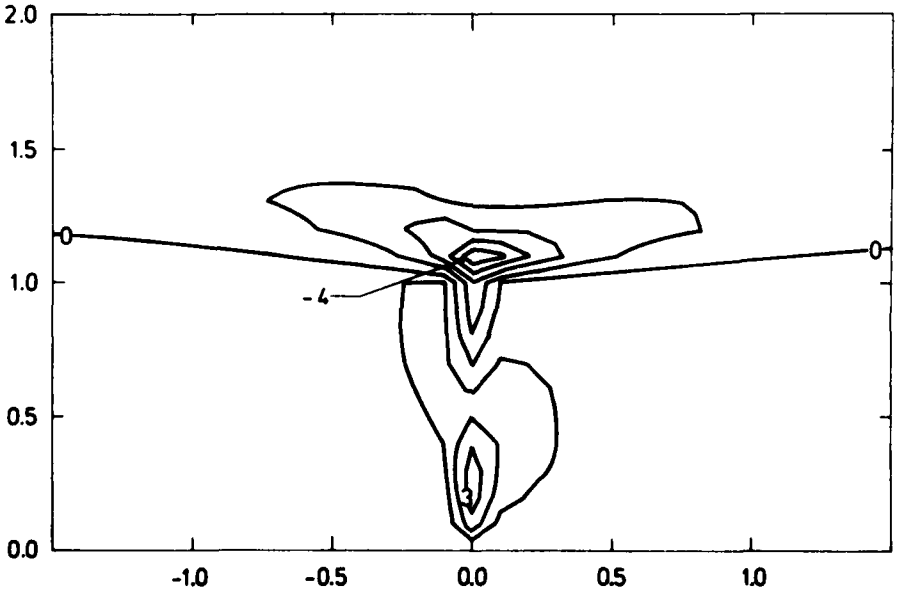

Fig. 2.16b. As fig. 2.16a, but with a background U with $k_U=4$ in both layers.

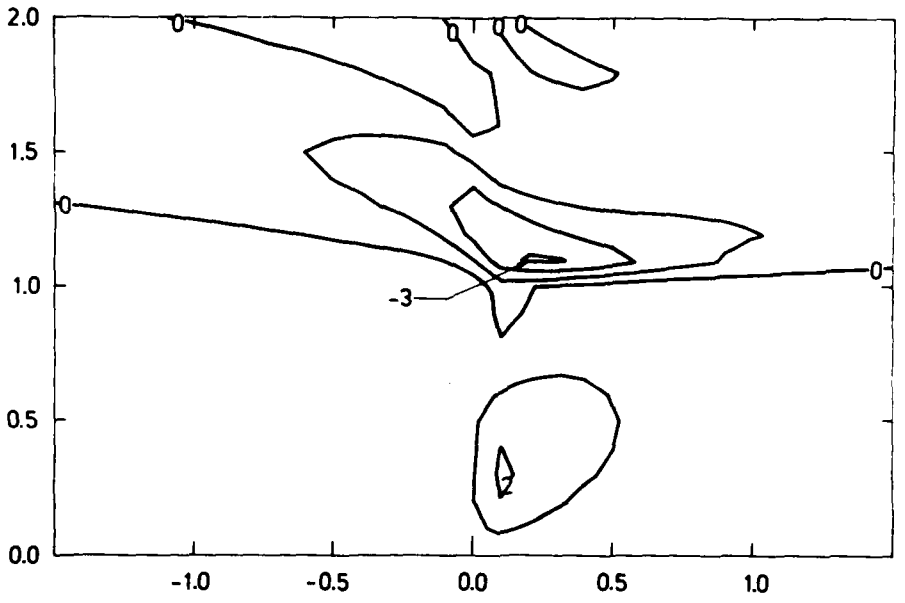

Fig. 2.16c. As fig. 2.16b, but with k_U=1.

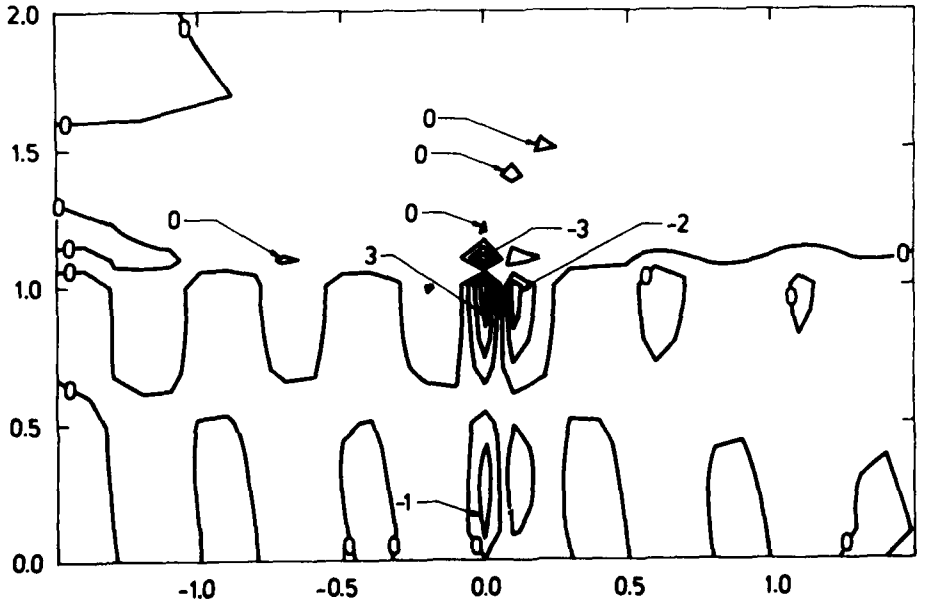

Fig. 2.17. As fig. 2.16b, but with k_U=4 in the lower layer, and k_U=-4 in the upper layer.

flow in the mixed layer and on the return flow near the inversion. In consistency with the treatment of a constant horizontal basic state velocity (section 2.6) and with the layered model treated here, different basic state velocities can be assigned to each layer to simulate this situation. For the two-layer model including windshear at the inversion results are shown on Fig. 2.16 for the cross isobar flow at the time of maximum surface temperature.

The effect of the inversion in concentrating the return flow and reducing the low level wind speed is apparent from these figures; the effect of a constant basic state velocity is qualitatively the same with and without the inversion. At the same distance inland the windspeed actually increases with increasing basic state velocity (decreasing k_U) because the maximum is displaced away from the coast in the direction of the wind. The maximum is decreased, however, as discussd in section 2.6.

The effect of different basic state velocity in the two layers is to displace the points of maximum low-level inflow and maximum return flow in the inversion layer away from each other in the horizontal. With larger shears the situation changes and disturbances generated in the shear layer appear equivalent to the unstable gravity waves which are generated at the interface between two homogeneous layers of different density and with a velocity jump across the interface (see, e.g. Gossard and Hooke, 1975). The stability analysis is complicated in the case treated here by the surface boundary conditions and the diffusivity in the two layers. In the model considered where all fields are assumed harmonic in time with frequency ω, and where θ is tied at the surface, these waves appear as finite disturbances which are amplified with increasing shear. This is obviously a model artifact and their structure in the real atmosphere cannot be analysed in the framework of this simple model. Waves are often observed in connection with the nocturnal boundary layer where they may form intermittently when strong shear is present. In the laboratory experiments by Britter and Simpson (1978) such waves are found behind the sea-breeze head on top of the layer

of protruding sea air simulated by a gravity current of a dense fluid undercutting a lighter fluid.

2.9. Circular island

In the previous sections we have considered the two-dimensional problem of flow across a straight coastline. In cases where the coastline is curved the flow will be subject to imposed divergence or convergence which in turn will induce vertical motions and pressure adjustments. Because of the 1/N dependence of horizontal velocity which is coupled to the thermodynamic equation through the adiabatic tooling term $w\Gamma$, the expected effect of increased convergence/divergence is to decrease the magnitude of horizontal velocity compared to the case of the straight coastline.

The effect can be studied by solving the linear flow problem for the case of a heated circular island. Assuming angular symmetry, and interpreting and horizontal coordinate ξ as the (scaled) radial distance from the island center, the dynamical equations Eq. (2.6) are unaltered except for the continuity equation, which in cylindrical coordinated becomes:

$$\frac{u}{\xi} + \frac{\partial u}{\partial \xi} + \frac{\partial w}{\partial \eta} = 0 \qquad (2.59)$$

The Fourier representation is impractical in this case and the fields are instead expanded in a Fourier-Bessel series:

$$u(\xi,\eta) = -\sum_{\ell=1}^{\infty} u(\ell,\eta)\, J_1(\sigma_\ell \xi/D) \;;\quad 0 \leq \xi < D \qquad (2.60)$$

for the radial velocity component u and similarly for the tangential velocity v. The temperature, vertical velocity, and pressure are given the expansion, viz for θ:

$$\theta(\xi,\eta) = \sum_{\ell=1}^{\infty} \theta(\ell,\eta)\, J_0(\sigma_\ell \xi/D) \;;\quad 0 \leq \xi < D \qquad (2.61)$$

The functions J_o and J_1 are Bessel functions of zero'th and first order, respectively, and σ_ℓ is the ℓ'th zero of J_o. Inserting the expansions (2.60) and (2.61) into Eqs. (2.6) with the continuity equation replaced by Eq. (2.59) leads as before to Eqs. (2.13) for the expansion coefficients. The wavenumber k now takes the discrete values $k_\ell = \sigma_\ell/D$, $\ell = 1,\ldots, \infty$. In particular we can rewrite the continuity equation for the ℓ'th term using the relation for the derivative of $J_1(x)$:

$$\frac{dJ_1}{dx} = -\frac{J_1}{x} + J_o \tag{2.62}$$

and obtain the form identical with (2.13). In analogy with the case of the straight coastline the surface boundary condition for the temperature is in analogy with the case of the straight coastline $\theta = 1$ over land and $\theta = 0$ over sea. This means $\theta(\zeta,\phi) = 1$ for $\zeta < r$ and $\theta(\xi,0) = 0$ for $\xi > r$, where r is the scaled radius of the island. This boundary condition leads to the following expansion coefficients (e.g. Charlton 1969):

$$\theta(\ell,0) = J_1^{-2}(\sigma_\ell) \cdot 2 \int_o^{r/D} y\, J_o(\sigma_\ell y)dy \tag{2.63}$$

or by performing the integration

$$\theta(\ell,0) = 2J_1(\sigma_\ell r/D)\; r\sigma_\ell/D \cdot (J_1(\sigma_\ell)\sigma_\ell)^{-2} \tag{2.64}$$

The solution can now be obtained as above employing the same boundary conditions. Since we have already scaled with the appropriate intrinsic length scale L, the flow structure depends only on the scaled radius r. For large radii $r >> 1$ the effect of curvature must be negligible and the results for all fields near the coastline should be identical to the results obtained for the case of a straight coastline. For radii comparable to 1 or smaller the maximum radial velocity should be influenced by the effect of curvature of the coastline. The result for the radial velocity at $\xi = r$ and $\eta = 0.3$ (where the maximum in u is found for large r) is shown in Fig. 2.18. No appreciable effect of the curvature is found when $r \gtrsim 1$, and the point where u_{max} is half the value at infinite r is the value r = 0.06. Using

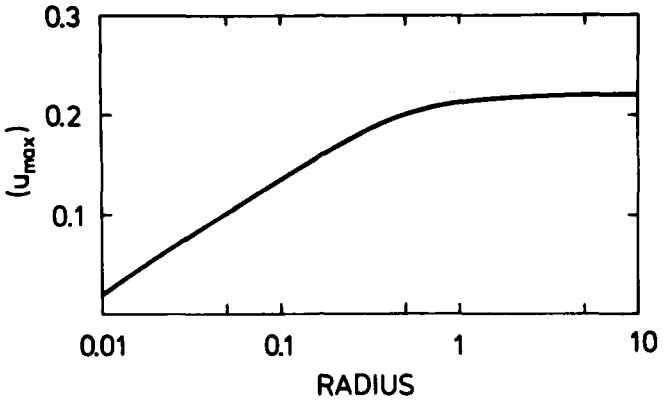

Fig. 2.18. Radial velocity (u-component) for the circular island at ξ=radius, and η=0.3, shown for diffent radii.

the values K = 5 m^2 s^{-1} and N = 10^{-2} s^{-1} the scale L becomes approximately 36 km and the radius has to be less than ~ 10 km before the maximum inflow velocity is influenced by the finite size of the heated area. The rather small value of r for which curvature effects are important for the maximum inflow velocity shows the importance of small scales. As discussed in section 2.6 these small scales are attenuated strongly in the presence of even a small basic state velocity across the coast. Also non-linear interactions become important for these scales even with small values of the surface temperature perturbation. As a consequence we must expect the curvature effects to be of importance at somewhat larger valves of r in the real atmosphere. The analysis could be extended as in section 2.6 by the introduction of a basic state velocity U; however, this will lead to a much more complicated mathematical problem since obviously the circular symmetry assumed here will be violated in this case, and the flow will become truly three-dimensional. It should be noted in passing that a rather simple technique has been devised for problems of this kind by Scorer (1956) and Olfe and Lee (1971). This latter work is of particular interest here since it deals with the urban heat island studied by linearized equations as in the present investigation. This technique is based on the superposition of solutions for two-dimensional surface heating distri-

butions. For the island flow discussed here the appropriate two dimensional problem is the flow over an infinitely long strip of land of finite width of say 2ℓ. This can be solved directly as in the case of the infinite land with the only difference that the expansion coefficients in the Fourier expansions now depends on ℓ as $(\sin(k\ell/L)/k)\cos k\xi$ for the temperature, pressure, and vertical velocity, and as $-(\sin(k\ell/L)\sin k\xi$ for the horizontal velocity. The solution can be found for any value of the basic state cross coastal velocity. Noting that any component of velocity along the coast will have no effect on the flow field the solution can be found for any orientation of a basic state velocity vector. Superposing solutions for all orientations of the strip of land keeping constant the basic state velocity in an absolute frame of reference leads to a three-dimensional solution for the flow over an isolated island with the surface temperature distribution given by the superposition as:

$$\theta(\xi,0) = \begin{cases} 1 & \text{for } \xi \leq \frac{\ell}{L} \\ \frac{2}{\pi} \arcsin \frac{\ell}{L\xi} & \text{for } \xi > \frac{\ell}{L} \end{cases}$$

This function is shown in Fig.2.19. By using distributions for the two-dimensional surface temperature field other than the "top hat" used here other three-dimensional distributons are obtained; the method will always give distributions with a tail $\sim \xi^{-1}$. In the urban heat island such distributions may adequately approximate the rather smooth surface temperature distributions observed, and in the study by Olfe and Lee (1971) the three-dimensional temperature field over a city heat island was studied using this technique. Their model differs from the linearized one described here in that rotation and viscous effects were neglected and the surface forcing was constant in time ($\omega = 0$). In this study we will not proceed along these lines but note that the periodically forced model can be employed for this rather complex flow problem and give semi-analytical solutions for the perturbation flow with proper boundary conditions.

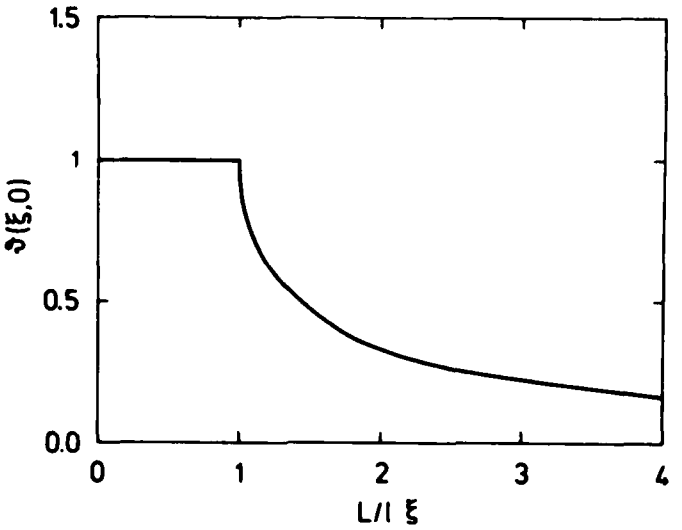

Fig. 2.19. Surface temperature distribution obtained from the superposition of infinite strips of width 2ℓ. (See text).

3. NUMERICAL MODEL

3.1. Basic equations

The model is based on the anelastic approximation (Ogura and Philips 1962, Gough 1969). The approximation is justified by scale analysis of the terms in the Navier Stokes equations treating the flow variables as perturbations on a basic state of constant potential temperature. The scale height of potential temperature is roughly four times higher than the density scale height, and the anelastic approximation is consistent with the continuity equation for "deep convection" (Dutton and Fictl 1969):

$$\nabla_3 \cdot (\rho_o \vec{v}) = 0 \qquad (3.1)$$

where ρ_0 is the height dependent density corresponding to the basic state of constant potential temperature. The inelastic approximation has been used in models of gravity waves and deep (cumulus) convection. The approximation effectively filters out sound wave solutions and is not based on the hydrostatic approximation. Neuman and Mahrer (1971) argue that it is necessary to include nonhydrostatic effects in their model of the sea-breeze; however, as pointed out by Walsh (1974) their argument is false, and from the point of view of scaling of the Navier Stokes equations effects of dynamical pressure is unimportant when the aspect ratio of the flow (typical height/typical width) is small. It cannot, however, be ruled out that nonhydrostatic effects are important in parts of the flow, and when modelling in detail the propagating sea-breeze front it should be expected that nonhydrostatic effects come into play. The modelling of such small-scale features requires a very high resolution, and since most model formulations require that model boundaries are effectively outside the influence of the flow, the number of gridpoints required (or equivalently the number of functions in a Fourier-type expansion) becomes very high. A typical extension for a sea-breeze flow is 100 km and in order to resolve in detail a frontal structure with dimension of the order of 1 km the gridsize required is of the order 0.1 km giving $\sim 10^3$ gridpoints assuming constant gridsize. The requirements on computer time and storage very easily becomes probibitive. Two possibilities are to use a nonuniform grid (Anthes, 1978), or a system of nested grids with different gridsizes (Walsh, 1974). The obvious disadvantage is a tendency to concentrate the fine structure in the region with a fine grid, excluding the possibility for the front to propagate away from the coast with a correct speed. Most published sea-breeze models utilize a grid with a gridsize effectively excluding flow structure with an aspect ratio of order one. Typical grid size of a few kilometers in the horizontal compared to the (possibly correctly resolved) vertical dimension of the flow of less than one kilometer limits the aspect ratio of the resolved flow to ~ 0.1 or smaller.

The basic equations employed can be written as:

$$\frac{\partial u}{\partial t} = - u \frac{\partial u}{\partial x} - w \frac{\partial u}{\partial z} - \frac{\partial \pi_h}{\partial x} - \frac{\partial \pi}{\partial x} + fv + \frac{\partial}{\partial z} K_m \frac{\partial u}{\partial z}$$

$$\frac{\partial v}{\partial t} = - u \frac{\partial v}{\partial x} - w \frac{\partial v}{\partial z} + f u_g - fu + \frac{\partial}{\partial z} K_m \frac{\partial v}{\partial z}$$

$$\frac{\partial w}{\partial t} = - u \frac{\partial w}{\partial x} - w \frac{\partial w}{\partial z} - \frac{\partial \pi}{\partial z} + \frac{\partial}{\partial z} K_m \frac{\partial w}{\partial z} \qquad (3.2)$$

$$\frac{\partial R}{\partial t} = - u \frac{\partial R}{\partial x} - w \frac{\partial R}{\partial z} + \frac{\partial}{\partial z} K_n \left(\frac{\partial T}{\partial z} - \Gamma_c \right)$$

$$\rho_o \frac{\partial u}{\partial x} + \frac{\partial}{\partial z} \rho_o w = 0$$

where

Θ = constant basic potential temperature independent of height.

$R = \frac{\theta - \Theta}{\Theta}$ = relative deviation of potential temperature.

$\pi_h = \int_z^{z_{top}} gR \, dz$ = hydrostatic pressure function.

π = perturbation (nonhydrostatic) pressure function

ρ_o = height-dependent constant basic state density corresponding to the basic state potential temperature

$$= \frac{p_{oo}}{R_g} \left(1 - \frac{z}{H_s} \right)^{\left(\frac{C_p}{R_g} - 1 \right)}$$

where p_{oo} is a standard surface pressure and H_s the scale height $C_p \Theta g^{-1}$. Here Rg is the gas constant and C_p the the heat capacity at constant pressure.

The π functions are related to the real pressure through $\pi = C_p \Theta (p/p_{oo})^{Cp/Rg}$.

Γ_c = counter gradient flux correction (see below).

K_m, K_n are the turbulent diffusivities for momentum and heat, respectively, calculated as discussed in the next section.

3.2. Turbulence parameterization

The one-dimensional version of the model results from assuming horizontal homogeneity as :

$$\frac{\partial u}{\partial t} = f(v - v_g) + \frac{\partial}{\partial z} K_m \frac{\partial u}{\partial z}$$

$$\frac{\partial v}{\partial t} = - f(u - u_g) + \frac{\partial}{\partial z} K_m \frac{\partial v}{\partial z} \qquad (3.3)$$

$$\frac{\partial R}{\partial t} = \frac{\partial}{\partial z} K_n \left(\frac{\partial R}{\partial z} - \Gamma_c\right)$$

The turbulence closure is obtained by the utilization of the equation for the turbulent energy in connection with a prognostic length scale equation :

$$\frac{\partial e}{\partial t} = K_m \left(\left|\frac{\partial \vec{v}}{\partial z}\right|^2 - \frac{\phi m}{\phi_h} g \left(\frac{\partial R}{\partial z} - \Gamma_c\right)\right) + c_2 \frac{\partial}{\partial z} K_m \frac{\partial e}{\partial z} - c_3 \frac{e^{3/2}}{\ell} \qquad (3.4)$$

$$\frac{\partial \ell}{\partial t} = \frac{\ell_s - \ell}{\ell / c_3 \sqrt{e}} \qquad (3.5)$$

with $K_m = \ell\sqrt{c_1 e}$. The first term in Eq. (3.4) is the shear and buoyancy production terms assuming again fluxes to be proportional to the local gradients. The second term is a parameterization of the divergence of the sum the fluxes $\langle w'e' \rangle$ and $\langle w'p' \rangle/\rho$ as in Shir (1973) and Yamada and Mellor (1975). The last term in Eq. (3.4) is the dissipation term. The definition of K_m implies a proportionality between the mixing length scale and the dissipation length scale. Eq.(3.4) can be rewritten as

$$\frac{\partial e}{\partial t} = \frac{e_s - e}{\ell/c_3\sqrt{e}} + c_2 \frac{\partial}{\partial z} K_m \frac{\partial e}{\partial z} \tag{3.6}$$

with

$$e_s = \ell^2 \sqrt{c_1} c_3^{-1} \left(\left| \frac{\partial \tilde{v}}{\partial z} \right|^2 - \frac{\phi_m}{\phi_h} g \left(\frac{\partial R}{\partial z} - \Gamma_c \right) \right). \tag{3.7}$$

Neglecting the transport term, Eq.(3.6) describes the relaxation of turbulent energy towards the value e_s, where production and dissipation are in balance, with a time scale $\tau = \ell/c_3\sqrt{e}$. Equation (3.5) for the length scale is based on the assumption that the length scale likewise tends to an equilibrium value ℓ_s with the same relaxation time scale. ℓ_s is assumed to be determined from the boundary layer height H:

$$\ell_s = \begin{cases} \min(c_4 \cdot H,\ kz\phi_m^{-1}), & \text{for } z < H \\ 0 \quad , & \text{for } z \geq H \end{cases} \tag{3.8}$$

The length scale equation (3.5) was originally proposed by Busch et. al. (1977). They, however, combined this equation with the assumption $e=e_s$, which under conditions of weak surface heating, and moderate to strong wind can be further simplified by neglecting the buoyancy production term in (3.7). Also their definition of the equilibrium length scale was different and given as:

$$\ell_s = kz\phi_m^{-1} \left(1 - \frac{z}{H}\right) \quad , \quad \text{for } z < H \ . \tag{3.9}$$

Near the surface both formulations give $\ell_s = kz/\phi_m$ in consistency with surface layer similarity. The constants c_1, c_2, c_3 and c_4 are found from known surface relations under equilibrium conditions. The transport term in Eq.(3.6) can be neglected for $z/L << 1$ (e.g. Wyngaard and Coté 1970), and we have $e=e_s$ and $\ell = \ell_s$; introducing this into (3.7) and rewriting yields

$$e_s = \sqrt{c_1}\, c_3^{-1}\, u_*^2 \left(1 - \frac{\kappa z}{\phi_m L}\right) \tag{3.10}$$

and

$$K_m \frac{\partial u}{\partial z} \equiv u_*^2 = u_*^2 \sqrt{c_1} \cdot \sqrt{\sqrt{c_1}\, c_3^{-1} \left(1 - \frac{kz}{\phi_m L}\right)} \tag{3.11}$$

For $z/L<<1$ we have $e_s = \sqrt{c_1} c_3^{-1} u_*^2 \approx 5u_*^2$ (Busch,1973) and from Eq. (3.11) $c_1^{3/2} c_3^{-1} = 1$, yielding $c_1=0.2$ and $c_3 = 0.2^{3/2}$. The constant c_4 in Eq. (3.8) is determined by requiring the length scale to scale with the peak in the vertical velocity spectrum, which under convective conditions is found to approach a maximum value $\lambda_m \approx 1.5H$ in the upper part of the boundary layer (Kaimal et.al., 1976), whereas for $z<<L$ $\lambda_m \approx 2z$ (Kaimal et. al.,1972). This gives $c_4 = 1.5k/2 = 0.26$. The constant c_2 is set equal to 0.5 here; results are very insensitive to the choice of this constant. The countergradient flux term Γ_c appearing in Eqs. (3.3) and (3.7) is taken from Bodin (1978) as

$$\Gamma_c = \frac{\gamma_c}{\theta} = \frac{10 \cdot \overline{w'\theta'_0}}{\theta \cdot H \cdot w_*} \tag{3.12}$$

where $w_* = (g/T_0 \langle w'\theta' \rangle H)^{1/3}$ is the convective velocity scale. The justification for the use of this counter gradient flux term in the convective boundary layer is discussed in Deardorff (1966). The height of the boundary layer is an important parameter entering into the dynamical equations as the limiting mixing length under convective conditions,and is determined from the temperature profile as the height of the intersection of the temperature profile with the line passing through the minimum with the line passing through the minimum temperature and having a slope equal

to γ_c. This procedure is similar to that devised by Bodin (1978).

Under neutral and stable conditions H is determined as the height where the bulk Richardson number Ri_B exceeds the value 1 with

$$Ri_B = \frac{g}{\theta_o} \cdot \frac{(\theta - \theta_o) \cdot z}{(u^2 + v^2)} \qquad (3.13)$$

The value 1 for the "critical" bulk Richardson number is somewhat higher than the values found by Mahrt (1980). It was chosen by calibrating against the observed nocturnal boundary layer height for Wangara day 33/34 (see below). The flux gradient relationships ϕ_m and ϕ_h are based on the expressions from Businger et al. (1971). The expressions for unstable stratification are changed by using the exponent -1/3 in both ϕ_m and ϕ_h in contrast to the original values of -1/4 and -1/2, and changing the coefficients to z/L to give an unchanged slope for $z/L \to 0$, this leads to the expressions:

$$\phi_m = \begin{cases} \left(1 - 11 \frac{z}{L}\right)^{-1/3} & \text{for } \frac{z}{L} \leq 0 \\ 1 + 4.7 \frac{z}{L} & \text{for } \frac{z}{L} \geq 0 \end{cases} \qquad (3.14)$$

$$\phi_h = \begin{cases} 0.74 \left(1 - 14 \frac{z}{L}\right)^{-1/3} & \text{for } \frac{z}{L} \leq 0 \\ 0.74 + 4.7 \frac{z}{L} & \text{for } \frac{z}{L} \geq 0 \end{cases} \qquad (3.15)$$

Under strongly convective conditions -L could become arbitrarily small in the model, whereas in the real atmosphere the convective motions on the scale of the depth of the boundary layer will induce horizontal motions near the surface, which in turn will generate small-scale turbulence. This mechanism is discussed in Businger(1973). The effect is simulated in the model by redefining the friction velocity entering into the definition of L as:

$$u_s^2 = u_*^2 + 0.002\ w_*^2 \tag{3.16}$$

here u_s is the redefined velocity scale, u_* the usual friction velocity and w_* the convective velocity scale. From Eq. (3.16) the minimum value for -L becomes

$$-L_{min} = 2.5 \cdot 10^{-4} \cdot H \tag{3.17}$$

More properly, the minimum -L should depend on the ratio H/z_o (Businger, 1973); this can be argued as suggested by Jensen (1982, personal communication) as follows: Under strongly convective conditions the geostrophic drag law can be written as (Wyngaard et.al., 1974)

$$\frac{G}{u_*} = k\ell n\left(-\frac{L}{z_o}\right) \tag{3.18}$$

with vanishing forcing $G \to 0$ and $u_* \to 0$ the average wind profile induced by the convection should match the velocity of order w_* well above the surface layer,and the induced velocity scale u_s is then determined by substituting u_s for u_*:

$$a\,\frac{w_*}{u_s} = k\ell n\left(\frac{T_o}{kg}\,\frac{u_s^3}{\langle w'\theta'\rangle}\right) = 3k\ell n\left(\frac{H}{kz_o}\,\frac{u_s}{w_*}\right) \tag{3.19}$$

Here a is a constant of order one. Eq.(3.19) can be solved give $u_s = f(H/z_o)w_*$ and $L_{min} = g(H/z_o)$. The expression gives only the scale velocity in the asymptotic case of vanishing u_* and Eq. (3.16) is a simple but somewhat arbitrary way of ensuring this asymptote. Businger(1973) argues that the effect can explain, at least qualitatively, why the asymptotic behaviour of ϕ_h, $\phi_h \sim (-z/L)^{-1/2}$ found from measurements differs from what is expected from free convection scaling $\phi_h \sim (-z/L)^{-1/3}$; it is clear, however, that a quantitative evaluation of the effect requires observation of H*) in addition to surface micrometeoro-

---

*) Or measurements of the low-frequency power spectrum for the horizontal wind components.

logical measurements, and the results cannot be composited using Monin-Obukhov scaling.

3.3. Simulation of Wangara day 33/34

The extensive field programme, The Wangara Experiment (Clarke, 1971) was in part aimed at providing good datasets on the boundary layer structure under rather ideal conditions, and the data

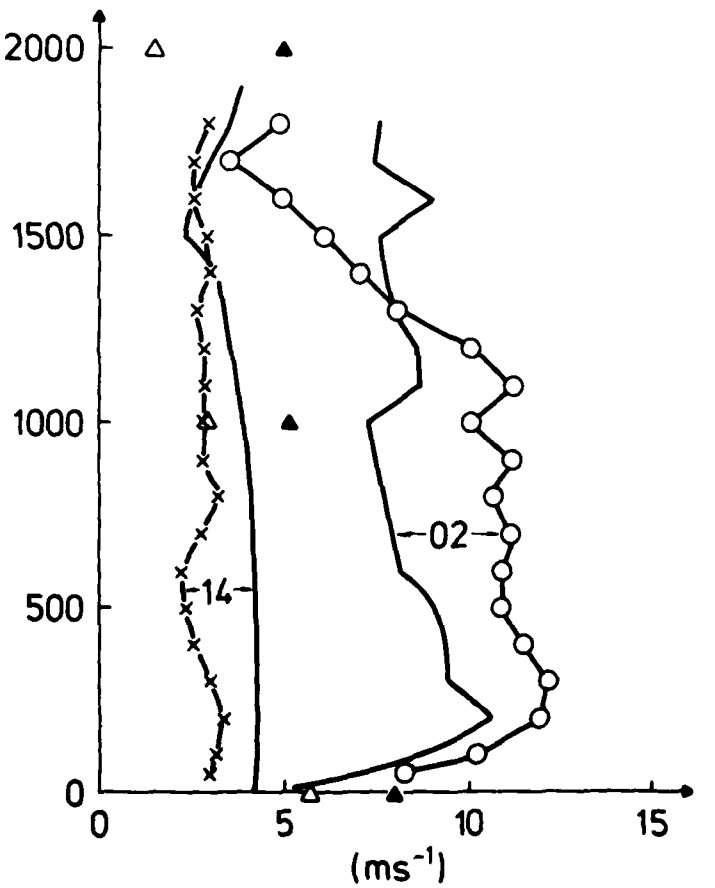

Fig. 3.1. Wind speed profiles at 14 h day 33 and 02 h day 34 of the Wangara experiment.(——): Model results,(×-×-), (o-o-o): Observations. (Δ): Geostrophic wind speed at 14 h, (Δ): Geostrophic wind speed at 02 h.

obtained naturally lends themselves to the evaluation of the quality of model simulations. For a number of boundary layer models day 33/34 of the experiment has been used for this purpose. The main reason for choosing these two days is the relative absence of large synoptic scale or mesoscale phenomena, which would seriously complicate the interpretation of the boundary layer processes. For the present purpose of the design of a mesoscale model particularly aimed at simulation of the sea-breeze, the diurnal variation of the boundary layer structure in response to the surface heating, and in particular the response of the wind profile is of interest. The wind profile was measured at the experiment using theodolite tracking of balloons, which were filled to rise at a constant, nominal rate enabling the wind profile to be determined up to 2 km. The initial data for the model was the observed wind and temperature profile at 06 hr day 33. The surface heating function was prescribed as pure sinusoidal during the day with maximum heating $\langle w'\theta' \rangle_{max}=0.15$ Kms^{-1} and following the observed net radiation. The surface radiational cooling at night was simulated by prescribing an exponential decay of the surface temperature, with decay rate and asymptotic value determined from the observed surface temperature at night between days 33 and 34. This ensures that the night temperature at the surface in the model closely follows the observed tempepeture provided that the surface temperature at sunset is correct. The geostrophic wind was specified as varying linearly in time and varying linearly between 1 km and 2 km, using the 3 hourly surface geostrophic winds from the synoptic network given in the dataset*).

The model was found to predict accurately the development of the daytime mixed layer height and temperature profile, and also the

*) The surface geostrophic wind was found by fitting a straight line to the observed values of each of the two components in the interval between 03 day 33 and 03 day 34.The thermal wind was observed only at 12 hourly intervals and the values used here were simply specified by the line connecting the values at 09 day 33 and 21 day 33.

development of the night mixed layer height. Figure 3.1 shows the predicted and observed windspeed profiles of day 33 hour 14, where the mixed layer is well developed, and at hour 02 of day 34, where a nocturnal jet has developed. The model shows good agreement with the observed wind profiles in particular in view of the uncertainty with which the geostrophic wind is measured. The most pronounced difference is the observed decrease of windspeed with height above 1200 m, a feature which is consistent through the night. The thermal wind specified in the model was, as mentioned, computed from the synoptic radiosonde network, using six stations with separations of around 500 km, and with three of them located at the coast (see Clarke (1971) for details). The observed decrease of windspeed above 1200 m could therefore possibly be explained by baroclinicity not resolved by the radiosonde network. A particular feature prominent in the data is the development of a strong nocturnal jet, this is well reproduced in the model, with regard to the level of maximum windspeed, time of maximum, and magnitude.

3.4. Two dimensional model

The set of dynamical equations (3.2) for the mean flow, and the turbulence parameterization described above form the basis of the model. Added in Eqs. (3.4) and (3.5) are advection by the mean flow of the turbulent energy and the length scale, respectively. The numerical solution of the system of equations is based on finite difference methods. To some extent the different physical mechanisms are treated in sequence using time splitting (Mesinger and Arakawa,1976). The first step consists of the calculation of the hydrostatic pressure by integration from the model top of the hydrostatic equation, assuming a linear temperature profile between gridlevels. The advection terms are calculated using centered differences in time and space, and the result after the first step are fields based on the inclusion of advection, hydrostatic pressure gradient, and coriolis terms only. The next step consists in the inclusion of the diffusion terms by first computing the forcing by surface fluxes. The numerical method used for

the diffusion terms is the finite-element method with implicit time differencing. The diffusion equation can be written:

$$\frac{\partial f}{\partial t} = \frac{\partial}{\partial z} K \frac{\partial f}{\partial z} \tag{3.20}$$

assuming both f(z) and K(z) are expanded in a series of some basic functions $\phi_i(z)$,viz. $f(z)=f_i\ \phi_i(z)$*) and $K(z)=K_i\ \phi_i(z)$. Then a set of equations can be obtained for the temporal development of the expansion coefficient f_k by inserting the expansions into Eq.(3.20), multiplying by ϕ_k and integrating over z to yield:

$$A_{ik} \frac{\partial f_i}{\partial t} = K_\ell\ f_i\ B_{\ell ik} \tag{3.21}$$

where the matrices A and B are constant and given by

$$A_{ik} = \int_z \phi_i\ \phi_k\ dz$$

$$B_{\ell ik} = \int_z \phi_k \frac{d}{dz} \phi_\ell \frac{d}{dz} \phi_i\ dz \tag{3.22}$$

These expressions are quite general for the spectral method for the solution of the diffusion equation, and Eq.(3.20) can easily be shown to give the least-square deviation for the expansion coefficients provided the expansions of f and K are correct. With orthonormal basic functions, A would become the identity matrix and no matrix inversion would be neccesary, but B would generally be complicated. In the finite element method the basic functions are chosen so as to make both A and B sparse. In the present model the ϕ's are chosen to be the "chapeau" functions. The k'th chapeau function is zero everywhere except in the interval form the (k-1)'th to the (k+1)'th gridpoint, it is piecewise linear ,and takes the value of 1 at the k'th gridpoint. With a function given as gridpoint values the expansion coefficients for the function on this grid simply become the gridpoint values themselves, and the expansion is correct only if the function is

*) Here summation over repeated indices is assumed.

piecewise linear. With this choice for ϕ_i the matrix A becomes tridiagonal, with main diagonal
$A_{kk} = 1/3\ (\Delta z_{k-1}+\Delta z_k)$ and $A_{k-1,k} = 1/6\Delta z_{k-1}, A_{k+1,k} = 1/6\Delta z_k$.
The elements of B are given by $B_{k-1,k-1,k} = B_{k,k-1,k} = - B_{k-1,k,k} = 1/(2\Delta z_{k-1})$, $B_{k+1,k+1,k} = B_{k,k+1,k} = -B_{k+1,k,k} = 1/(2\Delta z_k)$, and $B_{k,k,k} = B_{k-1,k,k} + B_{k+1,k,k}$.

All other terms are zero. The implicit scheme for the time differencing is a special case of the Cranck-Nicholson scheme, employed here for the extrapolation from timestep n to n+1:

$$A_{ik}\ (f_i^{(n+1)} - f_i^{(n)}) = K_\ell^{(n)}\ f_i^{(n+1)}\ B_{\ell ik}\ \Delta t \tag{3.23}$$

The next step consists in including the effect of the dynamical pressure term. After this step the fields at timestep n+1 are given by the result after the diffusion step plus the tendency from the π-terms:

$$\begin{aligned} u^{n+1} &= u^* - \left(\frac{\partial \pi}{\partial x}\ \Delta t\right) \\ w^{n+1} &= w^* - \left(\frac{\partial \pi}{\partial z}\ \Delta t\right) \end{aligned} \tag{3.24}$$

where u^*, w^* are the fields obtained after the diffusion step. Applying the divergence operator given as $D = (\partial_x, \rho_o^{-1}\partial_z\ \rho_o)$ to the (u,w) in Eq.(3.24) results in the equation

$$\begin{aligned} \partial_x u^{n+1} + \rho_o^{-1}\partial_z \rho_o w^{n+1} &= \partial_x u^* + \rho_o^{-1}\partial_z \rho_o w^* \\ &\quad - \partial_{xx}^2 \pi - \rho_o^{-1}\partial_z \rho_o \partial_z \pi \end{aligned} \tag{3.25}$$

where π has been redefined by letting it absorb the Δt. The continuity equation requires that the left-hand side vanishes, and we obtain a differential equation for π. The finite difference operators corresponding to ∂_x and ∂_z are centered differences. With $D^* = D(u^*,w^*)$ calculated π is obtained from the the solution of this Poisson-type differential equation. The boundary conditions for π are $\partial_z\ \pi$ at the lowest level and at

the top, and $\pi = 0$ at the lateral boundaries. The solution is obtained by a direct method, which consists in first performing a horizontal Fourier transform at each level. The system resulting for each Fourier mode π_k can be written as

$$\left[\frac{1}{2\Delta x^2}(\cos(2\Delta xk)-1) + \rho_o^{-1}\partial_z\rho_o\partial_z\right]\pi_k = D_k^* \qquad (3.26)$$

The first term in the parenthesis is the response function for the horizontal difference operator ∂_{xx}, and D_k^* is the k´th Fourier mode of D^*. The boundary conditions for u and w (see below) gives D^* zero at the lateral boundaries and the Fourier transformation can be written involving only sine terms. With a centred difference operator for ∂_z Eq.(3.26) results in a system of linear equations with a pentadiagonal coefficient matrix, which can be solved by standard methods. The final step then consists in applying the inverse sine transform to the expansion π_k at each level. To improve the speed in the computations the operator $\rho_o^{-1}\partial_z\ \rho_o\partial_z$ in eq.(3.26) was written as $(\rho_o^{-1}\partial_z\rho_o)\partial_z + \partial^2_{zz}$, and with $\rho_o^{-1}\partial_z\rho_o$ computed exactly from the analytical expression for ρ_o at each level. Using a finite element method similar to the method described above, the resultant linear equations have a tridiagonal coefficient matrix which is constant. This system is conveniently solved by using the the method described by Ahlberg (1977) performing the first decomposition step once and for all.

3.4.1. Boundary conditions

The computational domain is bounded at the top by a rigid lid where the initial values for u,v and θ are assumed to be maintained and where $\pi_h = \partial_z\pi = w = 0$. At the surface the usual no-slip conditions are assumed, i.e. $u = v = w = 0$, and $\partial_z\pi = 0$. The surface boundary conditions for the temperature are that over water the initial surface temperature is maintained, whereas over land the boundary conditions are

during the day: $\langle w'\theta'\rangle_o = \langle w'\theta'\rangle_{max} \sin\left(\frac{2\pi}{t_H}\, t\right)$

at night: $T_o = T_{initial} + (T_{sunset} - T_{initial}) \exp(-t/t_c)$

similar to the boundary conditions used in the simulation of Wangara day 33/34. These boundary conditions reflect the physical mechanisms of a daytime heated boundary layer with heating governed by the solar input at the surface, and a night-time boundary layer, where the ground surface temperature is primarily governed by direct long wave radiation to space. The lateral boundary conditions are $\partial_x u = \partial_x v = \partial_x \theta = w = \pi = 0$. The first ten meters above the surface are assumed to obey surface layer similarity theory, and the actual boundary conditions entering into the prognostic equations are the fluxes of momentum and heat at the first level at 10 m. This procedure is commonly used in boundary layer models as in the model by Busch et. al.(1977). The surface boundary condition for w is used as w(10m) = 0, thus assuming negligible convergence in the 10m layer.

3.4.2. Horizontal diffusion and filtering

The model equations (3.2) include no horizontal diffusion terms. As discussed in section 2.1 the effect on the mean flow structure from horizontal diffusion should be unimportant if the flow aspect ratio is much smaller than unity. In a numerical model the combined effect of truncation errors in the finite difference operators, and aliasing introduced by the nonlinear terms, will result in large errors if no precaution is taken to damp the small-scale features. In the present model, as in most mesoscale models reported in the literature, the resolution is insufficient to accurately resolve all the physical features which we want to model. We must therefore rely on the asumption that the smallest resolvable scales have only a negligible influence on the behaviour of the larger scales of motion. The relative success of large-scale weather prediction models, in spite of similar resolution problems with, for example, the proper resolution of fronts, suggests that this assumption is often justified, and the results with the present model in the simulation of the propagation of the seabreeze front described below also suggests that this is a minor problem. The one-dimensional advection-dif-

fusion equation with a constant advection velocity U and diffusivity K can be written

$$\frac{\partial \chi}{\partial t} = - U \frac{\partial \chi}{\partial x} + K \frac{\partial^2 \chi}{\partial x^2} \qquad (3.27)$$

With a finite difference approximation of this equation, truncation errors in the advection term will produce small-scale noise at a rate which must be proportional to $U/\Delta x$. Similarly, the destruction of small scales by the diffusion term must be proportional to $K/\Delta x^2$. If we define a grid Reynolds number as the ratio of these two numbers:

$$Re = \frac{U\Delta x}{K} \qquad (3.28)$$

we can control the amplitude of the small scales by specifying a maximum value of Re, that is letting K depend on U through (3.28) with Re fixed. The linear advection-diffusion equation (3.27) will not give rise to aliasing, but in the more general form in the model equations (3.2) aliasing will be present in the finite treatment of, for example, the $u\partial u/\partial x$-term, and also in the other nonlinear terms. In the present model the neccesary horizontal smoothing is accomplished by specifying Re as constant throughout the integration, and using the maximum value of $u(x,z,t)$ at every timestep as U in (3.28), giving the value of K used as the horizontal diffusivity. The diffusion term is computed, using a 3-point formula for ∂_{xx} and an explicit forward time extrapolation, as the final step in the sequence described in section (3.4).

The above consideration s also applies to finite difference operators acting in the vertical direction. In the model a minimum diffusivity defined for each vertical column of grid points is adopted, using (3.28) with $U\Delta x$ replaced by $(w(z_k,t)\Delta z_k)_{max}$. The turbulent diffusivities from the parameterization described in Section (3.2) are therefore limited from below by this minimum value before being applied in the model. To avoid the accumulation of noise near the lateral boundaries, an increased horizontal diffusion is applied in a zone near each of the lateral

boundaries. This is accomplished by the application of a 3-point filter (Shapiro, 1970) at every timestep in these diffusive zones.

3.5. Comparision with analytical model

The results from the linearized model described in the previous chapter should be approximately reproduced by the numerical model if the surface forcing is so weak that the nonlinear advection terms are negligible, and the turbulent diffusivities are externally specified as in the linear model. Comparisons between the models then yield an independent check on the numerical procedures with regard to accuracy, stability, and code errors. The stability and accuracy of the individual finite-difference operators in the numerical model can be performed by standard methods, and this kind of analysis is important in designing the model, but the adequateness of the model as a whole can probably be asserted only by using known solutions. The layered linear model enables a realistic vertical profile of the diffusivity and stratification in the boundary layer. This is important for the detailed vertical structure of the mean profiles, and specifically for the maximum wind velocities as discussed in Section 2.8. Furthermore, the most important physical mechanism in the sea-breeze flow is the vertical diffusive transport of heat and momentum; therefore, it is important that transport in particular be tested as realistically as possible. Figure 3.2a shows examples of such comparisons in the case where the diffusivities ($K_h=K_m=K$) are assumed to be closely parabolic up to the top of the boundary layer, and constant above the layer as shown in Fig. 3.2a. In addition to the diffusivity profile, this figure shows the computed analytical u-profile at the time of maximum surface temperature difference together with the corresponding result from the numerical model. Here the surface forcing is assumed harmonic also in the horizontal corresponding to the inclusion of only one wavenumber in the analytical model (Section 2.2); the wavelength is 7 gridunits in the numerical model corresponding to 28 km, and the Brunt-Väisälä frequency is $N=1/150\ s^{-1}$. Figures 3.bd show the u,v, and w components, using the same parameters except that the stratification below the 816 m level is reduced by a factor of five.

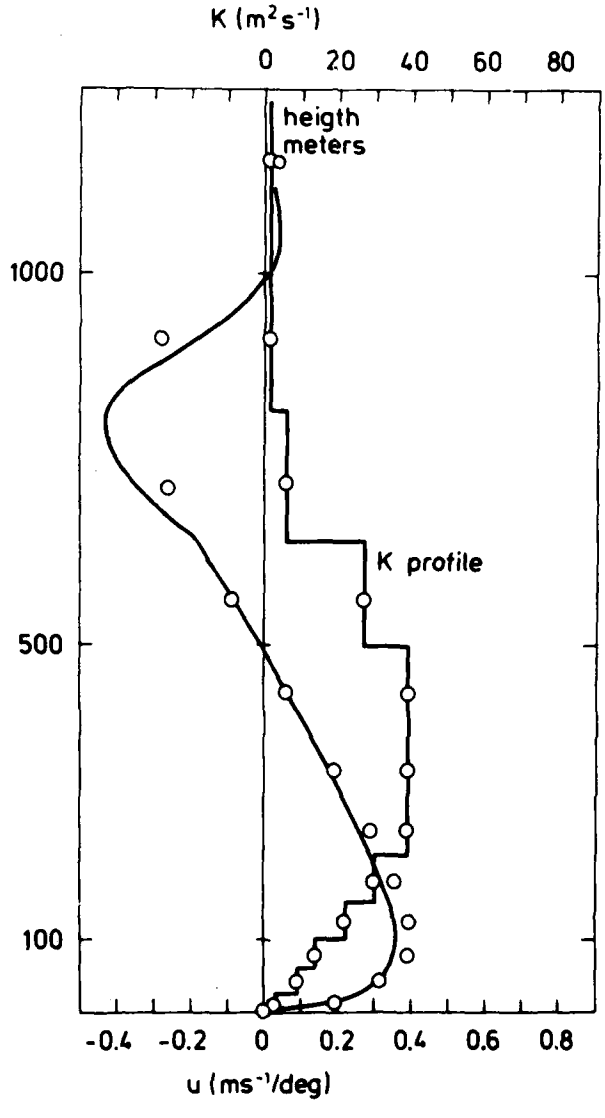

Fig 3.2a. u-component at t=6 h as function of height with N^{-1}=150 s, and a K-profile as shown on the figure (see text for details); (——): Analytical result, (o): Numerical result.

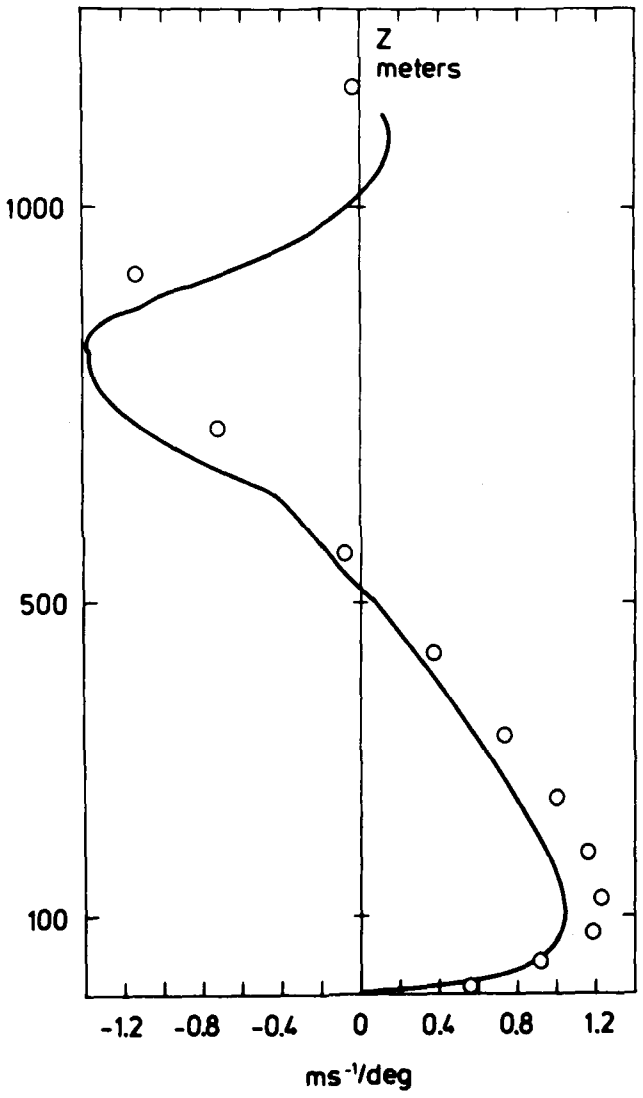

Fig. 3.2b. As fig. 3.2a, but in the case with a jump in stratification at 816 m with N_2^{-1}=150 s and N_1=0.2·N_2 (See text).

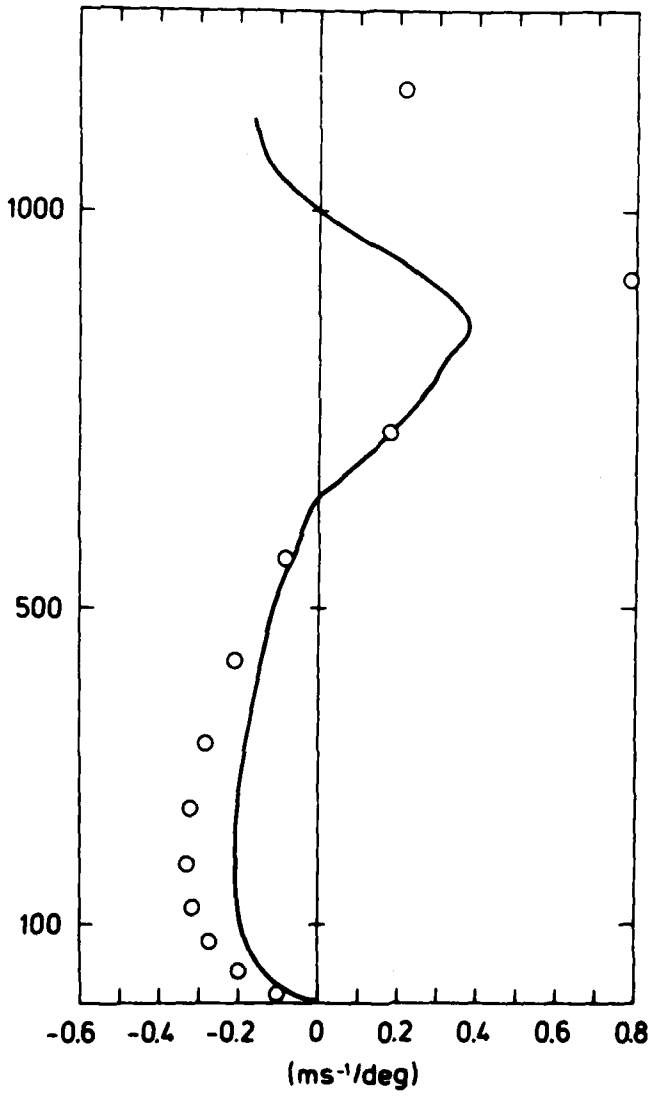

Fig. 3.2c. As fig. 3.2b, but for the v-profile.

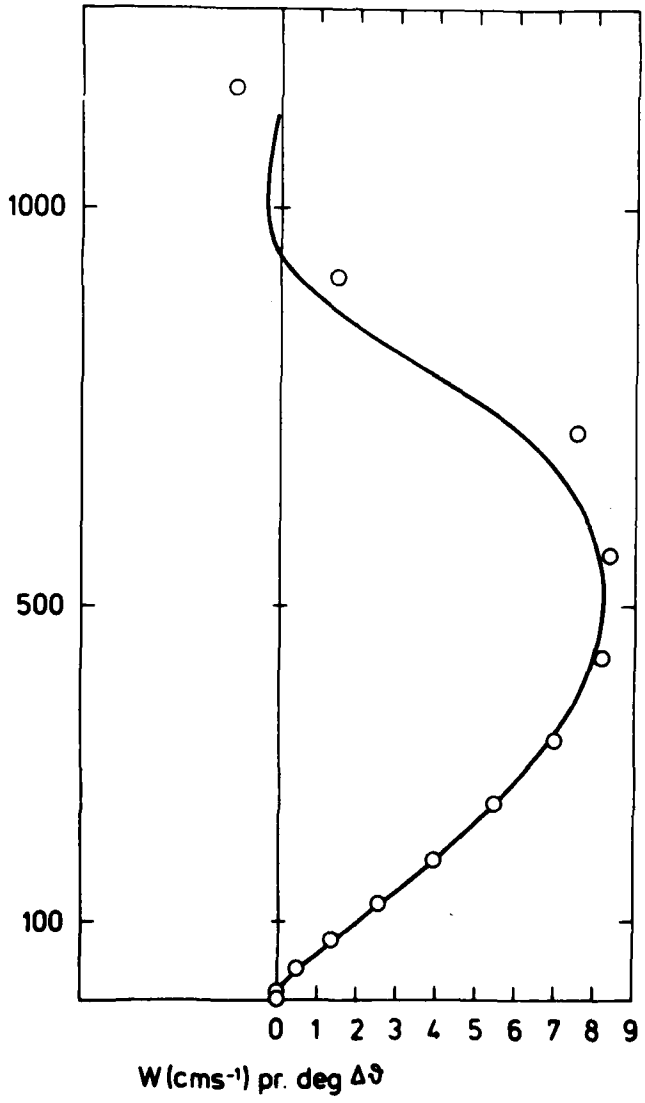

Fig. 3.2d. As fig. 3.2b, but for the w-profile.

The profiles are shown in ms^{-1} per deg in the surface temperature amplitude. Because of the vertical variation of the parameters, no simple scaling exists. Using the stratification below 816 m and the maximum diffusivity gives a length scale of 30 km in the linear model, and thus the nondimensional wavenumber is close to unity. This means that all terms in the linearized equations are of comparable importance. The u and w profiles show very good agreement between the numerical and analytical solutions. The numerical model initially assumes zero wind conditions at the start of the heating period, whereas the analytical model assumes periodic solutions, i.e. any transient solutions are neglected, and consequently differences should be expected due to the appearance of inertial-diffusive oscillations. In this case the numerical model was integrated for one period, and during this time the differences between the two models show a periodic variation with nearly constant amplitude. The contributions from these oscillations are most pronounced in the v-profile as should be expected, since this component is forced only through the coriolis term, whereas the u-component is forced more directly through the pressure gradient term. In all profiles the differences are largest at the higher levels in the boundary layer, partly reflecting the lowered resolution in the numerical model there. The comparisions show that the the numerical schemes are well behaved; in particular that the time splitting, and the sequential "corrector" method used for the calculation of the dynamical pressure term are not introducing systematic or accumulating numerical errors.

3.6. Sea-breeze simulations

The model has been integrated with a number of different specifications of the parameters pertaining to the synoptic or large-scale conditions. The aim has been to compare the model results with the qualitative response of the sea-breeze flow to variations in these parameters. A large amount of observational studies on the behaviour of the land- and sea-breezes has been reported in the literature (see, e.g. Schroeder et al, 1962 for references), and thus some general statements can be made re-

garding the interdependence of the synoptic situation and the sea-breeze flow (as summarized in Schroeder et al, 1962). Because of the number of parameters, which can be varied in the model, and the need to maintain physical realism, a complete study of model response is prohibitive. As a consequence variation of parameters was performed by using a reference set of parameters, and varying only one parameter at a time, keeping all other at their reference value. The parameters chosen is given by the following set with the reference values listed first, and the other values chosen are listed in parentheses:

Parameters varied:

Maximum surface heatflux over land: 200 (100,400) Wm^{-2}
Basic state surface geostrophic wind
u_g : 0 (-3, 3)ms^{-2}
v_g : 0 (-3, 3)ms^{-2}
Basic state thermal wind
x-component S_x , below 1500 m : 0 (-2, 2)ms^{-2}/km
above 1500 m : 0
y-component S_y : 0
Basic state stratification N :0.01 (0.02,0.005)s^{-1}
Grid Reynolds number Re : 2 (5)
Decay time for surface temperature excess over land at night (e-folding time) t_C : 4.2 (16.7)

Parameters kept constant:

Heating period 1/2 t_H: 12 hours
Coriolis parameter f : $1.21 \cdot 10^{-4}$ s^{-1}
Sea surface temperature T_o: 283 K
Initial surface temperature : 283 K
Surface roughness length
over land z_o: 5 cm
over sea : 0.01 mm

Horizontal grid

128 points with a seperation of 2 km, coast at gridpoint no 65. x=0 at coast positive inland.
Diffusive zone (sect. 3.4.2) at outermost 16 gridpoints near lateral boundaries.

Vertical grid

21 levels with increasing separation
z_1=10m , Δz_1 = 30m , $\Delta z_{i+1}=\Delta z_i \cdot 1.23$ ($\Delta z_i=z_{i+1}-z_i$)
resulting in $z_{top}=z_{21}$= 8074 m.

Timestep

0.8 times max allowable given as N^{-1}, and less than 2 min.

Table 3.1 shows some of the model results after integrating the model for 8 hours. The initial data was in every case a temperature field with constant Brunt-Väisäla frequency N, and a wind field given by the geostrophic values at all levels. At 8 hours, which is two hours after maximum heating over land, the sea-breeze is well developed, and the maximum of the onshore wind component u at the coast is found near this time in the case of no synoptic forcing. In the table each column gives results from choosing reference values of the parameters except for the parameter given at the top. The first row shows the u-component at the height of the maximum, which in all cases is near 100 m with a very small vertical gradient below this level. Similarly, the value of max(-v) at the coast is shown in the second row. The next four rows show the maximum u- and v-components, and the distance from the coast where they occur. In the case of no large-scale forcing (first five columns), the maximum winds are found near the coast, and the maximum values are close to those at the coast. With onshore geostrophic wind (u_g=3ms^{-1}), the maximum wind is displaced inland, and the strength of the onshore component relative to the background value ($u-u_g$) is reduced roughly by a factor of two compared with the reference value. In contrast we see that with the geostrophic wind directed offshore (u_g=-3ms^{-1}), the value of $u_{max}-u_g$ is increased by approximately 50%. This strong influence on the flow from even weak synoptic forcing is also evident from the differences in maximum vertical velocity. In the case of the synoptic forcing acting in the same direction as the sea-breeze, the maximum vertical vel-

Table 3.1. Key parameters from model simulations of the sea-breeze for different specifications of the synoptic situation at time 2 hours after maximum heating (8 hours of integration, corresponding to early afternoon). See text.

		ref.	N=0.02	N=0.005	H=100	H=400	u_g=3	u_g=−3	v_g=−3	v_g=3	S_x=2	S_x=−2	Re=5
u-comp at coast	ms^{-1}	2.75	2.47	2.77	1.94	3.86	3.81	−1.48	2.84	2.70	2.90	2.85	2.63
v-comp at coast	–	−2.13	−1.21	−2.41	−1.45	−3.11	−3.07	−0.69	−5.10	0.71	−1.99	−2.07	−2.05
Max u comp	–	3.07	2.57	3.58	2.05	4.49	4.52	1.44	3.14	3.01	3.37	2.96	3.10
Max u located at	km	4	2	6	2	6	16	−6	4	4	6	2	4
Max v comp	ms^{-1}	−2.17	−1.29	−2.47	−1.55	−3.11	−3.63	−0.44	−5.10	0.62	−2.00	−2.07	−2.17
Max v located at	km	−2	−2	4	−2	0	24	−14	0	2	−2	2	−2
Max w	cms^{-1}	6	4	9	4	10	2	16	6	7	2	13	7
Max w located at	km	20	20	20	14	32	24	0	22	18	36	12	20
Temp rise $\Delta T_\infty(0)$	K	9.8	14	7.7	6.5	15	9.0	9.1	9.1	9.1	9.5	9.6	9.8
Temp rise $\Delta T_\infty(10m)$	K	3.5	7.3	1.7	2.2	4.9	3.6	3.6	3.6	3.6	3.6	3.5	3.5
Position of front	km	19	17	17	13	30	24	−1	21	15	34	11	19
PBL-Height H_∞		1.6	1.0	3.0	1.1	2.4	1.6	1.6	1.6	1.6	1.8	1.8	1.6

vertical velocity is only one-third of the reference value. With u_g=-3ms^{-1} the maximum w is nealyr a factor of three larger than the reference value. These results are in accordance with observations (Schroeder et al, 1962). The row denoted $\Delta T_\infty(0)$ gives the surface temperature rise relative to the initial value (= sea surface temperature) at the gridpoint farthest inland, where conditions are nearly homogeneous in the horizontal. The boundary layer height at the same point is shown in the last row. The surface temperature is only slightly reduced in the presence of a large scale wind, and this decrease reflects the decrease of the superadiabatic temperature gradient near the surface, which can be seen by comparing it with ΔT_∞(10m), which is the temperature rise at the same point at the 10-m level. The frontal position is defined as the point with the steepest gradient of u at the 10-m level.

The position of the front, which at this hour is weak except when there is adverse large scale-flow present, is slightly behind the point with maximum vertical velocity, as expected. The greater part of the horizontal convergence is confined to the lowest few hundred meters above ground. Figure (3.2) shows the variation of the u-profile, at the point of maximum value, for the different values of surface heatflux over land. The maximum values are listed in Table 3.1, and we see that increasing the heatflux by a factor of four from 100 Wm^{-2} to 400 Wm^{-2} leads roughly to a doubling of both the maximum windspeed and depth of the inflow layer. We can compare these with the results obtained in section 2.6 (Eq. 2.53), which can be interpreted as the relation that the maximum speed u_{max} is proportional to the square root of the surface heatflux. This relation is followed by the model to within 10%. This square root dependence was also found by Pearson (1973). In contrast to this result we see a substantial dependence of u_{max} on the stratification N. In the linear model u_{max} is proportional to N^{-1}, whereas Eq. (2.53) predicts u_{max} independent of N. The numerical model thus gives a value in between these two extremes. Table 3.2 lists model results after 12 hours of integration, at the end of the heating period. At the coastline the u-component has decreased compared with the values at 8 hours, but the v-component has simultaneously increased as a re-

Table 3.2. Key parameters from model simulations of the sea-breeze for different specifications of the synoptic situation at time 6 hours after maximum heating (12 hours of integration, corresponding to early evening). See text.

		ref.	N=0.02	N=0.005	H=100	H=400	u_g=3	u_g=-3	v_g=-3	v_g=3	S_x=2	S_x=-2	Re=5
u-comp at coast	ms^{-1}	2.23	1.62	1.97	1.67	2.95	3.56	-2.11	2.23	2.70	1.76	2.63	2.12
v-comp at coast	-	-3.32	-1.37	-3.96	-1.82	-4.88	-0.75	-0.56	-6.23	-0.29	-3.21	-3.34	-3.40
Max u comp	-	3.87	3.37	3.50	2.45	5.42	4.54	0.67	3.85	3.96	3.40	2.81	4.35
Max u located at	km	36	32	26	22	50	74	-9	35	34	44	6	40
Max v comp	ms^{-1}	-3.84	-2.46	-4.25	-2.28	-5.55	-1.41	-5.70	-6.23	-1.44	-3.26	-3.45	-3.98
Max v located at	km	30	30	20	19	36	51	-22	0	30	8	6	32
Max w	cms^{-1}	15	10	13	7	27	-	17	14	17	5	27	23
Max w located at	km	42	36	42	28	62	-	-2	46	40	70	24	42
Temp rise $\Delta T_\infty(0)$	K	3.3	9.4	-	2.0	6.2	3.2	4.4	3.2	3.2	4.4	4.4	4.4
Temp rise $\Delta T_\infty(10m)$	K	4.1	7.4	2.0	2.6	5.8	4.0	4.0	4.2	4.2	4.1	4.2	4.2
Position of front	km	43	37	43	29	61	-	-1	47	41	70	23	43
PBL-Height H_∞		1.8	0.9	3.2	1.1	3.2	1.8	2.0	1.8	1.8	1.8	1.6	1.8
u_{max}/u_{front}		2.1	2.1	2.0	2.0	2.3	~ 1	large	1.9	1.9	1.4	3.5	2.2

sult of Coriolis turning, and the scalar windspeed has increased. There is one notable exception, namely the case with a strong initial stratification N=0.02 s^{-1}. In this case the v-component is relatively reduced both at 8 hours and at 12 hours. This reduction of the Coriolis turning, or increase of the cross-isobar angle of the flow, is consistent with the results obtained in

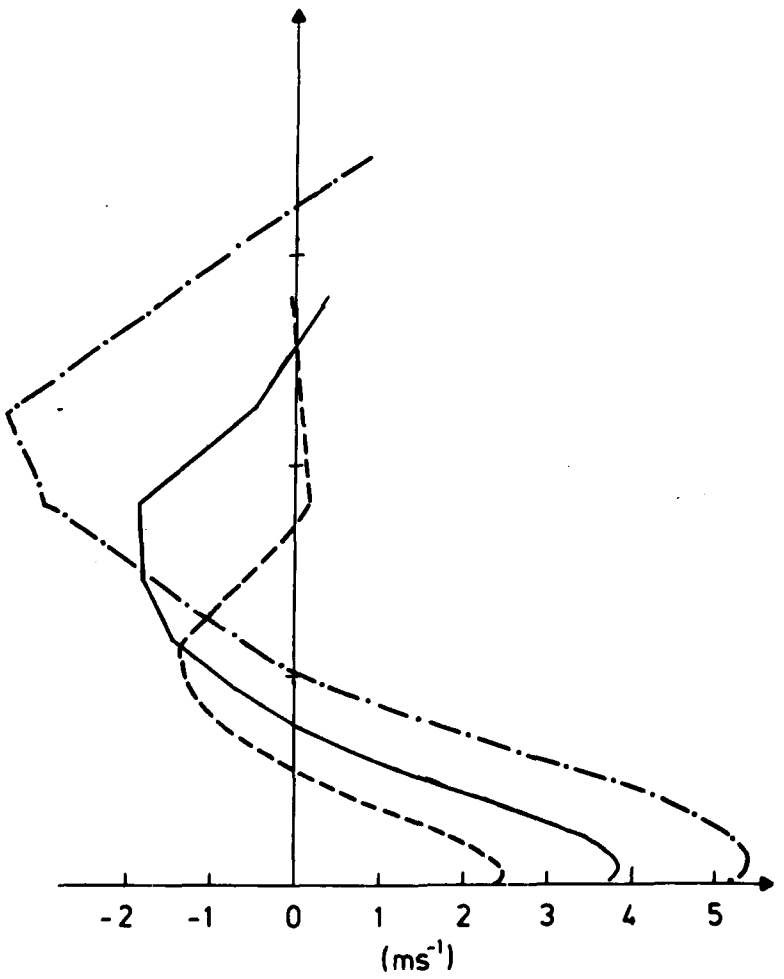

Fig. 3.3. u-profiles at t=12 h from the points with maximum values near the ground. Unit on vertical axis is 1 km. (——). Ref. with H_o=200 Wm^{-2} (profile at x=36 km), (-·-·-): H_o=400 Wm^{-2} (50 km), (---): H_0= 100 Wm^{-2} (22 km).

section 2.8. The point with maximum u and v has moved inland and the two maxima have risen. The surface front has likewise moved further inland, and has become stronger as is evident from the large increase in vertical velocity. The last row in Table 3.2 shows the ratio of the average maximum u-component to the average speed of the front between hours 8 and 12. We see that this value is close to 2 in all cases where there is no large-scale flow in the x-direction. This value agrees well with the value of ~ 2 reported by Simpson et al (1977), and the value 2.2 found by Kimura and Eguchi (1978). The strong dependence on the large-scale flow, which is evident from the table, suggests that this agreement may be fortuituous, however. The values obtained from the observational studies are based on the average of a large number of observations, and we could expect a dependency from the time of day as also suggested by Physick (1980). Table 3.3 gives the rate of advence of the front relative to the maximum u-component for different hours in the reference case, and for the case with larger heatflux.

Table 3.3. Progression of the surface sea-breeze front.
A: reference case . B: Heatflux = 400 Wm^{-2}.
In the last case the model was run with the double number of gridpoints in the x-direction.

A

hour	:	5	7	9	11	13	15	17
frontal pos. km	:	7	19	29	43	63	79	91
u_{max} ms^{-1}	:	2.5	3.0	3.2	3.6	3.7	2.9	2.4
u_{max} ms^{-1}	:	0.6	1.7	1.4	1.9	2.8	2.2	1.8
u_{max}/u_{front}	:	4.5	1.8	2.3	1.8	1.3	1.3	1.4

B

hour	:	5	7	9	11	13	15	17
frontal pos. km	:	17	30	43	61	89	111	131
u_{max} ms^{-1}	:	3.7	4.4	4.6	5.0	5.3	4.6	4.0
u_{front} ms^{-1}	:	1.7	1.8	1.8	2.5	2.5	3.1	2.8
u_{max}/u_{front}	:	2.2	2.4	2.5	2.0	2.1	1.5	1.4

We see that in the reference case the ratio u_{max}/u_{front} is rather variable with a value of ~ 2 only between hour 8 and 12 corresponding to the afternoon. After model sunset the front accelerates resulting in a decrease of the ratio. The value at 5 hours is not very well defined because the front is very weak at this hour. Figure 3.4 shows the u-profiles at 12 hours for the three values of stratification at the points where u is largest near the surface. We see that the profiles are nearly identical if a

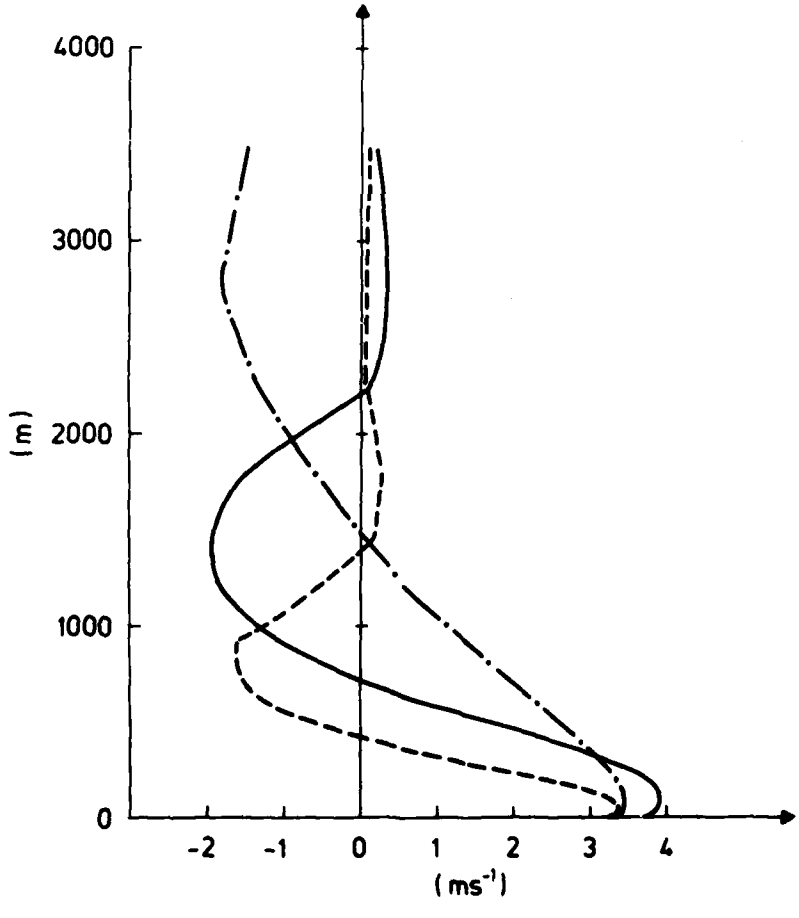

Fig. 3.4. u-profiles at t= 12 h and x=32 km. (——): Ref. with N=0.01 s^{-1}, (---): N=0.02 s^{-1}, (-·-·-): N=0.005 s^{-1}.

proper rescaling of the vertical axis is performed. The linear predicts a scale height proportional to $\sqrt{K}$. The model values of the maximum diffusivity K_m at the points corresponding to the profiles are 36,7.5, and 81 m^2s^{-1} for the three cases N=0.01 (ref.),0.02, and 0.005 $s^{-}1$, respectively, corresponding to the

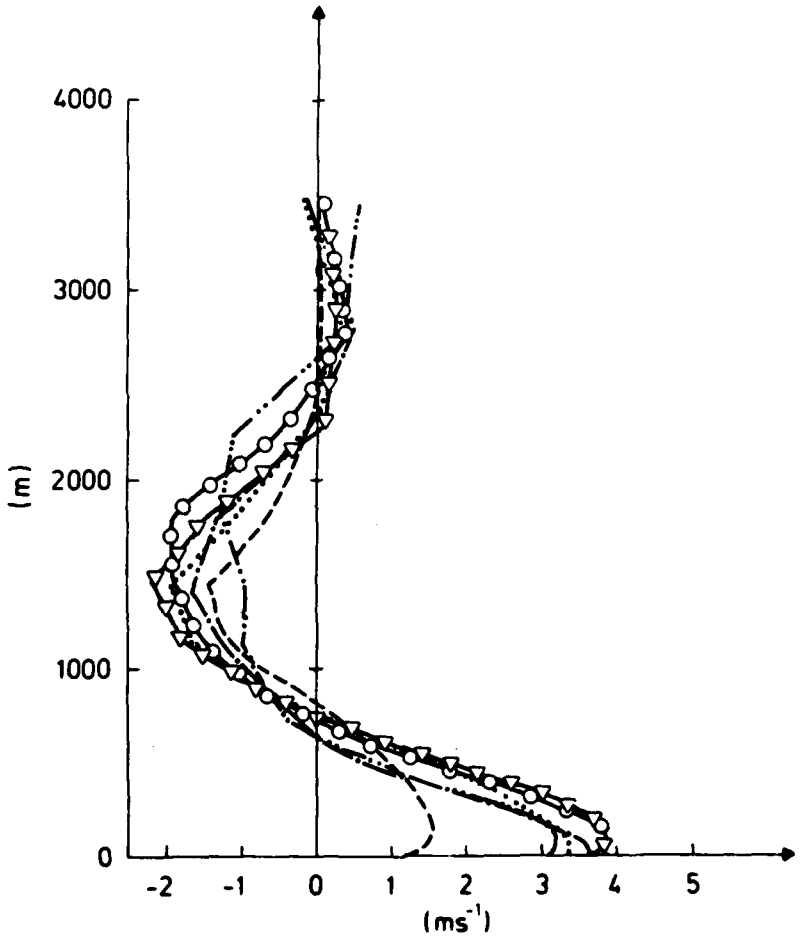

Fig. 3.5. The u-component relative to the large scale flow ($u-u_g$) at 12 h from the points with maximum values near the ground. (---): u_g= 3 ms^{-1} (x=74 km), (-·-·-): u_g=-3 ms^{-1} (-10 km), (-o-o-): v_g= 3 ms^{-1} (34 km), (-▽-▽-): v_g= -3 ms^{-1} (34 km), (-··-··-): S_x= -2 ms^{-1}/km (18 km), (····): S_x= 2 ms^{-1}/km (44 km).

ratios of $\sqrt{K}$ of 1:0.5:1.5. These ratios are close to the values which we would estimate from the figure. Figure 3.5 shows the profiles of $u-u_g$ selected as for Fig. 3.4 but for the different values of the large-scale wind field. The u-profiles relative to the large-scale values are seen to be relatively insensitive to the value of the latter, except in the case where they add to each other, in which case a large reduction of u_{max} results. It should be noted that the profiles are not taken at the same x-coordinate but at the points listed in the legend. Figure 3.6 shows the u,v, and w fields at 8 hours in more details. The maximum inflow is concentrated near the surface as is also evident in the profiles in Figs. 3.3-3.5 (at t=12 h). The asymmetry in both u and v is small only at this time, but in w there is a more pronounced difference between the up- and downdraught regions. The convective boundary layer over land slopes upward following the zero line in the w-plot until the maximum height of approximately 1.6 km is reached; from here it has a nearly constant depth as one moves inland. The downdraught is thus concentrated in a rather thin layer on the top of the boundary layer with a wide extension seaward with only weak subsidence. The same velocity fields 6 hours later (2 hours after model sunset) are shown in Fig. 3.7. At this time a stronger front has been established, and has moved inland as already described above. The definition of the frontal position used above, as the point with largest gradient in u at 10 m, is seen to be uncritical, since the isolines in both u and v are nearly vertical near the surface and essentially coinciding. At the coastline the surface wind is nearly parallel to the coast at this time with a comparatively large counter flow between 1 and 2 km. The maximum value of u has decreased relative to that at 12 hours, but we see on the other hand that the maximum value of w has actually increased indicating a strengthening of the front. Compared to the situation at 8 h, the w field at 14 h shows a downdraught with a strength much smaller than the updraught, but again located above and slightly seaward of the updraught zone. At this hour the land surface has cooled and a shallow stable surface layer has formed. The shear zone behind the surface front has generated a region of turbulence (Fig. 3.7d), and in the upper part of the old convective layer a decaying zone of turbulent

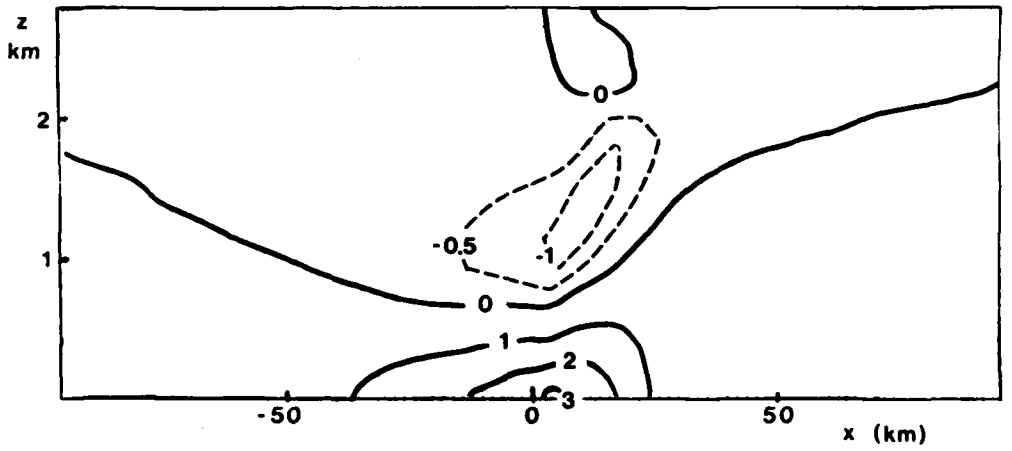

Fig. 3.6a. Contour plot of u-field at t=8 h. Unit on contours is ms^{-1}.

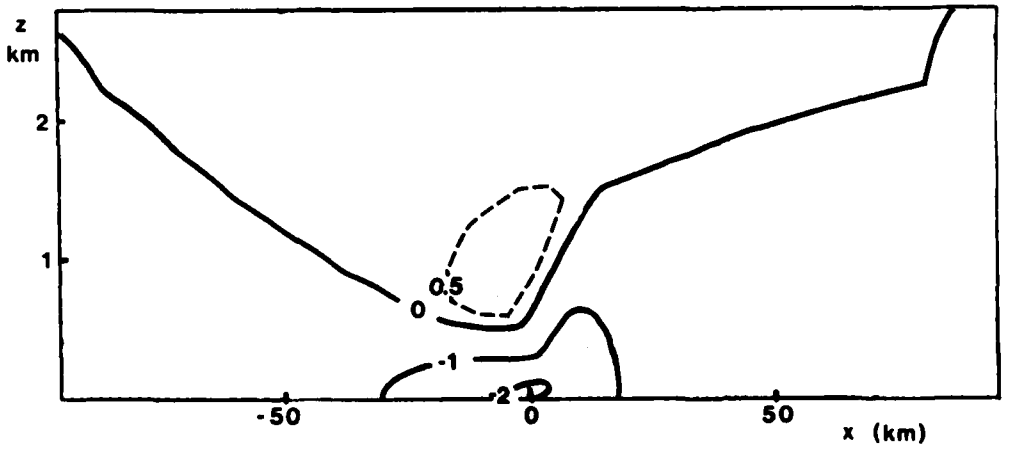

Fig. 3.6b. As Fig. 3.6a but for the v-field.

energy still remains. The turbulence length scale at the same hour is shown in Fig. 3.7e. The length scale at higher levels near the coast is seen to be very long-lived with large values in the old boundary layer where the turbulence energy has essentially vanished. The difference in the decay of e and ℓ is also

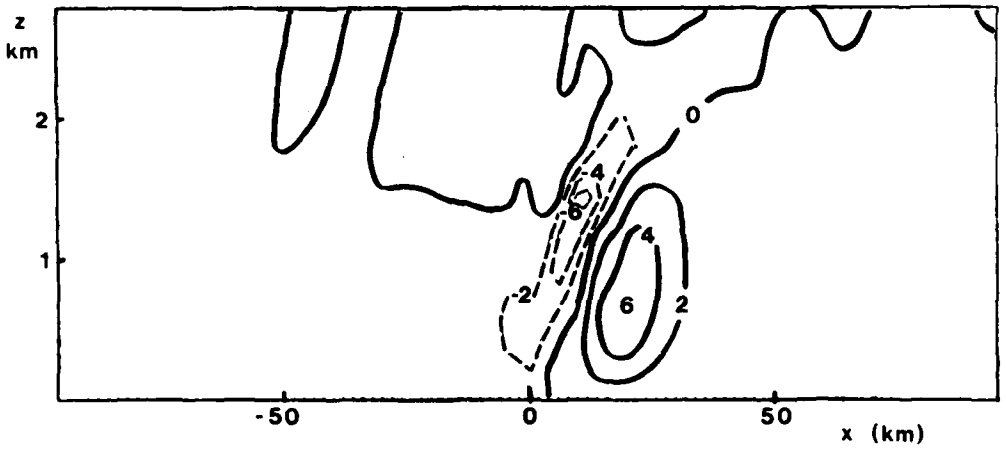

Fig. 3.6c. As Fig. 3.6a, but for the w-field. Contour interval is 1 cms^{-1}.

illustrated in Fig. 3.9 showing the fields of e and ℓ at 12 h in the case where the large-scale wind is directed seawards (u_g=-3ms^{-1}). Here the turbulence energy produced over land decays as it moves over the colder sea. The length scale survives much further, as shown in Fig. 3.9b. The mean flow in the model is influenced only by the turbulence fields e and ℓ through the diffusivity K ~$\ell\sqrt{e}$, and therefore this behaviour of ℓ has only a slight influence on the mean flow. The importance of predicting the turbulence length scale and the turbulence energy is primarily connected to the application of the model to air pollution problems. The study of coastal meteorology has been concentrated on the dispersion conditions in many studies in recent years, in which case knowledge of both the mean flow and the turbulence spectra are important. The simplest model of turbulence spectra which can be of use in this case must enable a determination of a timescale (Lagrangian integral scale), and a total variance. The case of dispersion from a single point in decaying turbu-

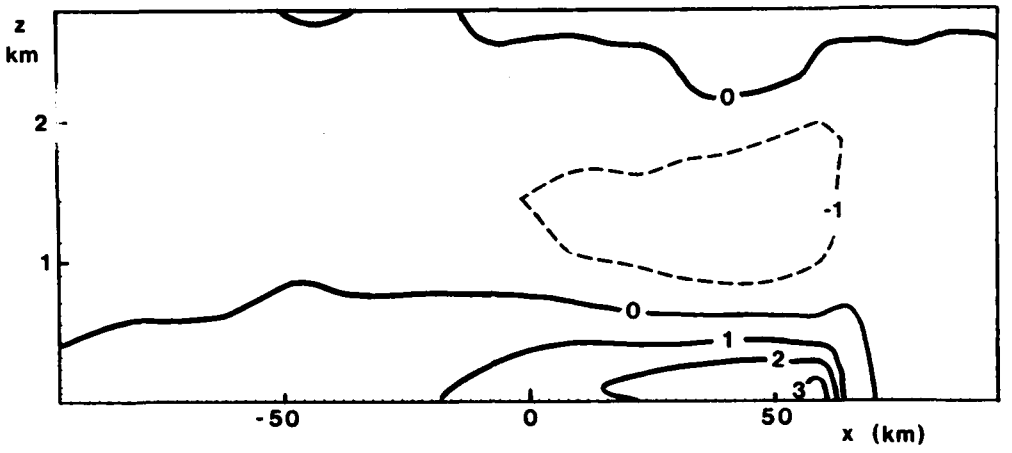

Fig. 3.7a. Contour plot of the u-component at t= 14 h (2 hours after model sunset). Numbers on contours in ms^{-1} (Reference case).

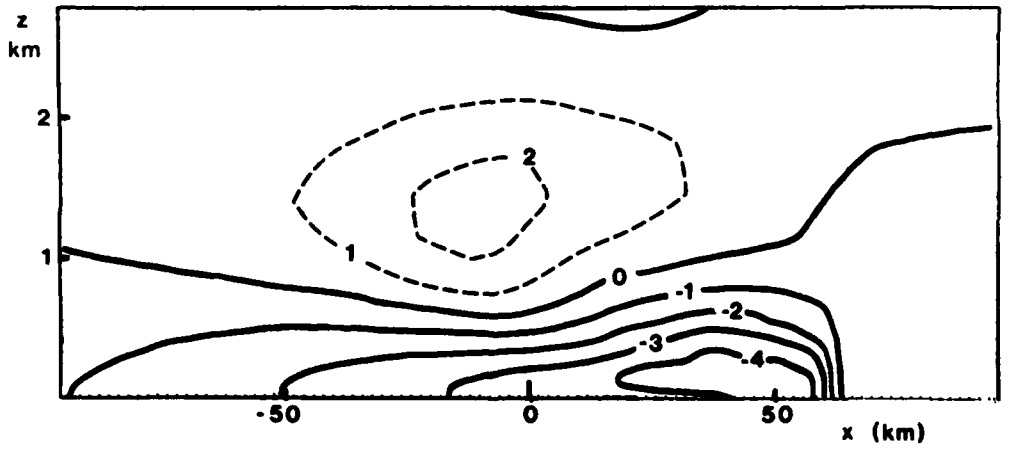

Fig. 3.7b. As fig. 3.7a, but for the v-component.

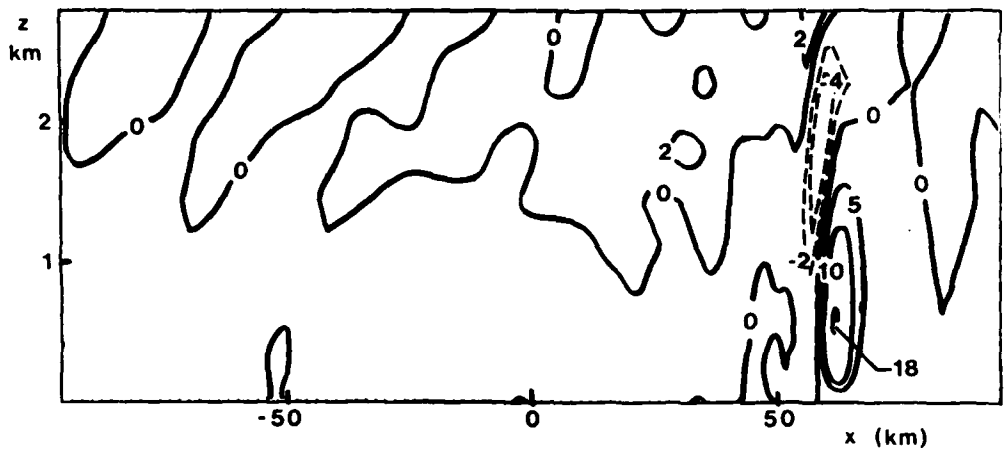

Fig. 3.7c. As fig. 3.7a, but for the w-field. Unit cms^{-1}.

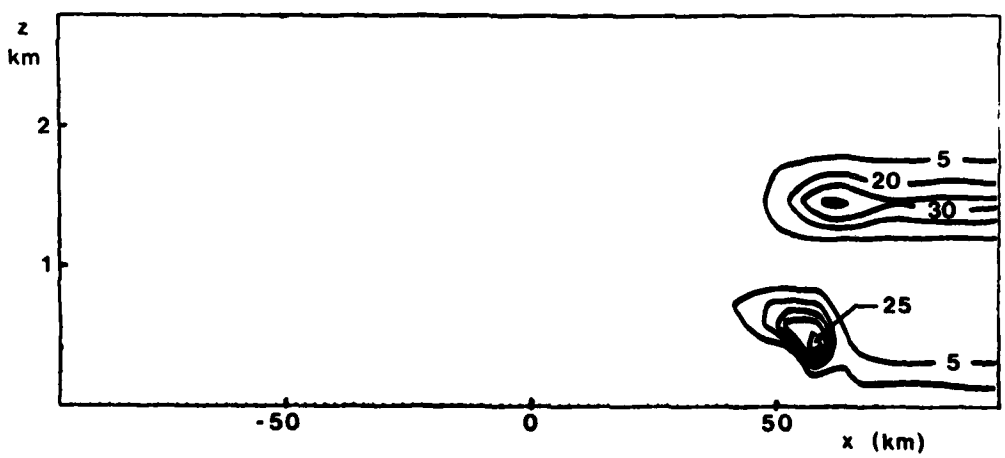

Fig. 3.7d. As fig. 3.7a, but for the turbulence energy. Unit on contours is 0.01 m^2s^{-2}.

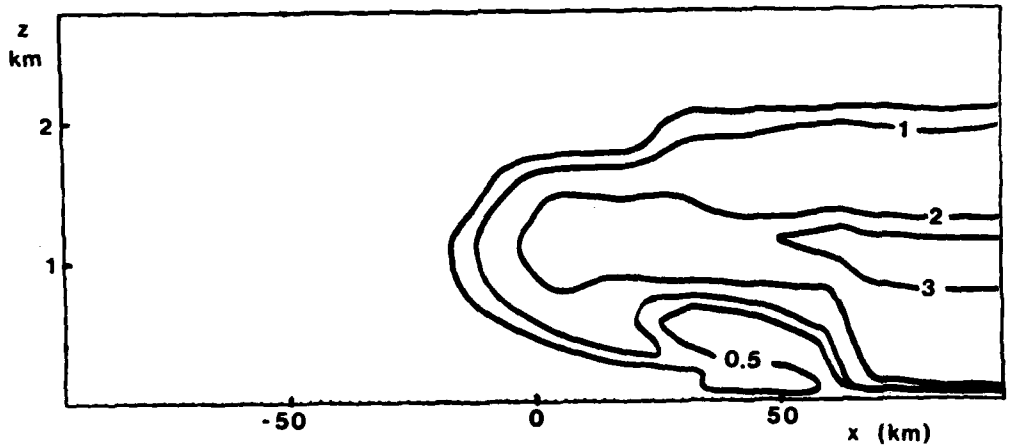

Fig. 3.7e. As fig 3.7a, but for the turbulence length scale ℓ. Unit on contours is 100 m.

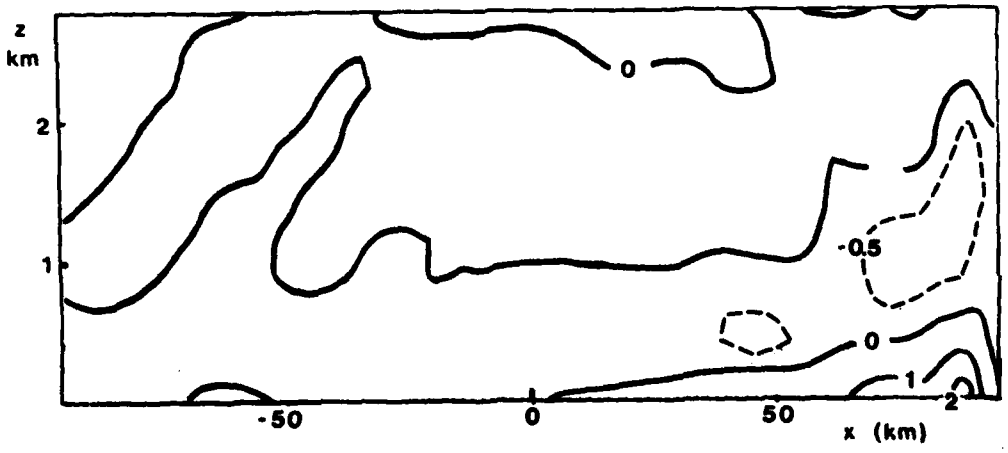

Fig. 3.8. As fig 3.7a, but for t= 18 h.

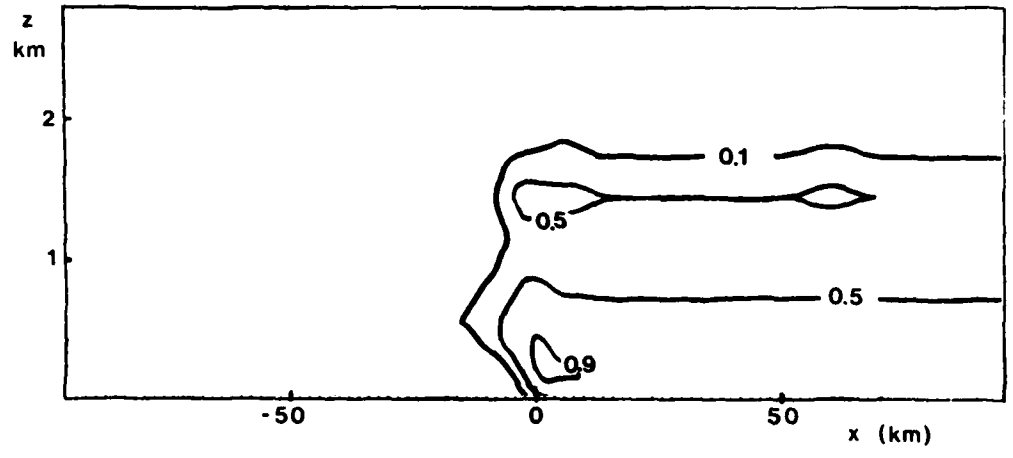

Fig. 3.9a. Contour plot of the turbulence energy at t= 12 h for the case with u_g=-3ms^{-1}. Contour unit is m^{2}s^{-2}.

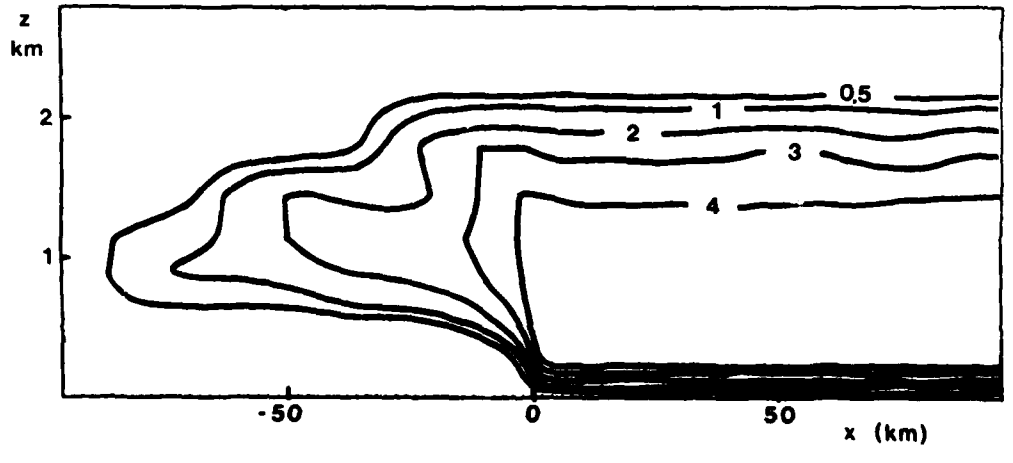

Fig. 3.9b. As fig. 3.9a, but for the turbulence length scale. Contour unit is 100 m.

lence using a simple two-parameter model is treated in Troen et al. (1982), where the the relevance of the knowledge of both e and ℓ is treated in more detail. With essentially constant length scale and decaying energy the timescale of the turbulence will increase, and the model thus predicts a stage in the decay with weak and slow fluctuations in the turbulence equivalent to the meandering often observed under light wind conditions (Kristensen et. al. 1981). The modelling of the length scale in the present model is obviously besed on a rather arbitrary prognostic equation which however, is simple and has the correct asymptotic behaviour in transitional periods, provided of course that the equilibrium values ℓ_s are correctly predicted. Using instead only the energy equation and a diagnostic value for ℓ equivalent to $\ell=\ell_s$ leads to a larger dissipation in the energy equation in the decay case considered. Returning to the behaviour of the sea-breeze front we present Fig. 3.8, which shows the u-field at 18 h, where the front has reached approximately 91 km inland. The maximum value for u has further decreased, but the maximum vertical velocity (not shown) has decreased from 18 cms^{-1} (at 14 h) to only 14 cms^{-1}. At this point only very little further inland progression of the front takes place.

4. CONCLUSION

The flow generated by periodic heating of the land surface while maintaining a constant sea-surface temperature (sea-breeze) has been investigated using analytical and numerical modelling. The linearized equations of motion can be nondimensionalized in such a way as to make solutions universal except for a dependence on the scaled coriolis parameter $f_s=f/\omega$, where ω is the frequency of the surface forcing. In the case when the breeze is superimposed on a large scale flow across the coast a strong attenuation of the breeze circulation results. It is suggested that when the linearization becomes invalid, at finite values of the surface forcing, the effect on the strength of the circulation can be

taken into account by a simple "self-advection" model. The analytical model has been generalized to include the effects of vertical structure on the diffusivity and stratification. The effect of an elevated inversion with a simultaneous jump in effective vertical mixing and stratification prescribed, is a decrease of the strength of the circulation when the inversion height is comparable with the scale height. This appears as a combined effect of the limitation of the vertical mixing and the increased stratification, which can be studied independently in the analytical model. The analytical method requires a simplification of the physical model, which in the case of the sea-breeze is substantial. The more detailed modelling of the flow requires the use of numerical techniques, with which the interplay of the mean flow and the turbulent transport can be handled more realistically. The numerical described in the present report employs a turbulence parameterization scheme, based on the turbulence energy equation and a simple prognostic equation for the turbulence length scale. The model is found to be able to reproduce a number of observed features in sea-breeze situations, in particular a realistic formation of a sharp sea-breeze front and the inland propagation of this front. The qualitative response of the sea-breeze to different synoptic situations is also found to be in qualitative agreement with observations. The prediction of the development of both the turbulence energy and length scale has applications to dispersion modelling in particular when a more accurate description than offered by K-models is required, but presently very little is known about the detailed evolution of the turbulence field under instationary conditions, and the study presented here offers only a simple model which should be tested by comparison with observational data before definite conclusions can be made as to this aspect.

The increase in frontal speed relative to the maximum speed in the evening leads to a structure of the flow, with a small region behind the progressing front, moving at a speed large enough to follow the front inland, without any further air from the sea entering into this region. This structure closely resembles the "cut-off vortex" described by Simpson et. al. (1977). A more ac-

curate modelling of this feature will probably require a larger resolution in the horizontal.

An increase in horizontal resolution down to of the order of hundreds of meters is possible within the nonhydrostatic model-formulation, with the exception that the treatment of the horizontal diffusion must be improved using possibly a formulation along the lines followed in the treatment of the vertical diffusion terms.

ACKNOWLEDGEMENTS

The interest in the analytical modelling technique was encouraged during a visit to Oregon State University, in particular as a result of the support given by Prof. Larry Mahrt. The visit was made possible partially by a grant given by the Nato Air-Sea Interaction Panel.

Drs. E.W. Peterson and T. Mikkelsen made a number of improvements of the text and helped in the preparation of the manuscript.

AD-A136 702 ANALYTICAL AND NUMERICAL MODELLING OF FLOW DRIVEN BY SURFACE DIFFERENTIAL HEATING(U) RISOE NATIONAL LAB ROSKILDE (DENMARK) I TROEN SEP 82 RISOE-R-452 2/2

UNCLASSIFIED F/G 4/1 NL

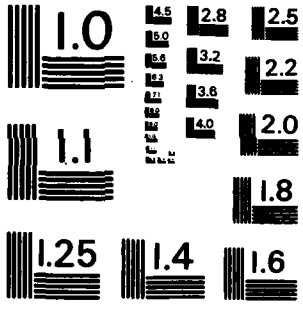

MICROCOPY RESOLUTION TEST CHART
NATIONAL BUREAU OF STANDARDS - 1963 - A

LIST OF SYMBOLS

a	$(f_s + 1)^{-1/2}$.
A_{ik}	Matrix defined by Eq. (3.22).
$A_\omega^{(k)}$, $A(\eta)$, $A_\omega^{(k)}(\eta)$	Amplitude function of a u component corresponding to wavenumber k and frequency ω.
b	$(f_s - 1)^{-1/2}$
$B_{\ell ik}$	Matrix defined by Eq. (3.22).
C	Constant defined on p. 19.
c_1, c_2, c_3, c_4	Constants in turbulence energy equation (p. 66).
d	Depth scale
D	Nondimensional value of outer radius in Fourier-Bessel expansion ($D >> 1$).
D	Divergence operator defined on p. 73.
D^*	$D(u^*,w^*)$
D_k^*	Fourier component of D^* with wavenumber k.
e	Turbulence kinetic energy.
e_s	Equilibrium turbulence kinetic energy (p.65).
f	Coriolis parameter.

Fr	Froude number.
f( )	function of ( ).
g	gravitational acceleration.
g( )	function of ( ).
G	Geostrophic windspeed.
h	depth scale
H, H_ω	depth scale, = $\sqrt{K/\omega}$
H	Height of boundary layer.
H_o	surface heatflux.
H_∞	Height of boundary layer at "infinity" $\equiv x_{max}$.
i	imaginary unit, index
J_o, J_1	Bessel functions of zero and first order.
k	wavenumber in x-direction.
$\hat{k}$	unit vector in z-direction.
k_U	= $N/U \cdot \sqrt{K/\omega}$.
K	diffusivity
K_m, K_h	diffusivity for momentum and heat.
ℓ	mixing length.
ℓ_s	equilibrium mixing length (p. 65).
L	Length scale = $N/\omega \cdot \sqrt{K/\omega}$.

L	Monin-Obukhov length.
m	stratification parameter (p. 11).
N	Brunt-Väisälä frequency.
p	pressure.
p_j	defined on p. 10.
p_{oo}	standard pressure.
q	heatflux = $\langle w'\theta' \rangle$
Q	heat source term.
r	scaled radius.
r	constant = $\sqrt{2}/2(1+i)$
r^*	complex conjugate of r = $\sqrt{2}/2(1-i)$.
R	Relative deviation of potential temperature = $(\theta-\Theta)/\Theta$
R_g	gas constant for dry air.
Ri_B	Bulk Richardson number (p. 67).
t	time.
T	timescale, temperature.
T_o	surface temperature.
t_c	relaxation timescale of surface temperature (p. 74).
t_H	length of day (p. 74).

u	velocity component in x-direction
$\tilde{u}$	dimensional value of u (in Ch. 2).
$u(\xi,\eta,\tau)$	scaled value of u as function of scaled coordinates.
$u(k,\eta)$	Fourier transform defined on p. 9.
$u^{(k)}$	= Re $\{u(k,\eta)\cos k\ \xi/k\ \exp(-i\tau)\}$.
u_*	friction velocity.
u^*	model u-component before adding $\partial_x\pi$-term.
u_s	x-component of geostrophic windspeed.
u_j	defined on p. 12-14.
$u_{max}^{(U)}$	max value of u in the presence of a large advective velocity U.
U	large-scale advective velocity in x-direction, horizontal scale velocity.
v	velocity component in y-direction.
$\tilde{v}$	dimensional value of v (Ch. 2).
$\vec{v}$	windvector.
$v(\xi,\eta,\tau)$	scaled v as function of scaled coordinates.
$v(k,\eta)$	Fourier transform of v defined on p. 9.
v_j	defined on p. 12-14.
v_g	y-component of geostrophic windvector.

w	vertical component of windvector.
$\tilde{w}$	dimensional value of w (Ch. 2).
w	vertical velocity scale.
$w(\xi,\eta,\tau)$	scaled w as function of scaled coordinates.
$w(k,n)$	Fourier transform of w defined on p. 9.
w_*	convective velocity scale = $(g/T_o\langle w'\theta'\rangle H)^{1/3}$.
w^*	model w-component before adding $\partial_2\pi$-term.
w_j	defined on p. 12-14.
x	distance inland from coast.
y	distance along coast.
z	height.
z_o	roughness length.
z_i	height of i'th gridpoint.
α, α_j	$= \pm\sqrt{\beta}$ with $Re(\alpha) < 0$.
β,β_j	characteristic roots (p. 10).
γ_j	$= (\alpha_j^2 + i)$
Γ	$= \partial\theta/\partial z$
γ_c	defined on p. 66.
Γ_c	defined on p. 66.
Δ	difference operator.

Δz_i	grid spacing = $z_{i+1} - z_i$.
η	scaled vertical coordinate = $z/\sqrt{K/\omega}$
η'	scaled vertical coordinate = $z/\sqrt{K/f}$
θ	potential temperature.
$\tilde{\theta}$	dimensional value of θ (Ch. 2).
$\theta(\xi,\eta,\tau)$	scaled θ as function of scaled coordinates.
$\theta(k,\eta)$	Fourier transform of θ defined on p. 9.
θj	defined on p. 12-14.
Θ	standard potential temperature.
λ	$= k^{1/3}\ \eta$.
ν	kinematic viscosity.
π	pressure function defined on p. 64.
π_h	hydrostatic pressure function (p. 64).
π_k	Fourier mode of wavenumber k of π.
ξ	scaled x-coordinate.
ϕ	latitude.
ϕ_s	defined on p. 20.
ϕ_i	"chapeau" function defined on p. 72.
$\phi_\omega^{(k)}, \phi_\omega^{(k)}(\eta), \phi(\eta)$	phase function of u-component corresponding to wavenumber k and frequency ω.

ϕ_o	direction of wind maximum (p. 26).
ρ	density.
ρ_o	standard density (p. 63).
σ_ℓ	ℓ'th root of J_o.
τ	scaled time = ωt.
τ_o	scaled time of wind maximum (p. 26).
ω	diurnal frequency, forcing frequency.
$\hat{\omega}$	scaled diurnal frequency = ω/f.
$\tilde{\omega}$	= k U/L "induced forcing frequency".
Ω	diurnal frequency.
Ω	length scale parameter = $(\ell/L)^{2/3}$.

REFERENCES

AHLBERG, J.H. and NILSON, E.N. (1967). The Theory of Splines and their Applications. Academic Press, New York 284 pp.

ANTHES, R.A. (1978). The Height of the Planetary Boundary Layer and the Production of Circulation in a Sea-Breeze model. J. Atm. Sci. 35 1231-1239.

BIGGS, W.G. and GRAVES, M.E. (1962). A Lake Breeze Index. J. Appl. Meteor. 1 474-480.

BODIN, S. (1979). A predictive numerical model of the atmospheric boundary layer based on the turbulent energy equation. SMHI reports, RMK 13, Sveriges Meteorologiske og Hydrologiske Institut, Norrköping. 138 pp.

BRITTER, R.E. and SIMPSON, J.E. (1978). Experiments on the dynamics of a gravity current head. J. Fluid. Mech. 88 223-240.

BUSCH, N.E. (1973). On the Mechanics of Atmospheric Turbulence. In: Workshop on Micrometeorology, Ed. D.A. Haugen American Meteorological Society, Boston. 1-61

BUSCH, N.E., CHANG, S.W. and ANTHES, R.A. (1976). A Multi-Level Model of the Planetary Boundary Layer Suitable for use with Mesoscale Dynamic Models. J. Appl. Meteor. 15, 909-919.

BUSINGER, J.A., WYNGAARD, J.C., IZUMI, Y. and BRADLEY, F.E. (1971). Flux Profile Relationships in the Atmospheric Surface Layer. J. Atm. Sci. 28, 181-189.

BUSINGER, J.A. (1973). Turbulent Transfer in the Atmospheric Surface Layer. In: Workshop on Micrometeorology, Ed. D.A. Haugen. American Meteorological Society, Boston. 67-100.

CLARKE, R.H. (1971). The Wangara Experiment: Boundary Layer Data. Tech. paper no. 19, Div. of Meteorological Physics. Commonwealth Scientific and Industrial Research Organization. Australia.

CHORLTON, F. (1969). Boundary value problems in Physics and Engineering. Van Nostrand Rienhold Company, London. 250 pp.

DUTTON, J.A. and FICHTL, G.H. (1969). Approximate Equations of Motion for Gases and Liquids. J. Atm. Sci. 26, 241-254.

DEARDORFF, J.W. (1966). The Counter Gradient Heat Flux in the Lower Atmosphere and in the Laboratory. J. Atm. Sci. 23, 503-506.

ESTOQUE, M.A. (1961). A Theoretical Investigation of the Sea Breeze. Quart. J. Roy. Meteor. Soc. 87, 136-146.

GEISLER, J.E. and BRETHERTON, F.P. (1968). The Sea Breeze Forerunner. J. Atm. Sci. 26, 82-95.

GOSSARD, E.E. and HOOKE, W.H. (1975). Waves in the Atmosphere. Developments in Atmosperic Science vol. 2. Elsevier, Amsterdam 456 pp.

GOUGH, D.O. (1968). The Anelastic Approximation for Thermal Convection. J. Atm. Sci. 25, 448-456.

KAIMAL, J.C., WYNGAARD, J.C., IZUMI, Y. and COTÉ, O.R. (1972). Spectral Characteristics of Surface Layer Turbulence. Quart. J. Roy. Meteor. Soc. 98, 563-589.

KAIMAL, J.C., WYNGAARD, J.C., HAUGEN, D.A., COTÉ, O.R., IZUMI, Y., CAUGHEY, S.J. and READINGS, C.J. (1976): Turbulence Structure in the Convective Boundary Layer. J. Atm. Sci. 33, 2152-2169.

KEEN, C.S. and LYONS, W.A. (1978). Lake/Land Breeze Circulations on the Western Shore of Lake Michigan. J. Appl. Meteor. 17, 1843-1855.

KIMURA, R. and EGUCHI, T. (1978). On the Dynamical Processes of Sea and Land-Breeze Circulation. J. Meteor. Soc. Japan 56 no. 2, 67-84.

KRISTENSEN, L., JENSEN, N.O. and PETERSEN, E.L. (1981). Lateral dispersion of pollutants in a very stable atmosphere - the effect of meandering. Atm. Environ. 15, 834-844.

MAHRT, L.J. (1979). Boundary Layer Mean Flow Dynamics. In: Workshop on the Planetary Boundary Layer. Ed. J.C. Wyngaard. Americal Meteorological Society, Boston (1980). 1-35.

MAHRT, L.J. (1980). Modelling the Depth of the Stable Boundary layer. Boundary Layer Meteor. 21 no. 1, 3-19.

MAK, M.K. and WALSH, J.E. (1976). On the Relative Intensities of Sea and Land Breezes. J. Atm. Sci. 33, 242-251.

MESINGER, F. and ARAKAWA, A. (1976). Numerical Methods used in Atmospheric Models. GARP Publications series No. 17, 1, World Meteorological Organization, Geneva.

MIKKELSEN, T., LARSEN, S.E. and TROEN, I. (1980). Use of a Puff-model to calculate dispersion from a strongly time-dependent source.In: Seminar on Radioactive Releases and Their Dispersion in the Atmosphere following a Hypothetical Reactor Accident. Risø(Roskilde) 22-25 April 1980. 575-614.

NEUMAN, J. and MAHRER, Y. (1971). A Theoretical Study of the Land and Sea-Breeze Circulation. J. Atm. Sci. 28, 1374-1388.

OGURA, Y. and PHILLIPS, N.A. (1962). Scale Analysis of Deep and Shallow Convection in the Atmosphere. J. Atm. Sci. 19, 173-179.

OLFE, D.B. and LEE, R.L. (1971). Linearized Calculations of Urban Heat Island Convection Effects. J. Atm. Sci. 28, 1374-1388.

PARK, S.U. and MAHRT, L.J. (1979). Oscillating, stratified boundary layers driven by surface temperature variations. Tellus 31, 254-268.

PEARSON, R.A. (1973). Properties of the Sea Breeze Front as Shown by a Numerical Model. J. Atm. Sci. 30, 1050-1060.

PIELKE, R.A. (1974). A Three-Dimensional Numerical Model of the Sea Breeze over South Florida. Mon. Wea. Rev. 102, 115-139.

PHYSICK, W.L. (1980). Numerical experiments on the inland penetration of the sea breeze. Quart. J. Roy. Meteor. Soc. 16, 735-746.

SCHROEDER, M.J., FOSBERG, M.A., CRAMER, O.P. and O'DELL, C.A. (1962). Marine Air Invension of the Pacific Coast: A Problem Analysis. Bull. Amer. Meteor. Soc. 48, 802-808.

SCORER, R.S. (1956). Airflow over an isolated hill. Quart. J. Roy. Meteor. Soc. 82, 41-56.

SHAPIRO, R. (1970). Smoothing, Filtering and Boundary Effects. Rew. Geophys. and Space Phys. 8, 359-387.

SHIR, C.C. (1973). A Preliminary Numerical Study of Atmospheric Turbulent Flow in the Idealized Planetary Boundary Layer. J. Appl. Meteor. 30, 1327-1339.

SIMPSON, J.E., MANSFIELD, D.A. and MILFORD, J.P. (1977). Inland penetration of sea-breeze fronts. Quart. J. Roy. Meteor. Soc. 103, 47-76.

TROEN, I., LARSEN, S.E. and MIKKELSEN, T. (1982). PPI-Theory for particle dispersion. 12. ITM/NATO CCMS Ile D'Embiez, France sept. 1982.

WALSH, J. E. (1974). Sea Breeze Theory and Applications. J. Atm. Sci. 31, 2012-2026.

WYNGAARD, J.C., ARYA, S.P.S. and COTÉ, O.R. (1974). Some aspects of the Structure of Convective Boundary Layers. J. Atm. Sci. 31, 747-751.

WYNGAARD, J.C., and COTÉ, O.R. (1971). The Budgets of Turbulent Kinetic Energy and Temperature Variance in the Atmospheric Surface Layer. J. Atm. Sci. 28, 190-201.

YAMADA, T. and MELLOR, G. (1975). A Simulation of the Wangara Atmospheric Boundary Layer Data. J. Atm. Sci. 32, 2309-2329.

APPENDIX

A1. Ekman problem in two-layer model

In a homogeneous stationary boundary layer the usual Ekman solution for the horizontal wind vector results from the equations of motion if a height-independent diffusivity for momentum is assumed. The solution for the case where the vertical mixing is limited to some depth H, for example as a consequence of an inversion layer at this height, can be obtained by assuming the atmosphere to be divided into two layers with different diffusivities in the two layers and matching the solutions for each layer at the interface. Using the Ekman depth corresponding to the diffusivity in the lowest layer for height scaling i.e. defining $\eta = z(2K_1/f)^{1/2}$, scaling wind velocity by the geostrophic windspeed G, and using complex notation as $V = G^{-1}(u-u_g + i(v-v_g))$ the dynamical equations can be written:

$$v + a^2 \frac{i}{2} \frac{\partial^2}{\partial \eta^2} v = 0 \qquad \text{(A1)}$$

where

$$a^2 = \begin{cases} 1 \text{ in the lower layer} \\ K_2/K_1 \text{ in the top layer .} \end{cases}$$

The solution in each layer can be written as a sum of two complex exponentials, and the four coefficients are fixed by application of the boundary conditions $V = -1$ at $\eta = 0$ (corresponding to u and v zero at the surface and the alignment of the real axis along the direction of the geostrophic wind vector), $V \to 0$ for $\eta \to \infty$, and the matching conditions at $\eta = b \equiv H(2K_1/f)^{-1/2}$ from the requirement of continuity of the wind vector and the momentum flux, viz

$$v_1(b) = v_2(b)$$

$$\frac{\partial v_1}{\partial \eta} = a^2 \frac{\partial v_2}{\partial \eta} \quad \text{at} \quad \eta = b \tag{A2}$$

The roots in the characteristic equation for Eq. (A1) are $\pm a^{-1}\sqrt{2i}$ and the solution can be written

$$v = A \exp((1+i)\eta) = B \exp(-(1+i)\eta) \tag{A3}$$

for the lower layer, and as

$$v = C \exp(-(1+i)\frac{\eta}{a}) \tag{A4}$$

for the top layer.

The boundary and matching conditions results in the following equations for the coefficients:

$$\begin{aligned} A + B &= -1 \\ Ap^b + Bp^{-b} &= Cp^{-b/a} \\ Ap^b - Bp^{-b} &= -Cap^{-b/a} \end{aligned} \tag{A5}$$

where $p = \exp(1+i)$. The solution to this system of equations is easily obtained:

$$\begin{aligned} A &= \left[\frac{a+1}{a-1} p^{2b} - 1\right]^{-1} \\ B &= -\frac{a+1}{a-1} p^{2b} \left[\frac{a+1}{a-1} p^{2b} - 1\right]^{-1} \\ C &= \left(1 - \frac{a+1}{a-1}\right) p^{\left(\frac{b}{a}+b\right)} \left[\frac{a+1}{a-1} p^{2b} - 1\right]^{-1} \end{aligned} \tag{A6}$$

For $a = 1$ corresponding to $K_2 = K_1$ (and no discontinuity) we obtain $A = 0$, $B = -1$ and $C = -1$ and the usual Ekman solution given by Eq. (A3). For the case of vanishing vertical mixing in the top layer we have $a = 0$, and Eq. (A6) simplifies to:

$$A = - [p^{2b} + 1]^{-1}$$
$$B = - p^{2b} [p^{2b} + 1]^{-1} \qquad \text{(A7)}$$

The coefficient C will tend to infinity as $a \to 0$, but as expected the wind tends to the geostrophic wind everywhere in the top layer as $a \to 0$ as can be seen by combining (A6) and (A4). With $K_2 = 0$ undamped inertial oscillations are also possible solutions in the top layer. The usual Ekman solution is again obtained from (A7) if the discontinuity tends to infinity. From (A7) and (A3) we finally obtain the wind profiles in the lower layer as

$$u/G = 1 - D[\cosh(\eta-b)\cos(\eta-b)\cosh b \cos b + \sinh b \sin b \sinh(\eta-b)\sin(\eta-b)$$
$$v/G = D[\cosh v \cos b \sinh(\eta-b)\sin(\eta-b) - \cosh(\eta-b)\cos(\eta-b)\sinh b \sin b] \qquad \text{(A8)}$$

with

$$D = [\cosh^2 b \cos^2 b + \sinh^2 b \sin^2 b]^{-1} .$$

These profiles are shown on Fig. A1 for different values of the thickness of the mixed layer b. Also shown is the wind vector at the top of the mixed layer obtained from Eq. (A8) by setting $\eta = b$.

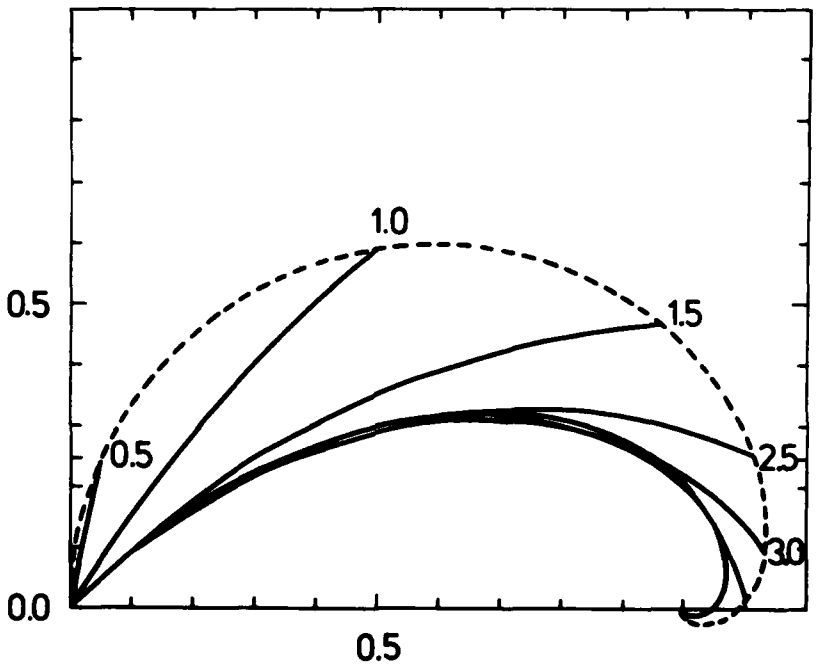

Fig. A.1 The Ekman spiral for different values of the scaled thickness of the boundary layer (see text). The numbers on the curves give the thickness. The endpoint of each curve corresponds to the top of the boundary layer, and the dashed curve connects all possible endpoints.
Geostrophic value in this (u,v)-plot is G=(1,0).

END

DATE
FILMED

2 84